Achim Michalke

Photocathodes Inside Superconducting Cavities

Studies on the Feasibility of a Superconducting Photoemission Source of High Brightness

Projekt Supraleitende

Photo-Elektronen-Quelle

Dissertation to acquire the doctor's degree
of the
Fachbereich 8 – Physik
der
Bergischen Universität - Gesamthochschule Wuppertal
English translation by the author

WUB-DIS 92-5

January 14, 1993

Updated Electronic Version, 2009

Contents

Abstract

We have done studies and experiments to explore the feasibility of a photoemission RF gun with a superconducting accelerator cavity. This concept promises to provide an electron beam of high brightness in continuous operation. It is thus of strong interest for a free-electron-laser or a linear collider based on a superconducting accelerator.

In a first step we studied possible technical solutions for its components, especially the material of the photocathode and the geometrical shape of the cavity. Based on these considerations, we developed the complete design for a prototype electron source. The cathode material was chosen to be alkali antimonide. In spite of its sensitivity, it seems to be the best choice for a gun with high average current due to its high quantum efficiency. The cavity shape was at first a reentrant-type single cell of 500 MHz. It is now replaced by a more regular two-and- half cell shape, an independent half cell added for emittance correction. Its beam dynamics properties are investigated by numerical simulations; we estimated a beam brightness of about 5×10^{11} A/(m×rad)^2. But the mutual interactions between alkali antimonide photocathode and superconducting cavity must be investigated experimentally because they are completely unknown.

For this purpose we built up two experiments: The first setup was a vacuum chamber to prepare and characterize alkali antimonide photocathodes. There we learned to handle this type of material. We could define a preparation process enabling us to produce reliably Cs_3Sb layers with 4% quantum efficiency at 543 nm. Using a more sophisticated process we were even able to produce a Cs_3Sb layer with 10% efficiency. Usually, the layers did not show any decay during two to four weeks storage in the chamber. The 10% layer even had the same efficiency after half a year of storage. Hydrogen and nitrogen gas at a pressure of $l0^{-5}$ mbar did not do any harm to the Cs_3Sb layers; other gases have not yet been investigated. The photocathode layer thickness had no influence on the quantum efficiency down to 60 nm; for yet thinner layers on niobium the efficiency was reduced.

In the second setup photocathodes can be transferred into a superconducting cavity and operated there. By renouncing to produce a defined beam we could keep the setup very simple and flexible. We measure the current extracted by the high RF field with and without illumination as well as the RF properties. The photocathodes behaved like expected, if one takes into account secondary electron emission. Quantum efficiency and secondary emission parameters could be determined comparing the measured curves with simulations. Also in RF operation we could achieve quantum efficiencies up to 10%. During operation the characteristic parameters of the photocathodes showed strong variations due to the bombardment by backaccelerated electrons and reaction with residual gases, which is unavoidable during operation with a continuous laser. Therefore the lifetime of the photocathodes under normal operation conditions cannot be tested until a pulsed laser is available.

All Cs_3Sb layers showed strong RF losses inside the cavity; the conductivity of Cs_3Sb at 4.2 K could be determined as $\sigma = 0.045$ A/Vm. Thus the layers did not shield the RF field, but caused dielectric losses in the high electric field area. The resulting heat dissipation will put heavy requirements on the cryogenic system of a prototype source. The photocathodes also showed field emission starting already at electric fields as low as 2-3 MV/m. The field emitters showed typical Fowler-Nordheim behaviour with high $\beta \approx 500$ and could be processed; their properties are obviously not intertwined with the photoelectric parameters. This effect limited the fields which we could apply on the photocathodes to 5-7 MV/m. We also investigated whether the Cs_3Sb photocathodes permanently contaminated the superconducting cavity by material transfer. Within our accuracy, we could not find such an effect.

Introduction

The present paper describes our studies and experiments towards a photoemission source of high brightness using a superconducting cavity. They are done in collaboration with our partners at INFN Milano, Italy, and at CEBAF, Newport News, VA. They base on an idea of H. Piel and C. K. Sinclair: Equipping the recently very successful photoemission RF guns with a superconducting cavity should enable them for continuous operation, then being applicable also to superconducting accelerators.

As a first step we have studied the requirements on the components of such a gun, especially on cathode and cavity. We've assessed and developed possible technical solutions for them. Based on these data we have developed a complete design for a prototype gun of this type. The parameters of the prototype were initially guided by the requirements of a compact free- electron-laser (FEL) with superconducting accelerator [2]. The material of the photocathode was chosen to be alkali antimonide. This material requires excellent vacuum conditions due to its sensitivity against active gases. Nevertheless, it seems to be the best solution for applications with high average current due to its high quantum efficiency. This design study was done in collaboration with colleagues from the MHF group of DESY Hamburg and from the electrical engineering department at our university.

In parallel to this design study we built up a vacuum chamber to prepare and characterize alkali antimonide photocathodes. The company Interatom GmbH (now Siemens AG) helped us to construct this experiment. It has been taken into operation in 1989. Initially, we learned the techniques of preparing and handling alkali antimonide cathodes on this setup. Later we investigated the dependence of the quantum efficiency on parameters like layer thickness and reaction with residual gases. Finally, the activities on this first experiment have been reduced in favour of the second experiment.

While most properties of the prototype gun (like beam dynamics) could be calculated from existing data, the mutual interactions between alkali antimonide photocathode and superconducting cavity were completely unknown. Both are extremely surface-sensitive systems; one can imagine various mechanisms of mutual interference. Therefore it is absolutely necessary to test and investigate the common operation of these two components in advance of building a prototype gun. For this purpose we have built a setup like a simplified prototype gun, but renouncing to produce a definite beam: Photocathodes can be produced in a preparation chamber and transferred into a superconducting cavity. There they can be operated under various conditions in the high RF field. This experiment has been taken into operation in 1991. Meanwhile, six Cs_3Sb layers have been operated and investigated in the superconducting cavity.

In parallel to these experiments we have continuously improved our prototype design. The proposal of the superconducting linear collider TESLA [204] defined a new application for the superconducting RF gun. In collaboration with our partners in Milano we have revised our design and adapted it to the requirements of TESLA [6]. This improved design is now included in the proposal of a TESLA test facility at DESY [158]. However, the possible application at TESLA doesn't diminish the meaning of application in free electron laser projects: While most probably only one linear collider (and not necessarily a superconducting one) will be built worldwide, free electron lasers will in future probably gain more and more importance.

1. Electron Sources of High Brightness

The following chapter is a summary of theory and history concerning our project. It shall serve as an introduction into this very topic of research as well as a summary of the most important definitions. Thus it does not base on proper research, but is collected from various publications.

1.1. The Meaning of Electron Beams with High Brightness

1.1.1. Particle Accelerators and Particle Beams

Particle accelerators accelerate charged atomic or subatomic particles (electrons, positrons, protons, ions, etc.) by means of electromagnetic fields. The final energies range from a few MeV up to several TeV. The produced ensemble of particles being strongly correlated in phase space is called a beam. Particle accelerators have been developed for nuclear and elementary particle physics which completely base on this instrument. But they increasingly find further applications in physics and engineering, because they can transfer large amounts of well concentrated energy. In this context electron accelerators are of special importance, because electrons can easily be generated and simply be accelerated due to their high charge per mass. In the broadest sense TV tubes, electron beam welding machines, and electron microscopes belong to the electron accelerators family. However, here we'll only consider applications with energies above 1 MeV, which require large accelerators with more than one stage.

The complete characterization of a beam would contain the phase-space coordinates of all particles involved. However, the macroscopic behaviour can be described by a few statistical parameters: The longitudinal phase space is normally described by time and energy; characteristic parameters of the beam are therefore average energy, energy spread, and time structure. The correlation between them is given by the longitudinal emittance, giving the phase space volume occupied by the particle bunch. Characteristic quantities of the transversal distribution are radius and divergence of the beam. Their correlation is again characterized by the transversal emittance. The brightness of the beam is a mixed quantity describing its intensity independent of the local beam-optical situation.

1.1.2. The Definition of Emittance and Brightness

The emittance is the phase-space area occupied by the beam in one real-space direction. Thus there are one longitudinal and two transversal components of the emittance [187]. One must distinguish between the (direct) emittance ε in the distance-angle-phase space and the normalized emittance $\varepsilon_n = \beta\gamma\cdot\varepsilon$ in the distance-momentum-phase space. They differ by the relativistic factor $\beta\gamma = p/mc$. According to Liouville's theorem, the product of all three emittance components is invariant as long as no statistical forces like space-charge forces or synchrotron radiation occur: Beam optics and acceleration devices change the shape, but not the volume of the phase-space distribution. If there is no coupling between the three directions, also the single components of emittance will remain invariant. Without acceleration of the beam, the factor $\beta\gamma$ doesn't change, and also the direct emittances will be invariant. However, nonlinear optical elements will distort the phase-space area, thus the effective emittance, defined by the enclosing ellipse, will be increased. As a matter of fact, this distortion can be corrected by suitable optics, restoring the initial low emittance of the beam. Various different definitions of emittance are used in scientific literature, for example the area of ellipses containing all or 90% of the particles in the beam. The most common one is the root-mean-square (rms) emittance

(1) $$\varepsilon_x = \sqrt{\langle x^2\rangle\langle x'^2\rangle - \langle xx'\rangle^2} \text{ resp. } \varepsilon_{nx} = \frac{1}{mc}\sqrt{\langle x^2\rangle\langle p_x^2\rangle - \langle xp_x\rangle^2},$$

averaging over all particles in the beam.

While the beam passes through the accelerator, the normalized emittance is altered only by a few effects: The repulsing forces between the charged particles, initially leading to an increase of emittance, are suppressed by a factor $1/\gamma^2$ during acceleration. A reduction of emittance is possible only by interaction with other particles, for example by emission of synchrotron radiation or interaction with a cold beam of lower emittance. The emittance can also be reduced by means of emittance filters, capturing all particles outside a given phase-space area. But this device also reduces the beam current, thus it cannot increase the beam brightness.

The brightness of an electron beam is defined as beam current *I* divided by the product of the transversal emittances, in analogy to optics. Also here one must distinguish between direct and normalized brightness:

(2) $$B = \frac{2I}{\pi^2\varepsilon_x\varepsilon_y} \text{ resp. } B_n = \frac{B}{(\beta\gamma)^2} = \frac{2I}{\pi^2\varepsilon_{nx}\varepsilon_{ny}}$$

In the following text the notions brightness and emittance always mean the normalized quantities without explicitly denoting it. The brightness characterizes the achievable beam intensity at a given beam divergence and thus the achievable interaction rate or luminosity. This makes it a good measure of beam quality and performance. However, brightness is not an invariant quantity like emittance, because the beam current can be altered for example by bunch compression. But the increase of brightness is limited to factors typically between 5 and 20 by the longitudinal phase-space distribution of the beam. Thus the brightness is a quantity which as a rule decreases along the beam line (for example by beam current losses or emittance aggravation). An increase of brightness is limited and requires strong technical efforts. Consequently, if a high-brightness beam is required at the exit of the accelerator, the injected beam must already have a corresponding brightness. In today's accelerator physics especially two applications require electron beams of high brightness exceeding the performance of conventional techniques: Linear e^+e^- colliders and free-electron lasers.

1.1.3. High-Brightness Electron Beams for Linear ee Colliders

Actually the particle collisions with highest center-of-mass energy are produced in ring colliders. In these machines protons can be accelerated to about 10 TeV (LHC, SSC [188]) and electrons up to about 30 GeV (LEP [181], HERA [184]) with acceptable technical expenditure. At yet higher energies the energy loss of electrons by synchrotron radiation can no longer be compensated; protons require too high magnetic fields for bending. For further progress in high energy physics (to look for the top-quark and Higgs boson, to cross-check the supersymmetrical theory, and to search new physics phenomena) one would like to extend electron-positron collisions up to 1-2 TeV center-of-mass energy. In comparison with hadronic collisions at about 10-20 TeV center-of-mass energy producing about the same physics phenomena they are easier to be evaluated due to their defined initial state and higher yield. Actually, electron beams of this energy range can only be produced by linear accelerators without appreciable deflection [186]. Thus several proposals exist to build a linear collider composed of two opposite linear accelerators [148][178]. The luminosity of about $L \approx 10^{33}\text{cm}^{-2}\text{s}^{-1}$ common to all these proposals requires electron and positron beams of extreme brightness. Thus as a rule these projects contain damping rings to reduce beam emittance. Nevertheless, an electron source of high brightness is always required, too. Some of

these projects with less extreme requirements on beam quality could eventually be operated without damping ring if an electron source of corresponding brightness could be provided.

1.1.4. High-Brightness Electron Beams for Free-Electron Lasers

A second application requiring electron beams of extremely high brightness are free-electron lasers [163] in the ultraviolet range. In principle a free-electron laser [173][174] can be built tunable in any wavelength range with extremely high pulse and average output power. Thus one of the preferrably aimed applications is a tunable ultraviolet laser [172] which cannot be built in conventional laser technique [176]. To achieve a sufficient light amplification a maximum overlap of electron and photon beam must be realized. The necessary electron beam brightness rises quadratically with the photon energy [177]. Using electron beams from existing accelerators lasers with photon energies up to 2 eV could already be realized [161][166][179]. Specially designed accelerators must be employed to surpass this value. Actually several corresponding projects exist, which partially use linear accelerators (CEBAF [171], BNL [162], AFEL [165], JAERI [175] and others) and thus are dependent on electron sources of extreme brightness [47].

1.2. The Constructon of High-Brightness Electron Sources

Every electron source consists of a cathode emitting electrons into vacuum, and an acceleration gap, where the electrons are accelerated and confined to a beam by means of an electromagnetic field. To produce an electron beam of high brightness both components must fulfil special requirements: The cathode must be capable of emitting a beam of this brightness, and the acceleration gap must accelerate this beam up to the desired energy with a minimum of emittance growth. In addition both components must be harmonized (for example in their timing) to ensure optimized operation. The following sections describe the fundamental setup of both components and the development of high-brightness electron sources.

1.2.1. Principles of Electron Emission at the Cathode

The cathode must emit the electrons from the solid into the vacuum. The electrons must either gain enough energy to surmount the potential barrier, or the barrier must be made so thin that the electrons can pass it by tunneling. Several corresponding mechanisms are well known, like thermionic, secondary, photo-, and field emission. The initial beam brightness B_n^0 at the cathode can be described by the cathode current density j_C and the initial transversal energy $E_\perp$ of the emitted electrons:

$$B_n^0 = \pi \frac{m_e c^2}{E_\perp} j_C \tag{3}$$

Thus one will choose an emission process with high current density at low remaining energy.

The standard process to produce free electrons is thermionic emission. Electron sources for accelerators use this process nearly exclusively, too. The temperature of the cathode is increased, until enough electrons in the material have sufficient thermal energy to surmount the potential barrier towards the vacuum. The emitted current density is determined by the density of electrons with thermal energies above the barrier height (work function) Φ and their transmission probability; it is described by the Richardson-Dushman equation

$$j = AT^2 \exp\left(\frac{-\Phi}{k_B T}\right) \tag{4}$$

For ideal metals $A_{ideal} = 4\pi e m_e k_B^2/h^3 \approx 120$ A/(cm·K)^2; for real metals A ranges between about 40 and 60 A/(cm·K)^2. The average transversal energy of the emitted electrons is determined by the cathode temperature, thus $\langle E_\perp \rangle \approx k_B T$. Consequently, the initial beam brightness increases with increasing cathode temperature and is limited by the thermal destruction limit of the cathode.

Electron sources for accelerators normally use large-area high-performance thermionic cathodes indirectly heated by a tungsten wire [115]. Actually the best performance is given by dispenser cathodes. Their active W-O-Ba surface layer is based on a porous tungsten substrate. Barium diffuses through the pores during operation and continuously refreshes the surface layer. This principle allows a long lifetime even at fair vacuum conditions. Scandate cathodes of the most recent generation have a work function of 1.85 eV and can produce current densities up to 100 A/cm^2 at an operation temperature between 900°C and 1050°C during a lifetime of several thousand hours [118]. Their initial beam brightness of up to 10^{13} A/(m×rad)^2 is so high that the final brightness is completely limited by the emittance growth in the acceleration gap.

The relatively large thermal reaction time does not allow a quick modulation of the cathode by temperature variation. However, the emission can be modulated by a grid inserted in front of the cathode. The necessary grid capacity limits the minimum modulation time to about 1 ns, while an adaption to subsequent RF acceleration elements would require pulse widths of 10 to 50 ps. It also has been tried to heat metal surfaces by laser pulses to get short electron pulses of high current density [49]. If the laser pulses become too short, thermionic emission passes into multiphoton emission [107], because the electrons can no longer transfer their energy to the lattice of the solid [114][117][130].

In photoemission the electrons gain their energy directly from impinging photons [96]; every photon transfers its energy to a single electron. Thus the number of emitted electrons is proportional to the number of incident photons: $N_e = \eta_Q \cdot N_\gamma$, the resulting current density

$$j = \eta_Q \frac{e\lambda}{hc} S_\gamma \tag{5}$$

is proportional to the power density S_γ of the illumination. The dimensionless, wavelength- dependent quantum efficiency $\eta_Q(\lambda)$ describes the probability of excited electrons to reach the surface and to cross it. At photon energies below the work function ($hc/\lambda < \Phi$) the quantum efficiency is near zero, above the work function it acquires a material-dependent value between about 10^{-8} and 1 (see also section 2.1.1 at page 15). The transversal energy of the emitted electrons $E_\perp \approx hc/\lambda - \Phi$ is in the order of the difference between photon energy and work function. Therefore one will choose the photon energy just above the work function to get a considerable efficiency with low remaining energy. Also for photoemission the current density is limited only by the damage threshold of the cathode at extreme light intensities. Current densities far above 1000 A/cm^2 have already been achieved [8][92].

However, besides their wide-spread application for light detection photocathodes are actually used only in a few prototype electron sources. High-performance photocathodes are either made from semiconductor materials providing quantum efficiencies up to 30%, but being chemically very instable, or robust metals like copper with quantum efficiencies below 10^{-4}. The initial beam brightness can be as high as 10^{12} A/(m×rad)^2 [34][37]. The most important advantage of photoemission is the possibility of modulation by the incident light. The temporal broadening of the electron signal compared to the light signal is caused only by the drift of the excited electrons to the surface. For metals the typical time constants remain be-

low 1 ps [102][108]. Ultrashort electron pulses can thus be produced directly by corresponding light pulses.

Besides that, photoemission allows the generation of a polarized electron beam [50][54][81][61]. Experiments in nuclear and particle physics are often strongly interested in this possibility [52]. As a matter of fact, this is the reason why photoemission was first employed in an electron source [44], but in connection with a DC acceleration gap. The operation conditions which are necessary to produce a polarized beam differ considerably from the conditions for a bright beam. Thus a combination of both properties in a single source does not seem to make sense.

An electric field E_C is necessary to remove the electrons from the cathode. The required field strength increases with the current density to be removed. But a strong electric field at the cathode causes an increase of electron emission by two effects: Firstly, the work function will be lowered due to the Schottky effect by

$$\delta\Phi = -\sqrt{\frac{e^3 E_C}{4\pi\varepsilon}} \tag{6}$$

[127][131], leading to a higher current density in all emission processes. Secondly, the potential barrier becomes so thin that also non- or low-excited electrons can pass it by tunneling; this effect is called field emission. The current density of field emission is described by the Fowler-Nordheim equation

$$j(E,\Phi) = \frac{e^3}{16\pi^2\hbar}\frac{1}{t^2(y)}\frac{E^2}{\Phi}\exp\left(-\frac{4}{3}\frac{f(y)}{\hbar e}\frac{\sqrt{2m_e\Phi^3}}{E}\right) \tag{7}$$

there $f(y)$ and $t(y)$ with $y = \sqrt{e^3E/4\pi\varepsilon\Phi^2}$ are dimensionless correction functions with values close to unity [116]. At high gradients field emission superimposes and soon dominates all other emission processes. As a matter of fact, it occurs already at much lower gradients than expected by equation (7), confined to very tiny spots instead of originating from the whole area [126]. This effect is not yet fully understood, possibly it is caused by field enhancement at tiny tips or locally reduced work functions.

Stimulated by the extreme current densities at field emission tips, one tried to produce such tips in a controlled way and to use them as electron emitters. In fact, these efforts have been successful already at moderate current densities [25][132][133][208]. But at high current densities, these emitters are no longer stable, thus this technique is only of limited importance for high-brightness electron sources [46].

Between pure thermionic, photo-, and field emission also mixed and transition effects exist, like multiphoton photoemission [71][107], photoinduced field emission and photofield emission[112][113], and laser-induced thermionic emission [49]. Some of them could also be of interest for high-brightness electron sources. In addition, other processes can be used for electron emission, like secondary emission by bombardement of the cathode with electrons [123] or ions, plasma [128][129] and pseudospark electron sources [55][57], and ferroelectric emission [111][119][53][122]. Some of them are actually investigated as potential sources for bright electron beams, but yet no one of them is ready for application. Pseudospark and ferroelectric emission already demonstrated their ability to produce very high current densities. But the corresponding pulse widths are yet in the nanosecond regime and thus much too long for a subsequent RF accelerator.

1.2.2. Function and Meaning of the Acceleration Gap

From the point of view of an electrical circuit, cathode and acceleration gap form a diode. The dependence of the current density on the electric field resp. the anode-cathode voltage can be divided in two regions: At low voltage a space-charge cloud is formed in front of the cathode, which suppresses further emission due to its potential. The current density is exclusively determined by the anode-cathode voltage, described by the Langmuir-Child equation

(8) $$j = k \cdot \sqrt{U^3}$$

The perveance k is a factor describing the anode-cathode geometry. For parallel-plate geometry with acceleration distance d is $k = 2{,}334 \cdot 10^{-6}\ (\mathrm{A/V^{3/2}})/d^2$. The space charge strongly influences the potential distribution in comparison to the charge-free case: The gradient is zero at the cathode and continuously rises towards the anode. When the current density given by equation (8) with rising voltage approaches the current density j_{max} limited by the emission process, the influence of space charge decreases. The gradient at the cathode increases, and the potential distribution approaches the charge-free case. At very high voltages the current density increases again, because the gradient is no longer shielded from the cathode and augments the emission by Schottky effect and field emission. If short pulses are emitted instead of a continuous current or if the acceleration is performed in an alternating field, the situation becomes more complex, and dynamic effects must be taken into account [58]. In the limit of very short pulses the extractable current is given by the induced charge density at the surface

(9) $$\sigma = \varepsilon \cdot E_C$$

(Gauß law); the electric field is completely shielded behind this charge cloud.

The space charge effects lead to a reduction of beam brightness: They limit the current density of the beam, and the repulsing forces within the electron cloud lead to an increased transversal motion thus aggravating the beam emittance. Consequently, for a high-brightness electron source one will choose the gradient as high as possible to suppress the space-charge and in addition make the perveance large. The remaining increase of beam emittance by space- charge effects is suppressed by a factor $1/\gamma^2$ when the beam is accelerated to ultrarelativistic energy: In the center-of-mass system of the electron bunch the charge density is reduced by a factor $1/\gamma$ due to distance spread, and the repulsion of the electrons is slowed down by another factor $1/\gamma$ in the laboratory frame due to time dilatation.

The setup of a typical electron source for accelerators contains a high-performance thermionic cathode and a ring-shaped anode, where a DC voltage between 100 and 500 kV is applied [12]. This voltage range can easily be realized together with the required currents (up to 1 mA); yet higher voltages lead to considerable problems at the isolation. Thus ultrarelativistic velocities cannot be achieved in the first acceleration step. But further acceleration of the beam is possible only with RF fields and requires a bunched beam with a few picoseconds bunch size. Therefore the low-energy beam must first pass a modulation stage with appropriate drift spaces, where the space-charge forces which are not yet suppressed can act over a considerable time period. This type of acceleration is thus only desirable for moderate current densities.

To produce a beam with yet higher brightness the electrons must be accelerated to relativistic velocities immediately after emission. For this purpose one can place the cathode inside an RF acceleration cavity (RF-Gun) [39][48][62]. The emitted electrons are then directly accelerated by the high RF field of the cavity. The attainable gradients at the cathode are comparable with the DC gradients, but the final energy is no longer limited to several 100 kV. At a sufficiently low frequency or with a multicell cavity several MeV can easily be obtained;

there is no more principal limitation of the acceleration distance. However, with continuous emission at the cathode only the electrons emitted within about a quarter of the RF period (between 0° and a bit above 90°) will leave the cavity with a broad energy distribution between zero and the maximum energy (see also chapter 4.3.2 at page 55). A large fraction of the achieved brightness is lost again at the inavoidable subsequent energy selection [59]. As a matter of fact, the generated beam is already bunched and can be inserted directly into the RF accelerator. The electrons emitted between 90° and 180° will come back to the cathode, partially with a considerable energy [56][60]. To avoid a cathode destruction by electron bombardment at high current densities, this part of the beam must be deflected magnetically or dumped otherwise. But the method employed there will also have unwanted effects on the extracted beam.

In contrary, if the electrons are emitted in short pulses synchronized with the RF phase, all emitted electrons can also be extracted, and no cathode bombardment will occur. If the pulses are even short enough (typically a few degrees of RF phase), also the energy spread of the beam will be small, and energy selection is no longer necessary. Thus, photoemission with its excellent modulability seems to be predestined for utilization in a high-brightness RF gun.

1.2.3. History of High-Brightness Electron Gun Development

The development of high-brightness electron guns was initiated by the fast development of free-electron lasers in the beginning of the 1980's and the resulting demand of ultra-bright electron beams. In 1984, Madey and Westenskow built the first RF electron source at Stanford Linear Accelerator Center (SLAC) [62] using the microtron as model. This gun was equipped with a LaB_6 cathode [60] and delivered a beam brightness of 2×10^{11} A/(m×rad)^2, though with an energy spread of about 20%. Later, the same cathode was operated as photocathode with a Nd:YAG laser, enabling a beam brightness of 5×10^{11} A/(m×rad)^2, yet with the same energy spread. Both versions have been used to operate the Stanford FEL [13]. In the meantime other institutes have also built RF guns with thermionic cathode [51][63]. The first RF electron source with pure photoemission cathode was realized at Los Alamos National Laboratory (LANL) [68]. The photocathode material was initially Cs_3Sb, later replaced by K_2CsSb. Both materials have high quantum efficiency and low work function, they can be operated with a laser of relatively long wavelength (green spectral region) and moderate energy. But due to their chemical sensitivity they require extremely good vacuum conditions and still have an operational lifetime of only a few hours [167][92]. This type of photoelectron source has been further developed at LANL and used there at the FEL projects HIBAF [169] and AFEL [165]. In the meantime, it proved to deliver a beam brightness up to 3×10^{12} A/(m×rad)^2 [30]. A major problem of these photocathodes is their high dark current already at moderate gradients due to their low work function [31]. Polishing the cathode substrate suppressed this effect so far that operation without field emission was possible up to 30 MV/m gradient.

An alternative photocathode technique has been developed at Brookhaven National Laboratory (BNL) [9][28]. The copper photocathodes used there have a quasi unlimited lifetime also under bad vacuum conditions and can be operated up to 100 MV/m without field emission. But due to their low quantum efficiency and high work function they require a laser with extremely high power output in the ultraviolet range. This photoemission source produced a beam brightness of 1.2×10^{10} A/(m×rad)^2 [32][38]; it is used as injector for the BNL Accelerator Test Facility [182]. The photoemission RF guns developed at LANL and BNL define two opposite positions in photocathode philosophy. Both were prototypes and initiated a number of similar developments in other laboratories [160][167][168][45] (LANL type) [10][19][185][29] (BNL type).

The reported data show that the principle of photoemission RF gun is really capable of producing a high-brightness electron beam exceeding by far the values obtainable with conventional sources. However, all those sources operate a normalconducting RF cavity at very high gradients (up to 30 MV/m with alkali antimonide cathodes and up to 100 MV/m with rnetallic photocathodes) in order to suppress space-charge effects. Thus all these sources are pulsed with low duty cycles in order to enable an adequate cooling of the cavity and to provide the required RF power in the order of several Megawatts. Typical duty cycles lie between 10^{-4} and 10^{-5} for RF frequencies in L-band or S-band. Normally, the pulsed operation is not seen as a disadvantage of this source type, because the connected RF accelerator must also be pulsed for the same reasons.

However, there exist several projects using a superconducting linear accelerator and also demanding a high-brightness electron beam. The FEL projects at CEBAF [171][43], JAERI [175], INFN Frascati [164], and TH Darmstadt [159] belong to this group. They want to operate continuously their superconducting accelerators to achieve an extremely high average power of the free-electron laser as required for example by material sciences. There exists also the superconducting linear collider project TESLA [204]. It operates indeed with a moderate duty cycle of 0.8%, but uses very long macropulses of 800 μs duration. In this project a suitable high-brightness electron source could make the electron damping ring disposable, saving a lot of money. Thus all these projects demand a high-brightness electron source which can be operated continuously or with long macropulses.

1.3. The Concept of a Photoemission RF Gun with a Superconducting Cavity

Under these premises the concept of a superconducting photoemission RF gun seems to be obvious: the normalconducting cavity is replaced by a superconducting one. Theoretically, superconducting cavities can produce gradients up to 100 MV/m at the cathode in continuous operation. The limitation is not given by the gradient itself, but by the corresponding magnetic field at the superconducting surface: Superconductivity disappears, if the critical superheated magnetic field H is exceeded [146]. For niobium, the standard material, this is about 240 mT, corresponding to about 100 MV/m electric field at the cathode in a typical geometry. However, this thermodynamically limited value has never been achieved in continuous operation, but the gradient was always limited to lower values by defects (normalconducting spots or field emission tips). Thus the obtainable gradient depends on the preparation of the cavity surface [152]. With state-of-the-art preparation technique, about 30 MV/m at the cathode should be obtained reproducibly, and even 50 MV/m should be obtainable after a guided removal of defects [147]. These gradients are quite sufficient for the operation of alkali antimonide photocathodes. For metallic photocathodes they are lower than usual, but yet quite acceptable.

But superconducting accelerator cavities make completely other demands on their environment than normalconducting ones and also produce completely other effects on it. The photocathode inside the superconducting cavity is an important part of this environment, which effect is yet completely unknown. Thus the technical concepts of normalconducting photoemission guns cannot simply be copied, but have to be completely revised. It becomes apparent that the employment of a superconducting cavity produces additional advantages, but also bears novel physical and technical problems. Both shall be shortly presented here.

Because the cavity is operated at cryogenic temperatures ($T < 4.2$ K), only a very little heat load can be accepted at its surface. The additional heat load at the cathode depends on the cathode type: At metallic cathodes with low quantum efficiency it is mainly due to the absorbed light power, while at semiconductor photocathodes it is dominated by the RF losses

due to the low conductivity. Considering a superconducting cavity, metallic cathodes thus seem to be advantageous for low average current applications. High quantum efficiency semiconductor photocathodes however have advantages in high average power applications, especially with pulsed operation.

The cryogenic surface of the cavity and its adjacent components act as a cryopump for the beamline vacuum. All gas components except helium and low amounts of hydrogen are frozen at the cold surfaces. Consequently, neither active gases nor backaccelerated ions can occur and attack the cathode layer. The cathode itself is cooled to liquid helium temperature (≤ 4.2 K) as well, therefore thermal desorption of cathode material or components [70][85] should also be negligible. The quantum efficiency of the photocathodes however should not be altered by the cryogenic temperature [67][86]. Thus the three processes known to degrade semiconductor cathodes and to reduce their lifetime [27][33] – reaction with residual gases, ion bombardement, and cathode material desorption – should be strongly suppressed due to the cryogenic environment. For this reason the cathode lifetime is expected to be much higher than in normalconducting systems.

Nevertheless one should assume that semiconductor cathodes regularly need refreshment or new preparation, although probably with a much longer period. This cannot be done inside the superconducting cavity, because its performance is already affected by very little contamination. On the other hand, the cavity shall not be warmed up for every refreshment. Thus the cathode must be evaporated onto a stem transferrable to and from the cavity under high vacuum and in cryogenic environment. The RF losses caused by this stem must be kept so low that they don't affect the cavity performance. In particular, the (necessary) electrical contact of this stem must be shielded against the high RF field inside the cavity.

Another advantage of the superconducting cavity is that its geometrical shape can be chosen without being completely dominated by minimizing the shunt impedance. An appropriate shape of the iris area enables the focusing of the beam already by the RF field, resp. emittance aggravating effects of the RF field can be suppressed. However, the geometrical shape of the cavity will also be influenced by the suppression of effects limiting the RF field. The advantageous operation of superconducting cavities at low frequencies will also help to reduce the emittance. It will at the same time reduce the requirements on the laser performance concerning pulse width and jitter.

The insertion of a robust metallic cathode (made of copper or even niobium) should not lead to technical problems concerning the operation the cavity. The mutual interferences of a superconducting cavity and a semiconductor photocathode (of Cs_3Sb type), however, were yet completely unknown. The mutual physico-chemical interactions of these two extremely surface-sensitive systems have never been investigated before. Theoretically, a number of effects affecting the performance of one or both components could be imagined: Material desorption from the photocathode to the cavity surface could reduce maximum gradient or quality factor of the cavity. Electrons hitting the surface could activate frozen gas and thus initiate a degradation of the photocathode. In addition, the photocathode itself could cause unbearable RF losses due to its low conductivity or unbearable field emission due to its low work function. The real size of all these effects, however, is accessible by experiment only. As a first step to realize a superconducting photoemission source, such an experiment must be built up, the effects must be investigated, and suitable measures to suppress them must be developed and tested.

The concept of such a superconducting photoemission source of high brightness has been firstly proposed by us in 1988 [2][3]. Besides our own activities and those of our collaboration partners at CEBAF and at INFN Milano [183] another group at the Japan Atomic Energy

Research Institute (JAERI) has been active on this area [157], but has ceased its activities for the time being. Recently, a collaboration between University of Rochester and Cornell University in New York has started the development of a superconducting photoemission source. It shall deliver only a low average current and thus shall be equipped with a metallic cathode [15][21]. However, this collaboration also thinks about alternative cathode materials. Finally, a group at IHEP Beijing in China has expressed its intentions to become active on this research area [137].

2. Components for a Superconducting Photoemission Source

As first part of our project we have estimated the requirements to be fulfilled by components for a superconducting photoemission source and the possible technical solutions. Assuming a high average current application, we have developed a complete design based on these components and calculated its beam dynamics performance.

2.1. The High-Performance Photocathode

2.1.1. Characteristics of the Photoemission Process

In principle photoemission (external photoeffect) can occur at every surface of a solid or liquid. Incident light activates electrons and enables them to penetrate through the surface into the vacuum [97]. This process can be divided into three steps (Figure 1): As first step the photons penetrate into the material and are absorbed there. The whole energy hc/λ of a photon is as a rule transferred to a single electron. As second step the excited (and thus movable) electron drifts to the surface. Its drift velocity is roughly equal to the Fermi velocity v_F of the material. On its way to the surface the electron can loose a part of its activation energy by collisions with phonons or with other electrons. Collisions with another electron lead in average to an equal distribution of energy between both electrons, while the electron looses only a small part of its energy in a collision with a phonon. As third step the electron may penetrate the material surface, if its remaining energy yet exceeds the work function. The difference between electron energy and work function remains with the emitted electron as kinetic energy E_{kin} [79][89].

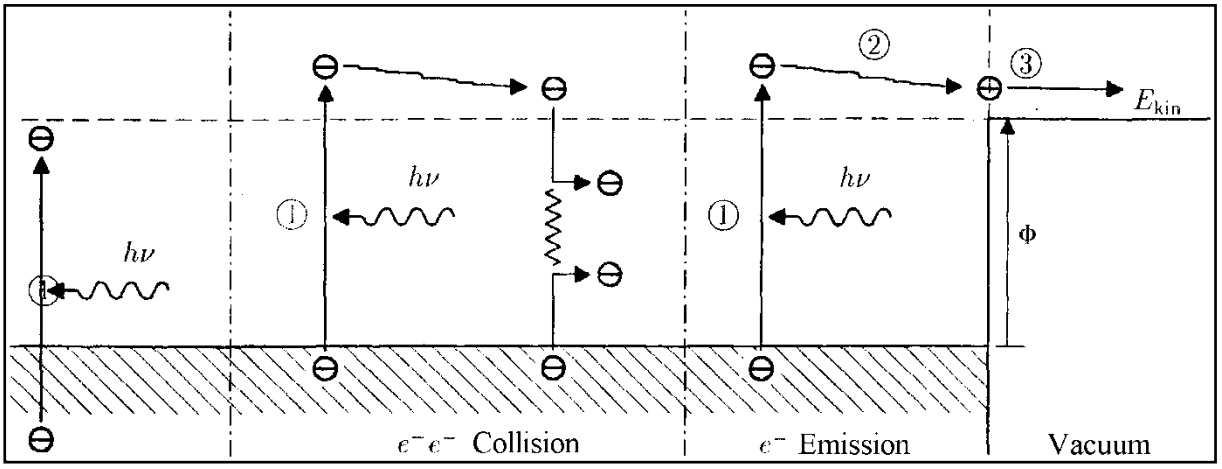

Figure 1 Three-step model for the photoemission process: Absorption of the photon and electron excitation (1), electron drift to the surface (2) with energy loss by collisions with phonons, and penetration through the surface (3)

The most important characteristic quantity of photoemission is the quantum efficiency $\eta_Q = n_e/n_\gamma$ as quotient between the number of emitted electrons and the number of incident

photons. The quantum efficiency depends on the material and on the wavelength of the light, but is independent from the light intensity within the validity range of the model presented above. All three steps of the emission process have influence on the quantum efficiency. Discussing their effects in detail one should distinguish between two types of material: Metals on one side and semiconductors or isolators with a certain energy gap E_G on the other side. In this context, the following considerations are mainly based on photon energies slightly above the threshold for photoemission.

As a rule, metals have a high optical reflectivity. A large fraction of the incident light thus cannot even excite electrons, but is reflected. Semiconductors, in contrary, normally have a much lower reflectivity. Besides that, they also have a much higher absorption coefficient for photons with $E_\gamma > E_G$, so that the electrons are excited quite near the surface. In metals there are a lot of electrons as potential collision partners for the excited electrons, and due to the efficient energy transfer already one or two collisions are sufficient to prevent all participating electrons from crossing the potential barrier. In semiconductors, however, the number of possible collisions is strongly reduced thanks to the forbidden energy gap, which both colliding electrons may not enter. Specially advantageous are low-electron-affinity (LEA) semiconductors, where the energy gap E_G is larger than the electron affinity E_A (Figure 2): Electrons excited to an energy between E_G+E_A and $2E_G$ cannot collide with other electrons at all, but have sufficient energy to leave the material. Consequently, these semiconductors normally have a high quantum yield.

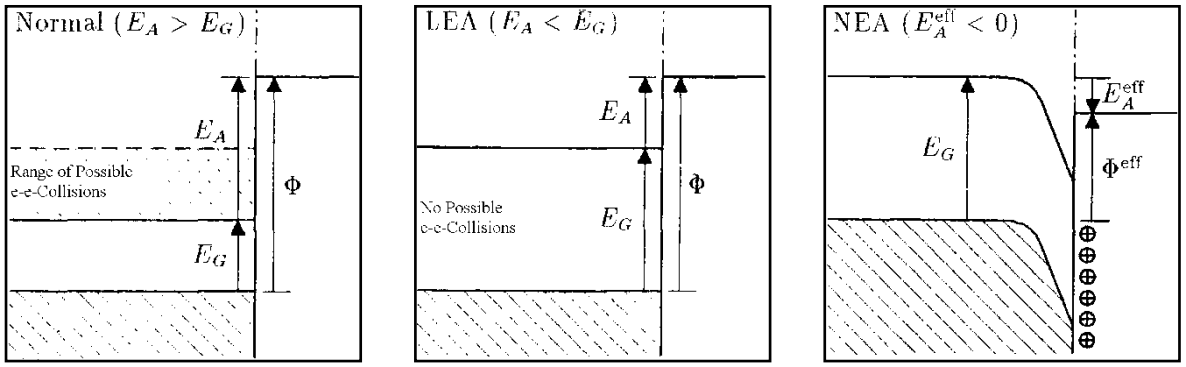

Figure 2 Band structure and emission process of semiconductors with normal (left), low (center), and effectively negative electron affinity (right)

Naturally, the quantum efficiency is strongly dependent on the wavelength λ resp. the photon energy $E_\gamma = hc/\lambda$ of the light. At photon energies below the work function Φ the yield is extremely small. Very few electrons can escape due to their additional thermal energy or due to multiphoton excitation. At the energy threshold the quantum efficiency rises sharply and approaches a constant value for higher photon energies. In the environment of the threshold energy $E_\gamma \approx \Phi$ the quantum efficiency approximately follows the function

$$\eta_Q = \frac{A\left(E_\gamma - \Phi\right)^{3/2}}{\left(E_\gamma - \Phi\right)^{3/2} + B} \tag{10}$$

where A characterizes the escape probability of the electrons and B the optical absorption (see Figure 3) [67][98][99]. The quantum efficiency below the threshold deviating from theory originates from donor levels. Metals show a typical quantum efficiency (above the threshold energy) between 10^{-6} and 10^{-4}, in exceptions up to 10^{-3}. Semiconductors of LEA type, however, can provide quantum efficiencies exceeding 0.1 just above the threshold (see Figure 4). At photon energies much bigger than the threshold energy $E_\gamma \gg \Phi$ the quantum

efficiency rises again, because a single photon can activate more than one electron above the work function.

The mechanism of photoemission implies that impurities in the material and especially on its surface strongly influence the quantum yield. Impurities in semiconductors can significantly alter the band structure and for example create states inside the band gap, enabling additional electron-electron collisions. Impurities at the surface can alter the work function already at very low concentrations (sub-monoatomic layer): A dipole field at the surface leads to band bending causing a different effective work function. With correct direction of the dipole (surface contamination with electron acceptors like O, OH, and F) even semiconductors with negative effective electron affinity can be created. Such NEA semiconductors have a very steep rise in quantum efficiency and achieve maximum efficiencies up to 0.3 [65][75].

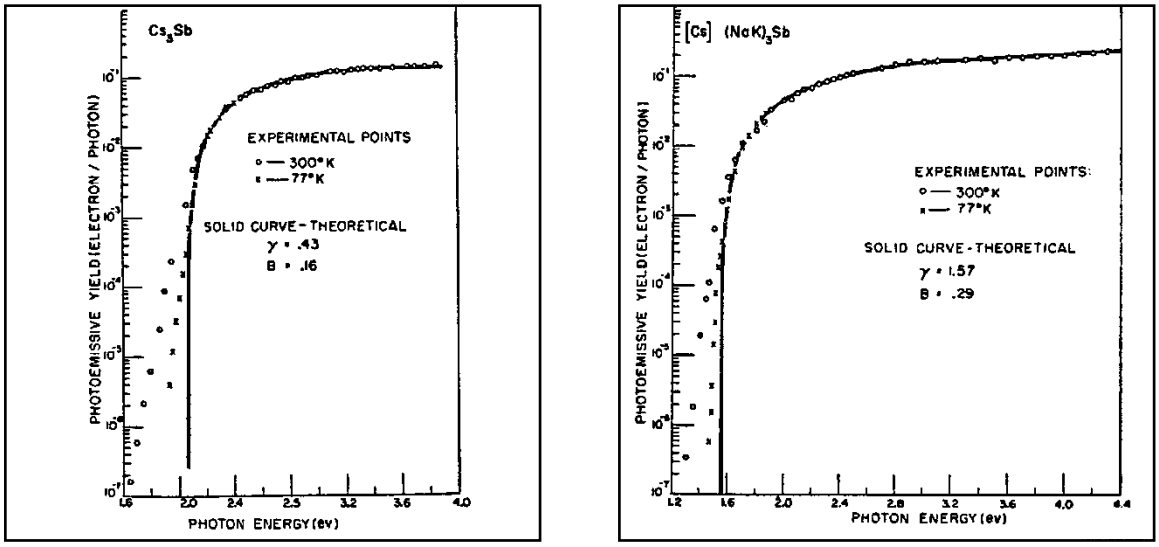

Figure 3 Quantum efficiency of Cs_3Sb (left) and [Cs](Na, $K)_3Sb$ (right) near the threshold photon energy, according to [98]

Further important characteristics besides the quantum yield are the energy distribution of the emitted electrons and the retardation between light incidence and electron emission. The average kinetic energy of the emitted electrons is approximately $E_{kin} \approx (E_\gamma - \Phi)/4$ above the emission threshold [79], but very near to the threshold and below it E_{kin} is dominated by the thermal energy. The mean retardation τ between light incidence and electron emission is approximately equal to the quotient of optical absorption depth and Fermi velocity. It shows a strong wavelength dependence via the absorption coefficient. The mean retardation determines also the spread of the electron signal relative to the photon signal, because the emission practically starts with the photon incidence. In metals the retardation is negligible ($\tau < 1$ ps), but in semiconductors, especially in NEA semiconductors near the emission threshold, it can be as large as 1 ns.

2.1.2. Comparison of Various Photoemissive Materials

The important parameters of several interesting photoemitter materials are listed in Table 1 and Table 2. It is clearly evident, that (until now) no material exists which can provide all desired properties [35]. These properties are low work function, high quantum efficiency, robustness against residual gases, and small retardation time. There exist groups of materials which are excellent in one or two of the desired properties, but are inevitably weak in other ones: Transition metals like copper or niobium are completely robust against atmospheric influences, but have weak photoelectric properties. Metals with stronger electronegativity,

like yttrium, barium, or cesium, provide better photoelectric properties and at the same time are more sensitive against active gases, too [91][109]. This is also valid for lanthanum boride and for the dispenser cathodes [64][90], which have initially been developed as thermionic cathodes. The listed LEA and NEA semiconductors have in common a very high quantum efficiency, but are chemically extremely sensitive, especially if they also have a low work function [82]. Isolators like cesium iodide are chemically less reactive, but have a very high work function and in addition a very low electrical conductivity, which is a problem at high average current levels. NEA semiconductors of the gallium arsenide type [87][88] are in addition distinguished by their capability of emitting polarized electrons [80]. However, the operation conditions required for the generation of a polarized beam inevitably lead to a very long retardation time and a low quantum efficiency.

Material		Cu	Nb	Y	Cs	LaB6	Ba-O-W*
Work Function Φ	[eV]	4,5	4,6	3,1	2,0	3,1	1,8
Quantum Efficiency ηQ		5×10-5	5×10-6	5×10-4	1×10-3	1×10-3	1×10-3
at Eγ	[eV]	4,7	4,7	4,7	2,3	3,5	2,3
Retardation Time τ	[fs]	<100					
Reaction with Active Gases		none	none	low	high	low	fair

* Dispenser cathode: porous tungsten surface covered with a monoatomic barium oxide layer

Table 1 Properties of metallic photoemitters

Material		GaAs:Cs,O*	Cs_3Sb	K_2CsSb	Cs_2Te	CsAu	CsI
Band Gap E_G	[eV]	1,4	1,6	1,0	3,3	2,6	>6,0
Electron Affinity E_A	[eV]	0,0 eff.	0,45	1,1	<0,5	1,4	<0,5
Work Function Φ	[eV]	1,4	2,05	2,1	3,5	4,0	6,4
Quantum Efficiency η_Q		0,3	0,1	0,15	0,1	0,1	0,05
at E_γ	[eV]	2,3	2,3	2,3	4,7	4,7	5,8
Retardation Time τ	[ps]	50-400	<2				
Reaction with Active Gases		very high	high	high	high	high	low

* Gallium Arsenide, surface-activated with cesium and oxygen

Table 2 Properties of semiconductor photoemitters

2.1.3. Selection Criteria for Cathodes in a Photoemission Source

The application in a superconducting photoemission source of high brightness imposes several competing requirements to the photocathode: The emitted current shall be as big as possible for a given laser power, thus the quantum efficiency at the laser wavelength must be as high as possible. However, the photon energy shall be located only slightly above the threshold energy in order to generate electrons with a low transversal energy. The photocathode should consequently provide a steep rise of quantum efficiency at the emission threshold. In addition, a powerful pulse-laser system should be availabe for the corresponding wavelength range (see section 2.3.2 at page 26). The requirements on the laser system are easier to fulfil, if the chosen photon energy is relatively low. A photon energy below the work function of the cavity material will in addition prohibit parasitic photoemission by scattered light. The length of the generated electron bunches should be only a few degrees of RF phase (e.g. a few pico-

seconds) in order to keep the resulting energy spread negligible. The retardation time of the photocathode therefore must be small enough, besides a correspondingly short laser pulse length.

Also the mechanical and chemical properties of a photocathode have to be considered for an application in a RF gun. It appears that all materials with a high quantum efficiency contain alkali metals, preferrably cesium. This is intelligible due to its high electronegativity (0.7 according to Pauling). Most of these materials – especially those with a low work function Φ – can be oxidized easily and instantaneously react with all oxidizing gases. Naturally, they loose their high photoelectric performance by oxidation. Therefore they have to be operated under ultrahigh vacuum conditions, but even then their lifetime is limited by reaction with residual gases. Other materials with lower photoelectric performance like yttrium or LaB_6 however can also be operated in fair vacua without affection of their photoelectric properties. Metals like copper or stainless steel are even robust against atmospheric conditions, but have poor photoemission properties.

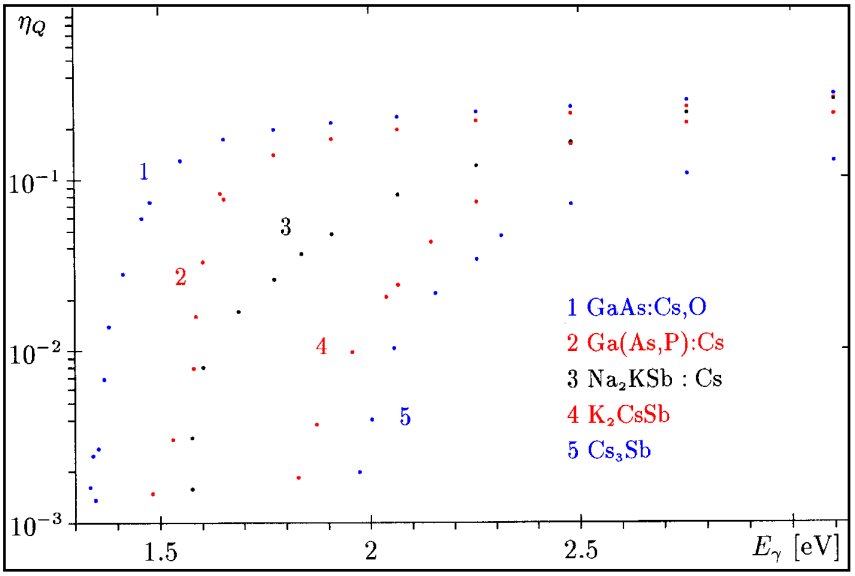

Figure 4 Spectral distribution of the quantum efficiency for the most important LEA semiconductors, according to [33]

Selecting a photocathode for a photoemission source therefore includes a tradeoff: On one side there is the high-performance semiconductor photocathode requiring high vacuum conditions and nevertheless needing periodical refreshment due to its limited lifetime. On the other side there are robust metal photocathodes, which require however a high-power ultraviolet laser system. In the development of normalconducting photoemission sources both choices have been realized, with photocathodes made from Cs_3Sb [26] resp. K_2CsSb [36] and from copper [9][22]. Also intermediate solutions using for example LaB_6 [13] or CsI [10] cathodes have been tried. The highest beam brightness until now has been achieved with K_2CsSb cathodes [37]. However, they must be refreshed already after a few hours of operation.

2.1.4. Selection Criteria for a Superconducting Photoemission Source

The application in a superconducting cavity puts other valences on the various properties of photocathodes. The evaluation done for a normalconducting photoemission source therefore cannot simply be adopted. All properties have to be reconsidered, taking into account the unique environment conditions which superconducting cavities demand and also provide.

The chemical robustness has less meaning than in a normalconducting system, because the superconducting system provides excelleiit vacuum conditions. The cold walls work as cryo-pump and freeze all gases. The residual atmosphere is extremely thin containing only helium and a few hydrogen (hydrogen pressure 2×10^{-6} mbar at 4.2 K) and does not react with the photocathodes. In addition, less gases are desorbed from the surfaces by impinging electrons, because superconducting cavities allow much wider apertures and can only be operated with negligible dark currents. A destruction of sensitive photocathodes by residual gases is therefore practically excluded. Desorption of cathode material or components (e.g. cesium) as another destruction mechanism should also be prevented due to the low temperature of the cathode. Consequently, the cathode lifetime should be much longer in a superconducting system, even for sensitive cathodes like Cs_3Sb. Experimental data on the actually achievable lifetime, however, are not yet available. Our own measurements (see section 4.5.1 on page 67) are not yet evident in this aspect due to the simultaneous electron bombardment in our experiment.

Most probably an indefinite lifetime of sensitive photocathodes must not be assumed even in a superconducting cavity, because electron or helium ion bombardment can never be prevented completely. Thus a system for periodical refreshment must be planned, if a sensitive photocathode shall be used. The relative expenditure on operation is reduced by the longer periods, but the expenditure on construction remains. It is even increased, because the superconducting system makes higher demands on the transfer system: It must work also in a cryogenic environment, and the additional RF losses must not load the cavity significantly.

Except for a metallic cathode like copper or niobium, it must be examined whether the cathode can contaminate the superconducting cavity by desorption. A purely thermal desorption can be excluded due to the low temperature, however, a desorption by electron or ion bombardment or by laser activation is yet possible. Normalconducting cavities don't care about these effects, but superconducting cavities are much more sensitive: Tiny normalconducting spots in a high magnetic field region can cause a thermal quench of the whole cavity [143][146]. Surface contaminations with low work function can cause parasitic dark currents at locations with high electric field. Such contaminations must be excluded in any case, because a periodic preparation of the cavity surface is surely not acceptable. Data about contamination by typical photocathodes were not yet available. Our own measurements are reported in section 4.5.3 on page 74. Within their accuracy, they don't show a contamination effect by Cs_3Sb cathodes, but their operation conditions are yet far from those of a prototype source.

The power dissipation at the photocathode is another important aspect in a superconducting system. While a normalconducting cavity can tolerate a power dissipation in the kilowatt range, it should be preferrably below about 1 W inside the superconducting system, because the power must be carried off at cryogenic temperatures. The first effect contributing to the power dissipation are dielectric and resistive losses of the RF field at the cathode:

$$P_C^{(H)} = \frac{1}{2} R_S \cdot \iint_C H^2 dF \quad \text{and} \quad P_C^{(E)} = \frac{1}{2} \varepsilon\omega \tan(\delta) \cdot \iiint_C E^2 dV \tag{11}$$

Both effects are quadratic in the field strength and cause a corresponding reduction of the quality factor. However, the cathode has a small area relative to the whole cavity and is located in a low magnetic field area, and metallic photocathodes shouldn't cause serious problems if properly cooled. Semiconductor photocathodes in contrary cause dielectric losses, which are high in the high electric field area, due to their low conductivity. Data on the conductivity of these materials were also unknown, especially at low temperatures. Our own measurements (see section 4.5.2 on page 71) showed unacceptably high RF losses at Cs_3Sb

layers, which were however rather thick (about 500 nm). Thus one will be forced to apply semiconductor photocathodes as thin as possible with yet acceptable yield. However, our data are not yet sufficient for reliable quantitative statements.

Another contribution to the power dissipation in the cathode comes from the incident light:

(12) $$P_C^{(L)} = P_{Laser}\left(1-R-\eta_Q\right) = \frac{h\nu}{e} I_e \frac{1-R-\eta_Q}{\eta_Q} = \frac{h\nu}{e}\frac{I_e}{\eta_Q'}$$

The dissipated power is proportional to the emission current *I* and inversely proportional to the internal quantum efficiency $\eta_Q{}^0$. The internal quantum efficiency, defined as number of emitted electrons per absorbed photon, is no longer dependent on the optical reflectivity *R* of the cathode. In semiconductor photocathodes with high quantum efficiencies this effect is negligible up to very high current densities. For metallic photocathodes, however, it becomes dominant at high current densities. Assuming an average current of 10 mA, a Cs_3Sb photocathode with 10% internal quantum efficiency dissipates 0.25 W laser power, while a copper photocathode with 10^{-3} internal quantum efficiency dissipates 50 W.

The energy dissipation caused by resistive losses of the emission current crossing the cathode

(13) $$P_C^{(I)} = d_C \iint_C \rho \cdot j^2 \, df$$

will probably cause no problems even at semicondnctor cathodes, if they are prepared thin enongh. Layers being as thin as the absorption depth of the light should even show photoconductivity: the electron holes generated by the excitation can be directly refilled with electrons from the substrate.

Another effect being relevant only in a superconducting cavity is parasitic photoemission at the cavity walls, generated by scattered light. The electrons thereby emitted are accelerated in the cavity field and normally hit the cavity wall again at a different location, dissipating their energy there. This effect increases the total power dissipation; in worst case a (electron-induced) quench can occnr at the cavity wall. Photocathodes with low work function prevent this effect, because the photon energy used is considerably below the work fnnction of niobium (4.5 eV). The effect is principally unavoidable if photocathodes of high work function are used. However, for metallic cathodes the diffuse reflection can be strongly reduced by polishing the cathode surface; at semiconductor photocathodes the light intensity is anyway much lower. Thus the total parasitic current is in any case lower than the direct emission current by several orders of magnitude. Nevertheless, caution is necessary, because especially in cavities of low frequency the parasitic electrons can gain a lot of energy until they hit the wall again: Scattered light from the cathode strikes the environment of the iris at the right phase, and the emitted electrons are maximally accelerated. In a 500 MHz cavity energies up to 3 MeV are possible; an average current of 10 mA with 10^{-4} portion of parasitic electrons leads to an additional power dissipation of 3 W.

Other aspects, like field emission occuring at cathodes with low work function, the maximum current density achievable with the specific cathode type, and the complexity of the required laser system, have the same value as in normalconducting RF guns. However, because superconducting cavities are preferrably operated at low frequencies (typicaliy 500 MHz vs. 3 GHz for normalconducting cavities), the requirements on the laser pulse structure (length and jitter) are significantly reduced.

A final assessment of the different cathode types with respect to a superconducting RF gun is obviously not yet available, because the data base is yet too small. Until now, no indications exist that certain photocathodes cannot be used in a superconducting RF gun. However, it seems reasonable that metallic photocathodes are the simpler and more reliable solution for applications with moderate average current (below about 100 µA). As simplest case, even the niobium wall of the cavity can be used as photocathode [15]. At high average currents (above about 1 mA), in contrary, and special demands on the beam brightness, the additional effort using semiconductor photocathodes like Cs_3Sb or K_2CsSb seems to be worth while. For pulsed sytems this evaluation must consider the average current within a single macropulse, because thermal equilibrium is quickly achieved, the current averaged over a lot of macropulses may be taken only for the load on the refrigerator.

The following design of a prototype source (section 2.4) is mainly oriented at FEL projects and TESLA. It is therefore designed for high average current and high brightness; it is consequently equipped with an alkali antimonide photocathode.

2.2. The superconducting cavity

The photocathode shall be operated inside a superconducting RF cavity, because there the necessary high electric field can be applied continuously. The design criteria for this cavity differ in several important aspects from the design criteria for a superconducting cavity in a pure accelerator segment. These differences shall be discussed in detail now.

2.2.1. Material and Production of the Cavity

According to the state of the art, elementary niobium of high purity is the best material to build high-performance superconducting cavities. Besides its excellent superconductivity properties (critical temperature T_C = 9.2 K, critical magnetic field H_C = 150 kA/m) it also provides (at corresponding purity) a high thermal conductivity at low temperatures [155]. Small defects can be cooled sufficiently in order not to produce a quench. Niobium can be machined and welded rather easily to cavities of any desired shape. Its surface can be prepared more or less defect-free by mechanical, chemical, and thermal processes [135]. The high-performance cavities actually used are nearly exclusively made from niobium. The experience gained at these systems should be utilized for a superconducting RF gun.

An alternative for using bulk niobium is sputtering a thin niobium layer on copper cavities. This procedure is cheaper for big cavities and also provides high thermal conductivity of the cavity wall; even tube cooling instead of bath cooling is sometimes possible [136]. However, the cavities produced (until now) have the disadvantage that their quality factor decreases at high field levels [134]. For a superconducting RF gun, which must be operated at high field levels, they seem to be less qualified. Other materials with theoretically better superconductivity properties like niobium nitride or Nb_3Sn were until now not able to achieve the same performance in cavities as niobium [150][151], mostly because their preparation is more complicated. For the time being, they are of no interest regarding a photoemission RF gun. In addition, it seems reasonable to use well-known and reliable technique for the cavity, because its combination with the photocathode will already produce enough technical problems.

The production of the cavity will be done as usual by shaping sheet or bulk material and electron beam welding. Its first surface preparation will be done by etching in an acid mixture and optional ultra-high vacuum annealing [145]. Annealing with an outside titanium evaporation in order to reduce interstitial impurities and increase thermal conductivity [154] as well as high-peak-power RF processing as in-situ technique [140] seem to be reasonable as further preparation processes. In contrary to standard accelerator cavities, the necessity of occasional

new preparations during operation cannot be excluded, if the cathode really contaminates the cavity. These preparations must have a negligible material removal in order not to generate a considerable successive frequency shift. They could consist of an etching, which does not attack the niobium itself, combined with an electro- or oxipolishing resp. an UHV annealing procedure. If experiments prove a cavity contamination by the cathode, this preparation will also have to be developed experimentally. The possible necessity of such a step, however, should already be considered in a prototype design.

2.2.2. Choice of the Cavity Geometry

The geometrical shape of normal- as well as superconducting accelerator cavities are optimized in order to achieve maximum acceleration gradient. However, the different mechanisms limiting the gradient require different actions. In normalconducting cavities the shunt impedance (the ratio between the square of the acceleration gradient and the power dissipation) must be optimized with highest priority. In superconducting cavities however the influence of defects must be suppressed primarily, by minimizing the peak surface fields as well as preventing the possibility of resonant secondary emission. As a rule, this procedure leaves more freedom to consider also the beam emittance when choosing the geometry (especially the environment of the iris). Based on the corresponding theoretical considerations [23] this optimization should be done with a suitable simulation program. In addition, the choice of geometry should also ensure that all parts of the surface can easily be accessed, liquids can run off without residues, and the surface can easily be dried.

Except for the shape of the iris environment, the typical shape of superconducting accelerator cavities [144] can be adapted. The beam tube and the RF coupler can be copied as well. A higher-order-mode coupler will probably not be necessary, if the cavity consists of only a few cells (see below) and the aperture of the beam line is big. The rear end of the structure is closed with a wall, the photocathode is located in the center of this wall. Its diameter results from the initial diameter of the electron beam required by beam dynamics. In order to reduce the RF losses at the cathode – especially with semiconductor cathodes – the cathode area should be chosen as small as possible, The cathode should neither project from nor stand back behind the wall, because the first situation would produce defocussing of the beam, and the second one would reduce the gradient at the cathode surface.

A robust metallic photocathode can be integrated into the rear wall by welding, brazing, or evaporation. As simplest case the niobium wall itself can be used as photocathode. A semiconductor photocathode with limited lifetime, however, must be removable in order to be refreshed without warming up the cavity or even dismounting it. A warmup of the cavity would also release a lot of gas from the cavity wall and thus degenerate the cathode quickly. Due to their low conductivity the semiconductor photocathodes must be evaporated as a thin layer on a well-conducting substrate. Typically, the substrate is a stem carrying the cathode on its top. This stem can be removed to the rear side from the cavity wall. It must be guided in a vacuum tube there to prevent cathode and cavity from atmospheric influences.

The cathode stern must have an electrical contact to the cavity carrying the emission current. This contact however must be shielded against the cavity RF field, otherwise high RF losses could occur at the contact zone. Thus the stem must not touch the cavity wall directly, but must be isolated from it by a gap. The contact is located behind that gap; a choke shifts a knot of the RF magnetic field to this location. The illumination of the cathode will probably come through the beam tube, leading to a perpendicular light incidence. A grazing incidence, as proposed to increase the quantum efficiency by the photofield effect [73][107], would require two openings in the cavity near the equator, but additional openings are not desirable with respect to cavity surface preparation.

2.2.3. Resonance Frequency and Number of Cells

Considering the beam quality, one would like to have – besides a high gradient at the cathode – a low frequency of the cavity. The acceleration of the electrons until the first zero crossing of the RF field is enlarged, and the electrons achieve relativistic energies already in the first cavity cell resp. first RF period. The consequent large aperture reduces the non-linearity of the RF field induced by the iris. At a given bunch length the energy spread of the bunch is reduced at low frequencies. Also the cavity performance profits from a low frequency: The BCS surface resistance increases quadratically with the RF frequency, thus a lower frequency leads (at a fixed acceleration gradient) to less power dissipation resp. to a higher operation temperature with the same power dissipation [141]. However, this advantage disappears when already at 4.2 K the defect-induced residual resistance dominates [142][156]; this becomes valid at about 300 MHz. On the other hand experience shows that it is more difficult to achieve high gradients in low-frequency cavities, probably because the larger surface is more difficult to prepare defect free. In addition, the large dimensions of low-frequency cavities make the system expensive and clumsy. Considering all these arguments, the optimum frequency for the superconducting RF gun seems to be about 500 MHz, enabling an operation at 4.2 K. The exact frequency must be a harmonic frequency of the microbunch repetition rate, thus being commensurable with the frequency of the subsequent accelerator. The proposed TESLA linear collider would favour an operation frequency of 650 MHz, while the proposed free electron lasers at CEBAF (operation frequency 1.5 GHz) and JAERI (500 MHz) could utilize a RF gun at 500 MHz.

The number of cells of the cavity depends on the desired electron energy at the gun exit. Again the low operation frequency has a positive effect reducing the number of cells. At an operation frequency of 500 MHz and a final energy of about 10 MeV only three or four cells are necessary. Together with the large aperture of the iris the low nomber of cells prevents the necessity of higher-order-mode couplers. In contrary to standard electron-accelerator structures the cells will not be identical: Due to the positive emission phase and due to the yet low electron velocity $\beta < 1$ at least the first cell will be considerably shorter than half a wavelength, probably about a quarter wavelength. At a fixed acceleration gradient all cells can be exactly adapted to the respective time of flight; the additional effort producing these cells is rather small.

2.2.4. Measures to Limit the Emittance Aggravation in the Source

The emittance at the exit of the RF gun can be distributed into five contributions: Besides the initial emittance at the cathode $\varepsilon_n = r\sqrt{2E/mc^2}$ (due to the transversal energy) linear and non-linear space-charge effects as well as linear and non-linear time-dependent transversal RF components contribute to the final emittance [11][14][24][189]. Non-linearity here refers to the radial dependence of the quantities. The initial emittance at the cathode has already been discussed with the emission mechanisms, normally it is small (about 1 mm×mrad) and completely dominated by the other effects. The linear space-charge forces can be compensated completely by proper focusing of the beam [11]. The emittance induced by non-linear transversal RF components is also small as a rule, especially in superconducting cavities due to their large aperture. Free shaping of the iris environment enables further linearization of the transversal components. Normally, the other two effects dominate the final emittance of the source. By proper choice of the emission phase their joint contribution can be minimized, but not completely suppressed [24]. However, in this case the resulting beam is strongly divergent and cannot be much compressed due to its longitudinal phase-space distribution.

There exist several propositions to correct the deformation of the transversal phase-space caused by the linear time-dependent transversal RF fields [17][18][41][42]. The simultaneous excitation of several TM-Modes of the cavity with exactly harmonic frequency relations seems to be quite impossible in a superconducting cavity due to the small bandwidth of its resonances. It would be necessary to tune the cavity simultaneously and independently at several positions in order to keep the modes in harmonic relations, requiring an enormous technical effort. The addition of an independently fed and phased, non-symmetric cavity, however, is no problem also in a superconducting system. Both cavities can be mounted and operated in a single cryostat. The achievable emittance reduction seems to be considerable, the beam brightness approaches the value required for direct injection into a linear collider.

2.3. The Pulsed and Synchronized Laser

The electron source makes several detailed demands on the light source concerning wavelength, brightness, pulse structure, and stability. They will be described now, and possible solutions according to the state of the art will be discussed.

2.3.1. Demands on Wavelength, Power, and Pulse Structure

The optimum wavelength λ resp. photon energy $E_\gamma = hc/\lambda$ for the respective photocathode is located slightly above the work function Φ as a rule. It results from a tradeoff between high quantum efficiency at higher photon energy (see Figure 3) and low transversal energy of the emitted electrons at photon energies close to the threshold. This tradeoff is simplified by cathodes with steep rise of quantum yield, because both demands can be satisfied. A deviation towards higher photon energies can easily be tolerated, while the work function poses a hard threshold in the opposite direction. Compensation of a lower quantum efficiency by higher laser power is limited by the resulting power dissipation in the cathode. In addition, at a too low difference $E_\gamma - \Phi$ the transersal energy is anyway dominated by the thermal energy $k_B T$. The quoted demands imply the mouochromaticity of the light source: Any spectral contribution outside the optimum range either increases the transversal energy or heats the cathode.

The choice of cathode material and corresponding wavelength determine the quantum efficiemicy. The required beam current then determines the necessary light power S_γ according to equation (5). It must be considered that the quantum efficiency especially of sensitive photocathodes is reduced with time, which must be compensated by the light power. The very high peak and average currents required for FEL's and linear colliders result in very high peak and average power demands on the light source. For example, a bunch charge of 8 nC and an average current of 8 mA (within a macropulse) are foreseen for TESLA. Assuming a Cs_3Sb cathode with 5% quantum efficiency at 2.3 eV photon energy, this results in a pulse energy of 400 nJ and an average power of 0.4 W. A niobium photocathode with a quantum efficiency of 10^{-5} would require a light pulse energy of 4 mJ at 4.7 eV photon energy and an average light power of 4 kW. Typically the cathode is not easily accessible, and its illumination requires an optical system with a very small aperture (typical acceptance 10 mm×mrad). Thus the light source must not only provide a high power, but also a high brightness light beam.

The presumably most difficult requirement on the light source is the necessary pulse structure. Pulse power and repetition rate are determined by the subsequent application. The pulse repetition rate at superconducting accelerators typically varies between 1 MHz (for linear colliders) and 1 GHz (for free-electron-lasers). The average beam current can be as high as several milliamperes. However, the pulse width demanded by the accelerator and the corresponding peak current will only be generated by pulse compression, the corresponding requirements on the light source are thus relaxed. The initial pulse width is limited to a few degrees of the

RF phase in order to keep the energy spread small. Here one profits again from the low freqilency of the cavity: At 500 MHz a pulse width up to 50 ps (about 90° RF phase) seems to be acceptable. The light pulses must be synchronized with the RF phase of the cavity in order to provide an emission at constant RF phase. The respective phase jitter should be small compared to the pulse width, otherwise the individual electron pulses would vary in energy.

2.3.2. Suitable Light Sources for a Superconducting Photoemission Source

The above mentioned requirements cannot be accomplished by conventional light sources, but can with lasers. The cost and complexity of the necessary laser technology increases with higher pulse power, shorter pulses, and higher photon energy. Usual laser media have only small gain bandwidth, where lasers can be realized relatively simply. Lasers at wavelengths outside these bands require a more complex technology, e.g. laser-pumped dyes. Consequently, the fixing of the light parameters should be done not exclusively considering the cathode requirements, but also the availability of suitable lasers.

Lasers can produce the desired pulse structure when they are mode-locked [218]. All modes of the laser oscillator within the gain bandwidth are phase-locked to each other, and their fourier synthesis results in a sequence of short pulses with fixed repetition rate. The width of the pulses $\Delta t = \lambda^2/(c \cdot \Delta\lambda)$ depends only on the gain bandwidth $\Delta\lambda$ of the laser material in the ideal case. The pulse repetition rate $\nu_{rep} = c/2d$ depends on the length d of the optical cavity; typical repetition rates are 50-100 MHz. Higher repetition frequencies can be produced by splitting the beam and reunifying it after different pathlengths; lower rates can be realized by selection of single pulses, for example by electro-optical switches. Yet too long pulses can be shortened by pulse compression, longer pulses can be produced by pulse stretching [16].

Lasers of the required power and pulse structure are commercially available, but the synchronization of the pulse repetition with the RF frequency yet requires constructive efforts. The repetition rate exclusively depends on the length of the optical cavity, thus the mirror distance must be varied. This can be done for example by piezo elements moving the mirrors, or by including an electro-optical phase modulator into the beam line. Then the optical cavity operates as free resonator being tuned to the master oscillator resp. to the RF cavity. The tuning information can be generated by mixing the RF signal with the signal of a fast photodiode. Synchronizations of this type can be realized; they already exist at other photoemnission RF guns and can be adapted from there.

Nd:YAG lasers and related systems (Nd:YLF and Nd:Glass) seem to be specially suited to RF gun applications. They emit however infrared light which photon energy (1.165 eV) is too low for any type of photocathode. But due to its high energy density it can easily be multiplied in frequency by a factor of two, three, or four. The resulting photon energies (2.331 eV, 3.496 eV, and 4.661 eV) cover the range of nearly all interesting photocathode materials. Even a Nd:YAG laser with frequency-multiplication by five has been realized to operate a CsI cathode [103]. Limited by the bandwith of the laser material, the pulse length of Nd:YAG lasers can be as short as about 70 ps; with Nd:YLF as laser material pulse widths down to 35 ps can be achieved [214].

A possible alternative in the ultraviolet range are excimer lasers which produce this photon energy directy without frequency multiplication. On the other hand, excimer lasers are much more expensive and maintenance-intensive than solid lasers, even with frequency multiplication stage. Another interesting alternative are Ti:Sapphire lasers which also emit in the infrared, but are tunable over a very broad range and thus can also produce extremely short pulses. For applications with moderate power requirements also an argon ion laser could be suitable, emitting in the blue and green range (up to 514 nm).

The sole light source except a laser being bright enough for this application is synchrotron radiation from a wiggler. This must be driven with an electron beam from a different accelerator with compatible frequency and pulse repetition rate, the pulse structure of the light being determined by the pulse structure of the drive beam. This system can deliver a very bright light beam with nearly any desired pulse structure. Also the synchronization of the light pulses with the RF frequency is much easier, because only the two accelerators must be phase-locked. The evident disadvantage of this concept is the enormous effort required to build the light source: A second electron accelerator with considerable performance is necessary. Thus also an alternative concept not requiring a second accelerator has been proposed [20]: The electron beam generated by the RF gun shall also be used as drive beam for the wiggler after acceleration. The feedback will automatically produce the correct pulse structure. However, this system is instable and will produce severe problems concerning ignition and stability.

2.4. Prototype Design for a Superconducting Photoemission Source

Based on the considerations discussed above, we have developed the design and partially also the detailed construction of a prototype electron source, in parallel and in completion to our experimental activities. The operation and performance parameters of this prototype source are adapted to the demands of the existing superconducting linear collider and free-electron laser proposals. They aim to maximum beam brightness at high average beam currents.

This work was mainly done in two steps: In 1988 we produced a first design with a single 500 MHz cavity, mainly dedicated to free-electron laser applications. This was done in collaboration with a group at DESY and colleagues from the department of electrical engineering in our university. Detailed constructions already exist for the cavity and several other components [1][5]. This first design has been continuously updated in parallel and with respect to our experiments. However, from our actual point of view, this design is obsolete and thus is only presented as a summary in the next section.

In 1991/92 we have completely revised this design in collaboration with our partners at INFN Milano [6]. The result, referred to as second design, is presented in more detail in the next chapters. Its parameters are specially designed to the requirements of the TESLA linear collider project. Thus we have proposed to use it as “Injector No.2” in the TESLA Test Bed at DESY [158]. Possibly, it could be the only system fulfilling the TESLA injection demands without additional damping ring. Several technical solutions naturally have been copied from the first design; the most important change concerns the cavity geometry. However, the optimization of the cavity geometry is not yet finished, and the beam dynamics data are yet preliminary. Nevertheless they show the progress with respect to the first design.

2.4.1. The First Prototype for a Superconducting Photoelectron Source

This design is distinguished by the fact that the complete source shall be very compact and easy to operate (Figure 5). Thus only a single-cell cavity at a frequency of 500 MHz is foreseen. This cavity has a reentrant shape with the cathode at the tip of a conical nose in order to keep the external dimensions small (Figure 6). The geometry factor of this cavity shape is only 90 Ω, but its diameter is as small as 270 mm. Thus it can be mounted in a relatively small cryostat and cooled with liquid helium under atmospheric pressure (operation temperature 4.2 K). The geometrical shape of the cavity, especially the surroundings of cathode and iris, are optimized with respect to minimum emittance. This has been done based on beam dynamics calculations with the computer code TBCI-SF at DESY [211]. The photocathode is a thin alkali antimonide layer evaporated on a niobium stem as substrate. It is illuminated via

the beam tube using a frequency-doubled Nd:YAG laser. These components are nearly identical in the second design and are described in detail there.

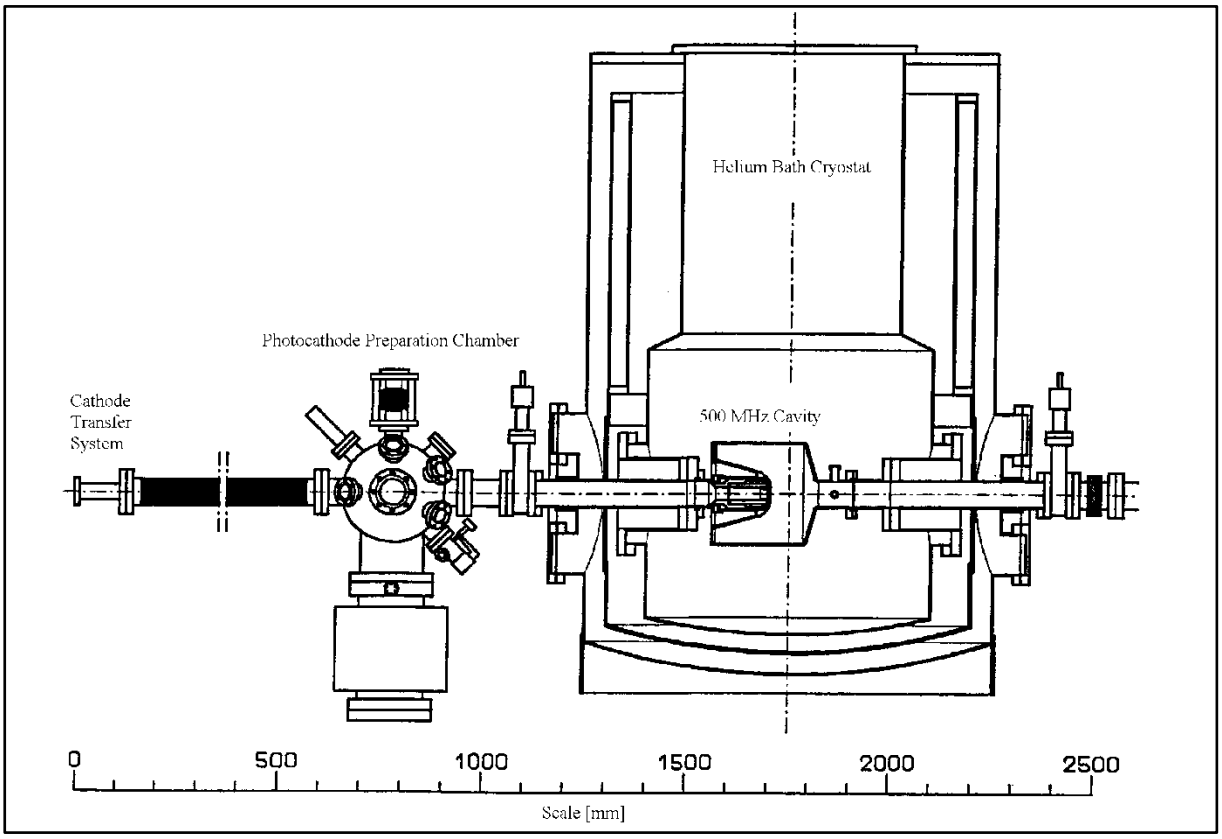

Figure 5 First design for a Superconducting Photoemission Source: Sketch of the setup

The parameters listed in Table 3 result from beam dynamics simulations with the ITACA computer code [217] performed by our collaboration partners from INFN Milano. They assume a moderate charge per bunch of 160 pC and also a moderate electric field of 16 MV/m at the cathode. Higher gradients at the cathode should lead to a further reduced emittance. The low charge per bunch enables a continuous operation of the source: At a pulse repetition rate of 50 MHz (occupation of every tenth pulse) the required RF power is about 6.4 kW. In spite of the simple construction the achievable beam brightness is already considerable. A further increase can be achieved by pulse compression, which is necessary to adapt the 70 ps long pulses to the subsequent accelerator.

2.4.2. Second Design for a Prototype: Components and Mechanical Setup

Our design for a TESLA injector contains a photocathode made of Cs_3Sb or K_2CsSb and a three-cell cavity made of niobium (Figure 7). According to the considerations discussed above, the frequency was chosen to be 650 MHz, half of the TESLA operating frequency of 1.3 GHz. The pulse repetition rate at TESLA is 1 MHz, thus every 650^{th} pulse must be occupied. However, the simple frequency relation enables a wide range of repetition rates; in principle every subharmonic of 650 MHz is a suitable rate. The first cell of the cavity is considerably shorter than the other ones due to the low electron velocity, and closed at its back side. The irises and the beam tube have a large aperture of about 20 cm to suppress emittance aggravation and to damp higher-order modes. Power input and monitor output couplers are built as beam tube side couplers. Due to the large aperture and the small number of cells higher-order-mode couplers have been renounced.

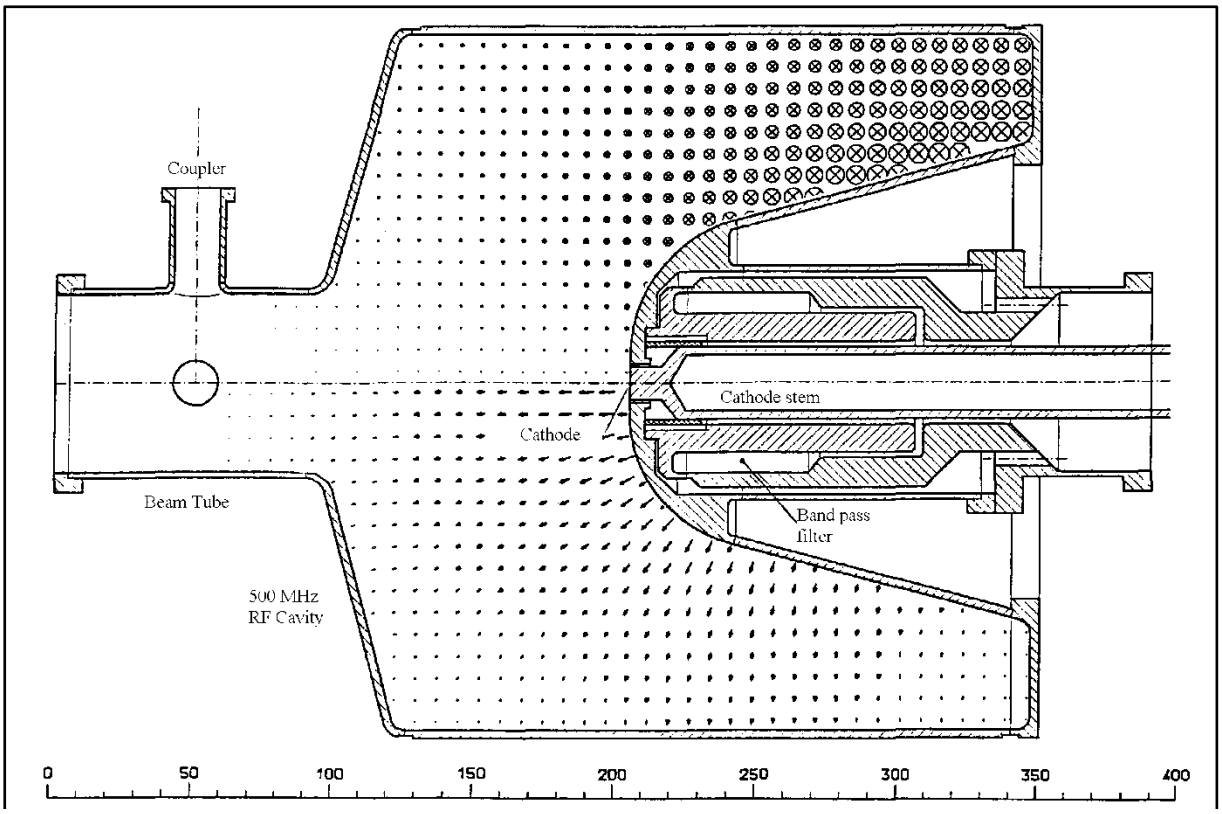

Figure 6 First Design for a Superconducting Photoemission Source: 500 MHz Cavity with Field Distribution

Machine Parameters	
Cavity: Material	Niob
Operation Temperature	4.2 K
Operation Frequency	500 MHz
Geometry Factor	90 Ω
Field Gauge Factor E_C^2/W	1.5 $(MV/m)^2/kJ$
Acceleration Distance	110 mm
Photocathode: Material	Cs_3Sb
Covered Area	1.1 cm^2
Geometry Factor	390 MΩ
Quantum Yield	1-5%
Laser: Material	Nd:YAG
Wavelength	532 nm
Pulse Length	70 ps
Pulse Intensity	≤ 2 μJ
Pulse Repetition Rate	≤ 50 MHz

Beam Parameters at the cathode	
Gradient at Cathode	16 MV/m
Bunch Charge	160 pC
Transversal Energy	0.2 eV
Bunch Length*	21 mm
Bunch Diameter*	5 mm
Emission Phase	52°
Beam Parameters at the Exit	
Kinetic Energy	795.5 keV
Energy Spread	±35.8 keV
Average Radius	8.2 mm
Average Divergence	30 mrad
Transversal Emittance	2.4 mm×mrad
Peak Current	1,55 A
Peak Brightness	2.7×10^{10} $A/(m\times rad)^2$

* Assuming a laser pulse gaussian in *r* and *t*

Table 3 Parameters of the first design for a Superconducting Photoemission Source: Technical data (left) and input/output beam parameters (right)

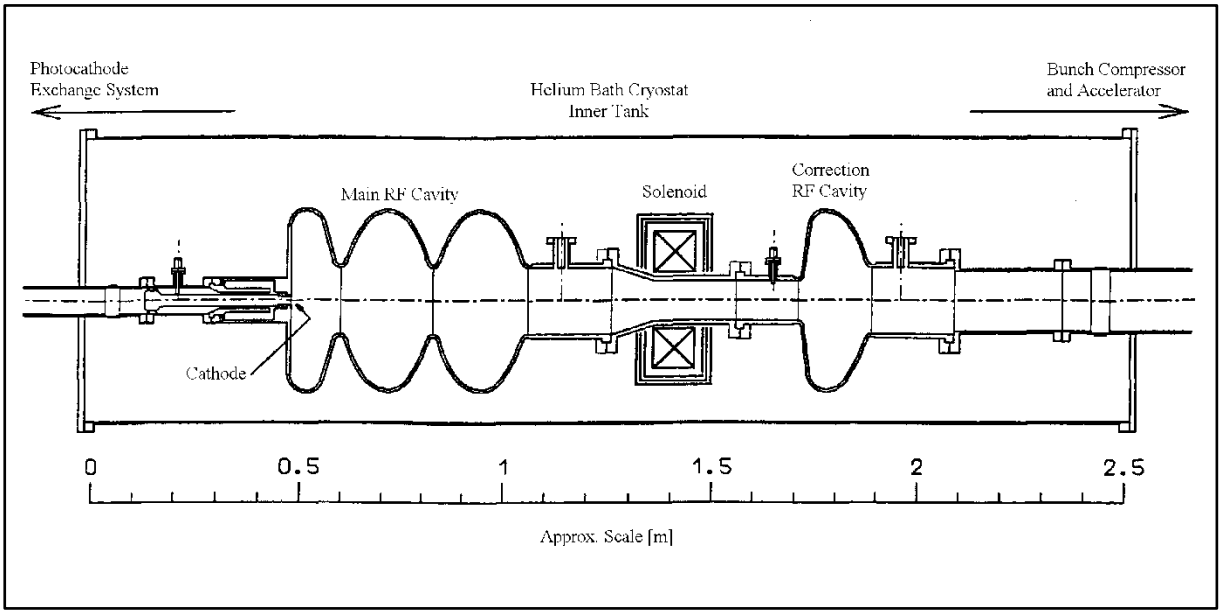

Figure 7 Second prototype design for a Superconducting Photoemission Source: Setup sketch for cavity and cryostat

An independent, unsymmetrical correction cavity is foreseen in the subsequent beam line [42]. A solenoid between both cavities shall turn the transversal phase-space distribution of the beam. After this turn the correction cavity can accelerate the beam instead of decelerate it during correction. When the solenoid is built in superconducting technology, all three components can be mounted together in a single cryostat, leading to a simple and compact setup. Superconducting sheets can shield the solenoid magnetic field completely from the cavities, preventing increased losses after an eventual quench. The operation temperature for all elements is 4.2 K; cooling can be done by liquid helium under atmospheric pressure. Thus a horizontal helium bath cryostat is foreseen, its inner tank would have a length of about 2 m and a diameter around 60 cm. The cryogenic power dissipation of the electron source being in any case small compared with the cryogenic power of the whole TESLA machine, the construction of the cryostat may be kept very simple.

The cathode has a diameter of about 20 mm; it is located in the center of the closed back wall. A thin layer (about 50 nm) of Cs_3Sb or K_2CsSb is evaporated on top of a niobium stem. This stem is mounted inside an opening of the wall, isolated by a gap of about 1 mm. The stem is beared about 20 mm farther back, the electrical contact there is shielded against the high RF field by a filter behind the gap. It is essential to install an excellent thermal contact between the stem and the helium bath in order to maintain the stem superconducting. This measure keeps the RF losses at the stem at an acceptable level and at the same time protects the photocathode against desorption.

The cathode is illuminated via the beam tube. If a beam deflection system (a dipole magnet or magnetic compressor) is installed in front of the injector, the optical beam can be mirrored directly along the beam axis, otherwise a slight angle must be chosen in order to prevent the mirror from the on-axis electron beam. The light source is a mode-locked, frequency-doubled Nd:YLF laser synchronized to the RF signal. Its photon energy of 2.3 eV fits the demands of Cs_3Sb and K_2CsSb cathodes well. The power behind the frequency doubler is sufficient to drive the photocathodes at full current, no optical amplifier is necessary. Thanks to the low cavity frequency, the pulse width achievable with mode-locking (about 35 ps) is sufficiently short even without compression. Thus the laser system (except the synchronization)

can be realized rather simply. The repetition rate of the laser is about 50 MHz. Single pulses can be selected by an electro-optical switch for example to achieve the repetition rate of 1 MHz required by TESLA.

The distribution of light intensity at the cathode (and consequently the initial charge distribution in the beam) can be determined by a few optical elements, for example in order to minimize beam emittance. In this context also flat (elliptical) distributions, as desired for some linear collider configurations [40], can be realized using cylindrical lenses. This variability of beam shape, pulse charge, and pulse repetition rate are highly desired for accelerator test facilities. In this case the whole surface of the stem would be covered with photocathode material. For regular operation, however, it would be advisable to adapt the evaporation area exactly to the required emission area in order to reduce its RF losses.

An UHV chamber containing several stems with completely prepared photocathodes is located directly besides the cryostat, at the cathode side. It is connected to the cathode by a vacuum transfer tube. When the cathode inside the cavity is degraded, it can be transferred to the chamber and exchanged against a new one without leaving the vacuum. The cavity must be switched off during the exchange (because its frequency is slightly shifted), but it can remain cold. Thus a quick cathode exchange is possible, avoiding long off-times of the accelerator. The time for one cathode exchange should be about five minutes. The number of stored photocathodes depends on the ratio between the cathode lifetimes in the chamber and in operation. Therefore the storage chamber should also maintain an excellent vacuum without active gases.

When all stored cathodes are used, the whole chamber is exchanged against another one with new cathodes. The preparation of the cathodes is done in a preparation chamber separated from the injector, where the storage chamber is connected to. The stems carrying used cathodes are then transferred to the preparation chamber. There they are either refreshed (by cesium evaporation) or cleaned (by heating) and again covered with photocathode material. The preparation chamber contains sources for antimony and alkali metals, gas leak valves, and corresponding measurement equipment (see also the following sections). The concept of a separated preparation and storage of cathodes also helps to reduce off-times of the accelerator and is already approved by the Los Alamos experiment [170]: The preparation of cathodes is no longer hampered by the gamma radiation near every operating accelerator. Just the exchange of the storage chamber requires a short presence at the injector.

2.4.3. Second Design for a Prototype Source: Prospective Operation Parameters

Based on the performance data of the various components, we have drawn a parameter list in collaboration with our partners at INFN Milano. We have estimated the prospective beam parameters (Table 4) with beam dynamics simulations.

The cavity containing the photocathode shall be operated with about 30 MV/in gradient at the cathode. The resulting maximum surface magnetic field is about 70 mT, the resulting averaged acceleration gradient about 15 MV/m. Achieving this gradient seems to be realistic with respect to both limitation mechanisms, defects at the superconducting surface and field emission at the semiconductor photocathode. With a resonance quality of about 2×10^9 at 4.2 K the continuously dissipated energy is about 10 W. The correction cavity has to be operated at about the same gradient and contributes another 3 W dissipated power.

Laser Parameters	
Pulse Length (2σ)	35-70 ps
Wavelength	532 nm
Pulse Energy	< 1 μJ
ModelockFrequency	81.25 MHz
Average Power	< 20 W
Kathoden-Parameter	
Diameter	20 mm
Material	Cs_3Sb
Quantum Yield	> 1%

* after magnetic compression

** depending on bunch charge, bunch length, and gradient

Beam Dynamics Results		
Charge per Bunch	≤ 20 nC	
Average Beam Current	≤ 10 mA	
Bunch Length*(2σ)	≥ 1 mm	
Peak Current in Bunch	≤ 2.54 kA	
Spatial Aspect Ratio	1 – 10	
Rel. Energy Spread**	$10^{-3} – 10^{-2}$	
Transv. Emittance**	$\approx 10^{-5}$ m×rad	
Emittance Asymmetry	$\varepsilon_x/\varepsilon_y \approx \sigma_x/\sigma_y$	
Max. RF Power	100 kW	
Cathode Field	20 MV/m	30 MV/m
Final Energy	7.5 MeV	11 MeV

Table 4 Second design for a prototype of a Superconducting Photoemission Source: Parameters for laser and cathode (left) and results of beam dynamics calculations (right)

To fulfil the TESLA demands the source must generate electron bunches with 8 nC charge at a rate of 1 MHz within the macropulse. According to the simulation results, the final energy of the electrons is about 11 MeV, the resulting power transferred to the beam is about 88 kW during the macropulse. The transferred power averaged over several macropulses however is only 700 W. Thus one needs a clystron which can deliver about 100 kW during 2 ms, but about 1500 W average power. The quality factor of the cavity loaded by the beam results in 3×10^5. A continuous operation of the cavity is nevertheless impossible, although the dissipated power without beam is negligible: Without beam the power requirement at the coupler is only reduced to 25%, because the coupler is adapted to the low quality. Thus most of the power is then simply reflected at the coupler.

Using a Cs_3Sb or K_2CsSb cathode one can expect a quantum yield of about 5%. However, with respect to its lifetime, the cathode should yet be operable down to a yield of about 1%. The necessary pulse energy of the laser is 2 μJ, leading to an average power of 100 W at a repetition rate of 50 MHz. This power is again required only during 2 ms; the required average power is only 1 W. When the light spot has a diameter of 12 mm the resulting charge density is about 70 $\mu C/m^2$. This value is smaller than the Gaussian limit of 266 $\mu C/m^2$ at 30 MV/m (see Formula (9)). The mode-locked laser should have a pulse length of about 35 ps, corresponding to about 8° RF phase. According to the simulation calculations this leads to an energy spread of about 200 keV. The resulting final bunch length of about 10 mm is too long for most applications, thus a bunch compressor is necessary as a rule. However, the longitudinal emittance is quite low due to the correction cavity, and a compression by at least a factor 10 seems realistic.

The achievable emittance with a round beam is about 5π mm×mrad according to the simulations. The resulting beam brightness is about 5×10^{11} A/(m×rad)^2, or even 5×10^{12} A/(m×rad)^2 after a bunch compression by a factor 10. Thus the potential of this source is well comparable with today's best high-brightness electron sources. A flat electron beam, as desired for TESLA, has been considered, too. An ellipse of $10\times1.6\pi$ mm^2 area at the cathode results in an electron beam of $25\times4\pi$ mm^2 cross section at the gun exit. Its transversal

emittances are 5π mm×mrad resp. 40π mm×mrad resulting in a beam brightness of 2×10^{11} A/(m×rad)^2.

The beam parameters presented in this sections base on a yet very preliminary cavity design. Consequently, the data also have preliminary character. However, the presented data are estimated so cautiously that we are sure they can be achieved. In future we intend to proceed with cavity optimization in collaboration with our partners in INFN Milano. Based on a more accnrate geometry, more realistic data on beam dynamics will then be available. Nevertheless, as already mentioned above, several parameters which are fundamental for the operation of the source are yet completely unknown, because no experimental data are available. With highest priority there are the lifetime of the cathode in its cryogenic, but high-gradient and high-current environment, and the lifetime of the superconducting cavity (characterized by maximum gradient and quality factor) with an operating photocathode inside. In spite of all models and extrapolations these problems can finally be solved by experiments only. In the next two sections, the experiments, which we built up especially for this purpose, will be described.

3. The Experiment on Preparation of Photocathodes

3.1. Intention of this Experiment

We have built up a vacuum chamber to prepare, characterize, and investigate alkali antimonide photocathodes. This has been our experimental entry into the project of a Superconducting Photoemission Source. Initially this experiment was useful to skill us in handling akali antimonide photocathodes. The working group of Prof. Piel has been active on superconducting RF cavities for fifteen years, thus corresponding technical experience was fully available. But there was no experience on operating photocathodes at all. However, preparation and handling of alkali antimonide is so difficult that experience of the operator is indispensable. The intention of this experiment is the definition of a procedure to reliably produce alkali antimonide photocathodes with high quantum efficiency. In addition, certain properties of these cathodes shall be investigated in more detail. Although the alkali antimonide photoemitters are well-known long ago (Cs_3Sb since 1936 [72] and K_2CsSb since 1963 [95]) and in parts have been thoroughly investigated [78][99][106] yet a lot of their properties being relevant for a superconducting photoemission gun are quite unknown. In particular, this is valid for their behaviour on various substrate materials, especially niobium, the dependence of quantum efficiency on the layer thickness on metallic substrates, their lifetime in actively pumped vacuum systems, and their reaction with various residual gases [82].

Actually this experiment is in a paradox situation: In spite of the promising initial results and the extensive experimental program yet to be done, it is actually inactive due to lack of personnel. The second experiment described in section 0 naturally has higher priority, and we have not sufficient staff to operate both setups at the same time. This is the reason why several of the questions discussed below had to remain unanswered, although the instrumentation was available to solve them.

3.2. Setup and Starting of the Experiment

3.2.1. The Vacuum System of the Preparation Chamber

An excellent vacuum inside the chamber is a fundamental requirement for most of the planned experiments in order to keep its effect on the performance of the photocathodes as low as possible. Already during construction, special care has been taken to suppress the eventual occurence of oxidizing gases and to improve their removal. The apparatus consists of a stainless steel recipient with about 40 l volume (Figure 8) being annealable at 300° C in total. All components are mounted on metal-sealed flanges and are annealed simultaneously. The volume of the chamber is divided in two parts by a baffle sheet. While the front part is dedicated to preparation and measurement of photocathodes, the rear part is used for vacuum niaintenance and control.

The vacuum quality is controlled by two devices: An extractor-type ionization gauge with an X-ray limit of 10^{-12} mbar measures the total pressure, and a quadrupole mass spectrometer with a sensitivity of 5×10^{-14} mbar up to mass 200 can determine the residual gas composition. Both are located in the rear part of the recipient, together with the opening to the 150 l/s ion getter pump. A baffle shields them against the preparation area to avoid contamination especially by alkali metals. If alkali metals condense on the gauges they can falsify the measurements due to their low work function. As a matter of fact, this effect can even be used to control alkali metal vapour partial pressures [101]. In addidion, metallic condensations on ceramic insulators cause side currents which also interfere with the measurements. However, in spite of the shielding this effect has been observed several times at the mass spectrometer. We

also have the suspicion that a defect at the channeltron of the mass spectrometer was caused by cesium vapour. An improvement of the existing baffle should therefore be considered in future.

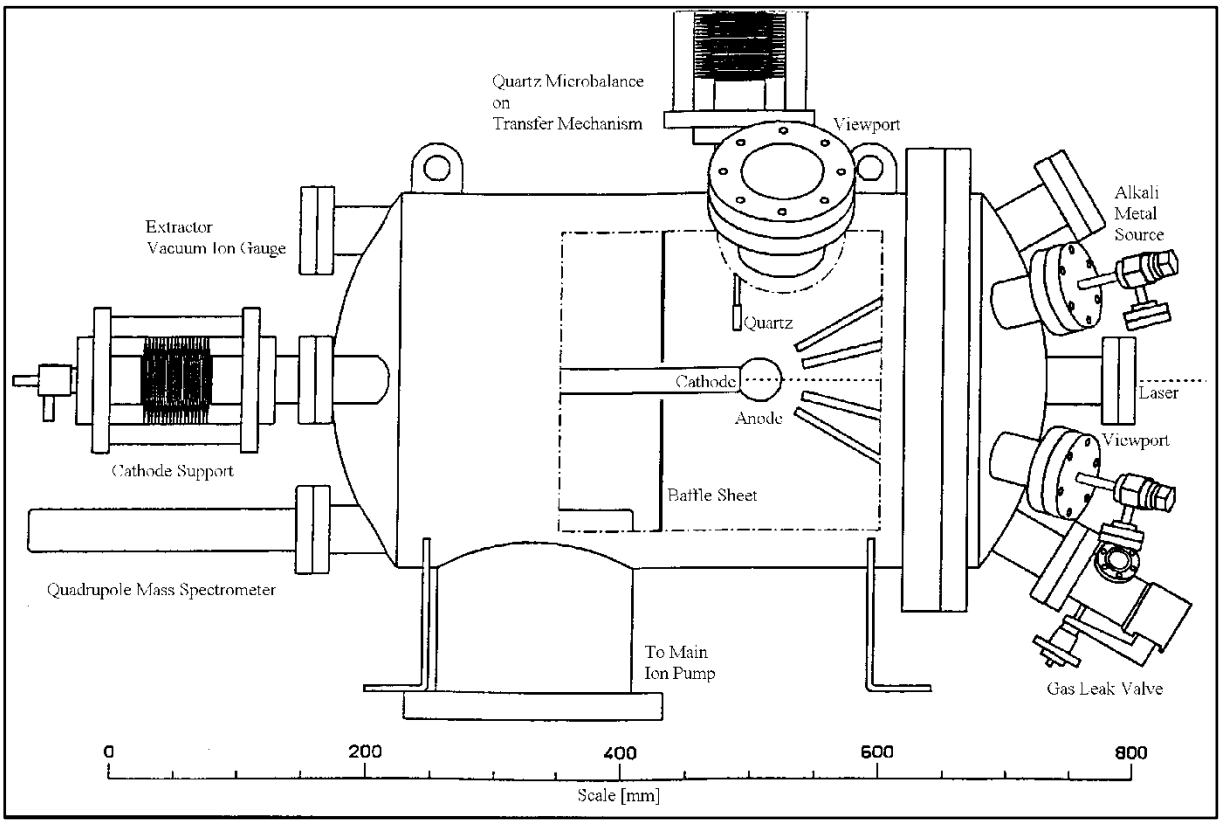

Figure 8 Vacuum chamber to prepare and investigate alkali antimonide photocathodes

When the recipient is at atmospheric pressure, it is evacuated initially by two sorption pumps down to about 10^{-3} mbar, then with an ion getter pump (30 l/s) being connected to the chamber via an all-metal valve. Depending on the status of the chamber surface, this ion getter pump evacuates down to a pressure between 10^{-7} and 10^{-8} mbar. As next step the complete setup is annealed at 300°C, while the desorbed gases are again pumped by the 30 l/s ion pump. The velocity of annealing depends on the gas desorption rate; the pressure should not rise above 10^{-5} mbar. The annealing is continued until a pressure of about 10^{-7} mbar is reached in the hot state. Depending on the initial state, this procedure takes between several hours and a few days. When the chamber is cooled down to 150°C, the big 150 l/s ion pump is started and the all-metal valve closed. This pump is directly connected to the recipient and annealed together with it. The described procedure ensures that the ion pump used in the high-vacuum state is as clean as possible and not contaminated by desorption products.

After cooldown to room temperature the total pressure of the chamber is about 10^{-9} mbar. Within a few days it typically falls below 10^{-10} mbar. The lowest basic pressure achieved until now is 3×10^{-11} mbar after several weeks of pumping time. The residual gas composition is typical for a very clean vacuum system: It consists nearly completely of hydrogen (H_2) and contains about 5-10% carbon monoxide (CO), 1% methane (CH_4), and 1% helium and argon. The hydrogen slowly diffuses through the steel walls; carbon monoxide and methane are probably generated from carbides in the steel. Helium and argon probably originate from the ion pump, where the gettering efficiency of noble gases is quite low. The partial pressures of reactive gases like carbon dioxide, oxygen, nitrogen, and water are below the detection limit

of 10^{-13} mbar. Thus the most dangerous component with respect to photocathodes is obviously carbon monoxide with its partial pressure between $\times 10^{-12}$ and 10^{-11} mbar.

3.2.2. Preparation of Alkali Antimonide Photocathodes

The substrate for the photocathodes is made from niobium to approach the conditions in a superconducting photoemission source. The photocathodes are evaporated on the front area of a long stem looming into the front section from the back wall. The face area has a diameter of 30 mm and is smoothed plain, but not polished. Finally, it has been etched chemically. The whole stem is hollow, thus the rear side of the front sheet is accessible under normal pressure. A heater is mounted in the front of this hollow space, which can heat the face controllably up to 600°C. It is floated with nitrogen gas to achieve a sufficiently homogeneous temperature distribution. The temperature is controlled by a two-point regulator, it is fluctuating only 1-2°C with a time constant of about 15 s in the hot state. Heating to 600°C takes about 15 minutes, cooling with a flow of cold nitrogen in the hollow tube about one hour. The temperature difference between heater (resp. controlling thermometer inside the heater) and face area have not been measured. Rough analytical estimates give a temperature difference up to 50°C in the hot state; at temperatues necessary for preparation (about 120°C) the difference should however amount to a few degrees only. The hollow stem can also be cooled to 77 K by filling it with liquid nitrogen, if the low-temperature behaviour of photocathodes shall be investigated.

The evaporation sources for antimony and the alkali metals are located opposite the photocathode stem, mounted at the front wall of the recipient. Antimony is a metal resistant against air at atmospheric pressure, melting at 631°C, but considerably sublimating already at 600°C. Hence the antimony source is simply a small crucible containing about 0.5 g antimony (6N purity) and heated by a tungsten filament. The evaporation rate is controlled by the heating current according to a calibration. The open area of the crucible (7 mm^2) is directed to the face of the cathode stem, its distance is about 100 mm. Assuming a $\cos(\theta)$ distribution, about 2% of the evaporated material reach the photocathode area.

Metal	Melting P.	Boiling P.	Temperature [°C] for Vapour Pressure			
	[°C]	[°C]	10^{-8} mbar	10^{-6} mbar	10^{-4} mbar	10^{-2} mbar
Antimony	630.7	1750	359	436	533	667
Sodium	97.8	892	71	121	189	285
Potassium	63.7	774	13	56	113	202
Cesium	28.5	690	-18	19	71	146

Table 5 Evaporation properties of antimony and alkali metals, according to [212]

Besides the antimony source, the chamber contains three identical evaporation sources for sodium, potassium, and cesium. With this combination the most important photoemitter materials Cs_3Sb, K_2CsSb, and Na_2KSb can be synthesized. The construction of the sources must take into account that alkali metals are more volatile than antimony and immediately react with air. The supply of about 1 g alkali metal is stored in a copper tube outside the recipient and connected to it by a miniature valve. A capillary tube leads the vapour from the valve opening to the cathode inside the chamber. The supply tube is heated and the valve opened for a definite time during evaporation, the evaporation rate is given by the temperature of the supply (typically between 120°C and 180°C). Valve and capillary tube are heated to a higher temperature than the supply (about 240° C) in order to prevent condensation there. The capil-

lary has a cross section of about 12.5 mm^2 and ends about 70 mm in front of the cathode. About 4.5% of the evaporated material reaches the cathode area.

In front of each tube a mechanical shutter is mounted, because the time constants of the sources themselves are too long for a precise preparation. The shutters can be operated from outside by a rotary feedthrough. The evaporation rates of all sources are controlled and calibrated by a quartz microbalance. This balance can be moved exactly to the place where the cathode is located during preparation in order to get the correct evaporation rate. The metals are evaporated onto a small quartz vibrator (frequency 6 MHz). Its resonance frequency *f* varies with the mass occupation i according to

$$\Delta f = 8{,}9 \cdot 10^6 \left[\frac{\mathrm{Hz}}{\mathrm{kg/m^2}} \right] \cdot \Delta\mu \tag{14}$$

Repeated calibrations at all sources prove a high reproducibility of the evaporation curves. Consequently, in normal operation one can use supply temperature resp. heater current as direct measure for the evaporation rate (Figure 9).

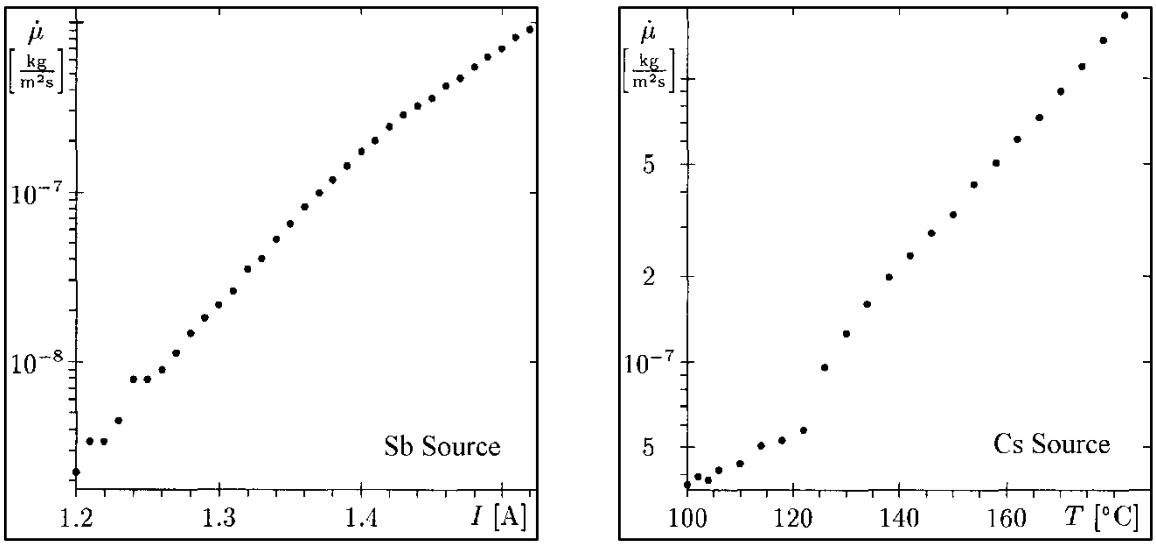

Figure 9 Measured calibration curves for evaporation rates of antimony (left) and cesium source (right)

In addition to the four sources, also a gas leak valve is mounted at the front side of the recipient. Also here a capillary tube conducts the gas towards the cathode. A gas supply system is connected to the leak valve outside the vacuum chamber, enabling the supply of various pure and mixed gases to the cathode. Actually, bottles for oxygen, carbon dioxide, carbon monoxide, and methane, a source for volatile liquids (like water or methanole), and an external connection, for example for nitrogen, are equipped. A constant, very small gas flow can be conducted to the cathode through the gas leak valve. The resulting partial pressures in the chamber can be controlled by the ionization gauge and the mass spectrometers. This component shall be used to activate cathodes with tiny amounts of oxygen or other electronegative media as well as for controlled exposition of photocathodes to active gases in lifetime experiments.

The preparation of alkali antimonide layers is done according to the usual process described in literature [77][97]: Initially, the substrate is covered with an antimony layer of defined thickness (between 5 and 100 nm). Then (in case of Cs_3Sb) cesium is evaporated at a cathode temperature of 125°C, until the (simultaneously monitored) quantum efficiency has reached its maximum. In recent preparations a bit more cesium was added during cooldown of the cathode to room temperature. Sometimes new cesium antimonide layers were evapo-

rated on top of existing layers, sometimes the niobium substrate was cleaned by annealing at 600° C for several hours. Except for some reference layers made from K_3Sb, no other material than Cs_3Sb has been used until now.

3.2.3. Determination of Quantum Efficiency

The cathode surface is illuminated with a laser, and the emitted electrons are collected at an anode. The anode is a cylindrical disc with a diameter of 35 mm in 50 mm distance from the cathode, kept on a positive potential U_0 versus cathode and vacuum chamber. The current collected by the anode is measured with an electrometer. In comparison to a measurement at an isolated cathode this method has the disadvantage that the measured current contains also electrons emitted from other components than the cathode, and that not necessarily all electrons emitted at the cathode are collected. However, an isolation of the cathode is difficult to realize. A control measurement with provisionally isolated cathode showed that anode and cathode current are nearly identical in the whole range of U_0 (Figure 10): the influence of parasitic currents is negligible. It can also be seen that a bias voltage of 100 V is already sufficient for the given current to suppress the formation of a space-charge cloud. All measurements mentioned below are thus done with a bias voltage between 100 and 150 V. The only error source which we corrected were leak currents; they can easily be measured by switching off the illumination. Sometimes the leak currents were rather high in this chamber (up to 100 nA with 100 V bias) and always showed a linear dependence on the voltage. However, the leak currents were always low again after bakeout. We suppose that the reason for the leak currents are condensations of cesium on the ceramic insulators.

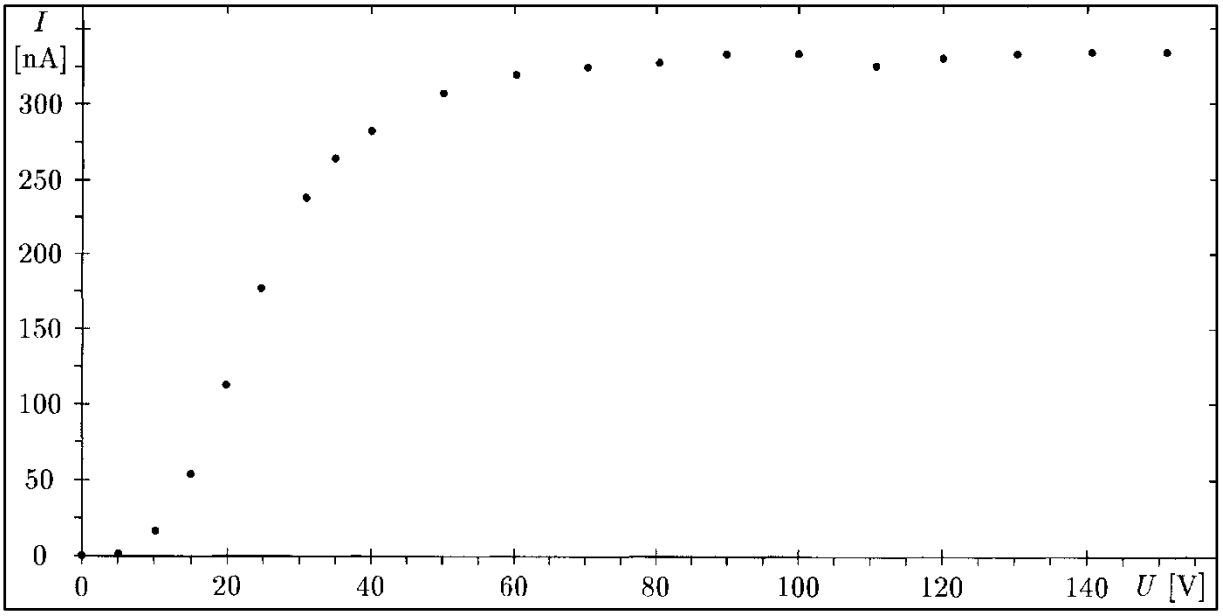

Figure 10 Characteristic curve of anode and cathode current versus bias voltage

The laser used for the cathode illumination is a green helium-neon laser with about 0.5 mW light power at a wavelength of 543 nm. Its beam is directed onto the cathode by a system of two lenses and a mirror. The lens system enables focussing to a spot below 0.1 mm diameter (limit of visual control) as well as blowing up to an area with 10 mm diameter at the cathode (2σ values of gaussian distribution). The tiltable mirror allows controlled scanning of the whole cathode surface with 30 mm diameter. An optical telescope is mounted parallel on the beam axis enabling visual control of the spot size and position. Until recently, no suitable laser powermeter was available, thus the incident laser power had to be estimated from the nominal laser power and the attenuation by lenses, mirror, and viewports. Now we can meas-

ure the light power in front of the viewport with such a device, and only the attenuation of the window must be corrected. However, a subsequent recalibration of former measurements is of limited significance due to the long-term variations of the laser power. We measured a laser power of about 0.4 mW according to a light intensity of 0.25 mW hitting the cathode; this is about half the value which we assumed before calibration.

3.3. Results in the Photocathode Preparation Chamber

3.3.1. Achieved Quantum Efficiencies

I want to emphasize again that all results (except the very last ones) of quantum efficiency have been estimated without knowledge of the correct light power. The assumed laser power at the cathode was 0.5 mW. The subsequent calibrations proved that this value was assumed too high up to a factor two. Consequently, the resulting quantum efficiencies were surely estimated too low. We did not try to correct the results because the power variation of the laser during that period is unknown. As a matter of fact, the laser tube was even exchanged one time. In the following discussion only emission currents are given, but no resulting quantum yields, in order to give no incorrect data. The relations between the measurements, however, are quite reliable, especially if they are performed within a short period. As rough orientation one can assume that 1 1A photocurrent corresponds to 0.5-1% quantum efficiency at 543 nm wavelength. The relative error of successive measurements should be about ±5-10% or even less.

Already at the very first preparation of a Cs_3Sb layer we could achieve at once a photocurrent of 3-4 μA, which proved to be well reproducible. An antimony layer was just heated to 120-130° C and covered with cesium, until the monitored photocurrent reached its maximum, and then was cooled down to room temperature. In this process we varied the evaporation rates, the temperature of the cathode, and its warmup and cooldown velocities. Naturally, this resulted in variations of the dynamic changes of photocurrent, but the maximum photocurrent always was in the same range mentioned above. However, with a cathode temperature above 130°C no photocathode preparation was successful. Finally, by carefully controlling the process, we succeeded to prepare layers with up to 5 μA photocurrent.

These preparations were done onto the clean niobium substrate as well as on already existing Cs_3Sb layers without significant differences. Cleaning of the substrate was done by annealing at 600° C for several hours. The superficial Cs_3Sb layers evaporate completely then. After the chamber was opened to air, the substrate was always annealed at 600° C prior to photocathode preparations.

3.3.2. Lifetime of Photocathodes

The lifetime of the Cs_3Sb layers could not be measured in operation with high current density, but only during storage, because the available laser power was too low. In the first hours after preparation the layers showed some slight variation obviously due to formation of the Cs_3Sb stoichiometry. Afterwards, however, they were completely stable. In several cases the layers were measured again after two to four weeks storage time, but no significant difference was found in any case. Thus the lifetime of Cs_3Sb layers in this recipient is surely far above four weeks.

However we suspect that a considerable cesium pressure exists in this chamber. Caused by the construction of the cesium source, large amounts of cesium vapour are emitted into the recipient during preparation. In some cases, a partial pressure of 2×10^{-10} mbar could be detected even by the mass spectrometer. However, a short period later the cesium pressure was

no longer detectable. The positive effect of a cesium partial pressure on the photocathode lifetime is well known [101]. However, it is not yet clear whether the cesium pressure prevents a net cesium desorption from the photocathode or whether it getters residual gases which otherwise could attack the photocathode.

The lifetinie measurements discussed above have been performed at the basis pressure of the vacuum chamber. Systematic measurements with artificially increased partial pressures of certain gases have yet to be done. In a first test we have checked the behaviour of Cs_3Sb in pure nitrogen. At a partial pressure of 5×10^{-5} mbar during 30 minutes no variation of the quantum yield could be detected. Also an activation with water vapour has been tested with one of the first layers. Due to the provisional setup the partial pressure of the water vapour could not be determined. The photocurrent initially increased from 3.8 μA to 7.5 μA instantaneously; more water vapour then destroyed the photocathode, as expected.

3.3.3. Further Results

The dependence of quantum efficiency on the thickness of the Cs_3Sb layers has been investigated in a series of preparations (see Figure 11). An antimony layer of defined thickness was deposited onto the substrate with the calibrated antimony source and activated with cesium. The thickness of the Cs_3Sb layers referred to result from a multiplication of the antimony thickness by a factor 6 [74][78], corresponding to a density of 4800 kg/m^3 [76]. The quantum yield increased already with very thin layers and reached its asymptotic constant value at about 100 nm thickness. This thickness has the same order of magnitude as the light absorption constant in Cs_3Sb [78]; the incident light is then completely absorbed. A maximum of the yield due to reflexion of light at the substrate surface [73] could not be detected. It is interesting that already the layer with only 30 nm thickness already has a considerable quantum yield. This result is important with respect to the reduction of RF losses at the cathode (see section 4.5.2 at page 71).

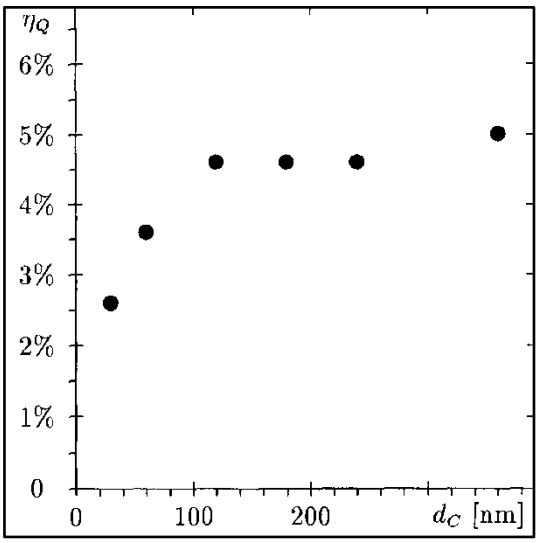

Figure 11 Dependence of the quantum yield on the thickness of Cs_3Sb layers evaporated on niobium

We also tested the homogeneity of the 7 cm^2 Cs_3Sb layers. As a rule the layers were as more homogeneous as higher the quantum efficiency was. A layer with 5 μA average photocurrent varied between 4.8 and 5.3 μA spot photocurrent. The layer shown in Figure 12 with a photocurrent of about 10 μA however has a significant maximum located a bit above the center.

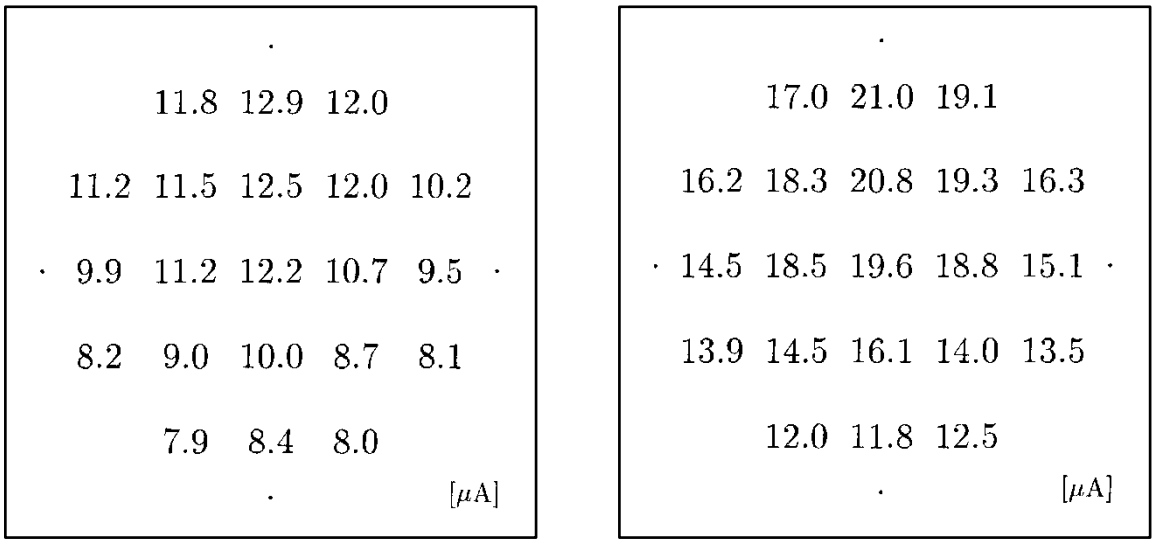

Figure 12 Homogeneity of a 32 mm diameter Cs_3Sb layer before (left) and after activation (right) with oxygen

In the most recent preparation we succeeded to generate a Cs_3Sb layer with more than 10 μA photocurrent by additionally evaporating tiny amounts of cesium onto the cathode during cooldown. Also this layer showed no significant variation over several days. Then we tried to activate it with oxygen. The photocurrent quickly increased up to22 μA. However, the activated cathode was not completely stable, and the photocurrent decreased to about 16 μA within a few days. Thereafter the layer was stored in the chamber for six months at a basic pressure of about 5×10^{-11} mbar. Then the layer was again controlled and yet showed a photocurrent of 10 μA; a calibration with the laser powermeter yielded a quantum efficiency of 10%. This measurement proves that activated Cs_3Sb photocathodes can achieve quantum efficiencies far above 10%, and that these layers can be stable over months in actively pumped vacuum systems.

3.4. Planned Programme of Future Measurements

With respect to most of the problems, the measurements presented above are only a first step and must be continued. The most important experiment concerning the Superconducting Photoemission Source concerns the reactivity of photocathodes with various residual gases. Data concerning a few gases like oxygen and water are available [82], for other important gases like carbon monoxide and methane future measurements are necessary. Identically prepared and comparable Cs_3Sb layers should be exposed to the different gases under controlled partial pressure. The dependence of the reactivity on photocathode thickness and preparation process is also relevant. These measurements should help to estimate the maximum lifetime of alkali antimonide photocathodes in a superconducting cavity. A more accurate knowledge of the reactions with active gases would also help to detect and separate eventual additional effects which also degrade the photocathode.

The activation of alkali antimonides with strongly oxidizing gases shall also be investigated in more detail. Also here the dependence on photocathode thichkness, preparation process, and activating gas should be examined. Besides oxygen also water and nitrogen fluoride NF_3 shall be tested, the activation capability of both is well known. From chemical considerations, also antimony pentafluoride SbF_5 should be a capable activator. Considering the superconducting photoemission source again, the influence of activation on the cathode lifetime and conductivity is of special importance.

However, a light source with variable wavelength should be availabe for these measurements, because the activation does influence not only the absolute height of quantum efficiency, but also its spectral shape [78]. Two main alternatives can be chosen: Lasers with several lines in the visible spectrum (for example Ar^+ lasers) offer only a few choices of wavelength, but produce sufficient brightness there. White light sources (tungsten lamp or xenon arc lamp) with spectral filters cover the complete visible range, but produce only a fair brightness, and special data acquisition techniqes (e.g. lock-in amplification) must be applied.

Other alkali antimonides, especially K_2CsSb [69][77], shall be prepared and investigated besides Cs_3Sb. K_2CsSb is of special interest, because it has a higher quantum efficiency and shall have a longer lifetime in photoemission RF guns due to an improved resistivity against active gases [101]. Thus it is an interesting alternative to Cs_3Sb in spite of its more difficult preparation process [105]. This preparation chamber is especially suited to learn its preparation and to compare its properties with those of Cs_3Sb. A detailed comparison is necessary to do a correct estimation between the performances of both materials for the proposed application.

Further photoemitting materials like Cs_2Te [94][104], CsAu [100], and GaAs:Cs [88] can be investigated in this preparation chamber, too. However, several components have to be replaced or added for this purpose. In particular, a tunable source for ultraviolet light, a corresponding viewport, and eventually a bearing for GaAs wafers would be necessary. However, due to the yet low importance of these materials for a photoemission source (see section 2.1.2 at page 17) their investigation will have a lower priority than the questions discussed above.

Also in future the preparation chamber shall be used to test new components for photocathode preparation before applying them in other experiments. This aspect will also concern the alkali metal dispenser sources, which already have been used in the second experiment (see next section) and which must be considered as potential source of the difficulties in cathode preparation observed there. In spite of its actual inactivity, this experiment shall remain a technical and scientific component of the superconducting photoemission source project.

4. The Experiment to Operate a Photocathode Inside a Superconducting Cavity

4.1. Intention of the Experiment

As already mentioned in section 2.4.2, the superconducting photoemission source is an interesting concept which proposes several advantages for specific applications. However, on the other hand several physical and technical questions are yet open and require an experimental solution. It is the intention of our working group to deliver an important contribution to this concept besides the startup experiment described in the recent chapter. In opposition to initial hopes, however, we had only fair financial, technical, and personal resources at our disposal: The complete financial volume for investments was about DM 60,000. Construction and operation of the complete experiment had to be done by one PhD thesis candidate and one or two masterthesis candidates within a few years.

Obviously the setup of a complete prototype source was impossible under these conditions. Thus we decided to set up an experiment which could investigate most of the unknown problems concerning the interaction between a semiconductor photocathode and a superconducting RF cavity, but was free of the technical effort to produce a high-brightness electron beam. In this case, it is indispensable to prepare a photocathode of desired type and quality, to transfer and operate it inside a superconducting cavity with high quality factor and high gradient. However, the generation of a definite electron beam with specified brightness, energy, or pulse structures and therefore all beam optics are dispensable. This enables the experimental setup to be much simpler and easier to operate, thus also more flexible for modifications.

We have constructed and built the experiment described below according to these guidelines. Initially, a cesium antimonide photocathode should be operated in the superconducting cavity for the first time as a proof of principle [4]. Then we want to determine the lifetime of photocathodes under various operation conditions and investigate the responsible mechanisms. In parallel, we want to see whether and how the photocathode affects the cavity performance. In addition, operating this setup shall bring us experience in handling the other components (preparation chamber, optics, transfer system etc.) and serve as test environment for new or modified components.

But the given funding was extremely short even for this program. Thus we were compelled to obey the following strategy: Initially, all components of the setup were constructed as simple as possible, even taking the risk that a few components would not or not completely fulfil the requirements. Components, which showed shortcomings during operation, were gradually replaced by improved constructions. Besides the very low cost (no component is more complicated than necessary) this strategy also has the advantage that first scientific results are available already at a very early stage. In addition, the components of the second generation are improved by first generation experience. The most important disadvantage is of course that no fixed time schedule can be set up, and it takes a very long time until all components are working perfectly.

In addition to this strategy a lot of time and money could be saved by re-using components from former projects. Here, the cryostat was formerly used for tests of multicell accelerator structures at 8 GHz and 3 GHz; it has only been shortened for easier handling. The preparation chamber together with its ion getter pump was formerly part of a furnance to prepare Nb_3Sn surfaces on niobium cells. Also several vacuum components could be taken over from former setups. The optical system as well as several control units are identical with those of the first experiment (section 3); therefore both experiments cannot be operated simultaneous-

ly. The cavity has been welded without charge by our collaboration partners at CEBAF, the deep-drawn half cell was kindly provided by the TH Darmstadt. These recycling actions made components with a total value of about DM 200,000 available for our experiment.

Construction and setup of this experiment were started in 1989; in 1991 the completed system was ready to be operated for the first time. During the first operations several components showed shortcomings as expected. Nevertheless, the system in total worked quite well, and already in the first test a semiconductor photocathode could be operated inside the cavity. Some of the problematic components could be replaced at once; they are described already in their improved version. In the meantime, four more tests have been performed, and especially the tests No. 4 and No. 5 yielded interesting results. The replacement of some other components will require a larger rearrangement of the setup, which is actually under construction and shall be realized within the next months. Shortcomings and planned improvements of these components are described below, too. These and other problems mentioned below should not be seen as disadvantages, but as natural steps in the development of this experiment.

4.2. Description of the Experimental Setup

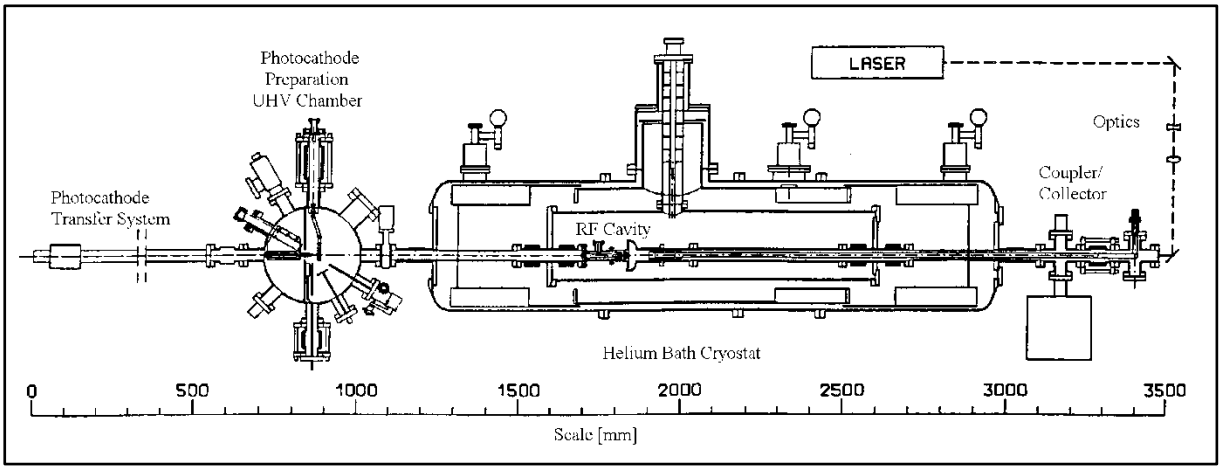

Figure 13 Experiment to operate an alkali antimonide photocathode inside a superconducting cavity: Overview sketch

In principle, the experiment consists of a specially shaped niobium cavity inside a helium bath cryostat, a photocathode preparation chamber with transfer system at one side, and an unit to collect the beam and to couple the RF at the other side (Figure 13). Photocathodes (and in principle any other material) can be transferred into the cavity during operation. The quantum efficiency of the photocathode as well as the operation parameters of the cavity (quality factor and gradient) can be measured under various operation conditions.

4.2.1. The 3 GHz Cavity

The niobium cavity (Figure 14) is shaped like half an S-band accelerator cell (with geometry like in the S-DALINAC accelerator [180]), closed with a plane sheet. Frequency and field distribution are the same as in a full accelerator cell, because the end plate is perpendicular to the electric field everywhere (Figure 15). The groove in the end plate near the equator is only for manufacturing reasons (better welding along the equator). The contours have been rounded in this area to prevent multipacting. Due to the groove in the high magnetic field area, the frequency is shifted from 3 GHz to 2.83 GHz. The most important parameters of the cavity are listed in Table 6, where a cathode radius R_C = 3 mm has been assumed. The electric

field strength at the iris depends strongly on its curvature radius. Due to the small radius, its determination is difficult with mesh codes. For an iris radius R = 3.2 mm, the computer code URMEL [220] found the peak electric field there, but the code URMEL-T found the maximum electric field at the cathode. The maximum magnetic field strength is located at the inner border of the groove in the end plate. As long as the cathode radius R is small, the magnetic field at the cathode surface can be approximately described by a constant normal electric field: $H_\varphi(r) \approx r\varepsilon E_C/2\omega$. Similarly the geometry factor of the cathode can be described by its field gauge factor E_C^2/W:

(15)
$$G_C = \frac{2\omega W}{\int_C H^2 df} = \frac{16}{\pi\omega\varepsilon^2 R_C^4}\left(\frac{E_C^2}{W}\right)^{-1}$$

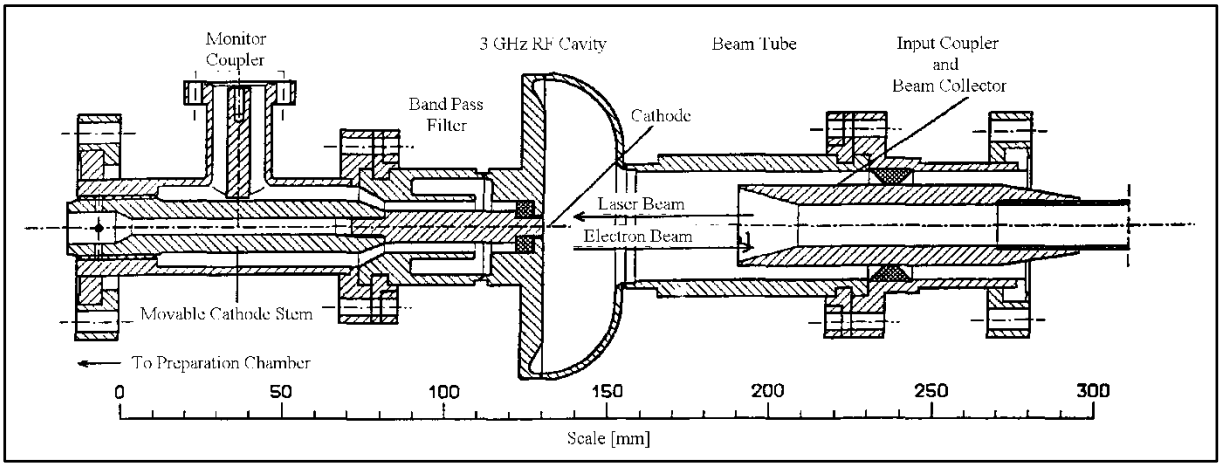

Figure 14 Detailed drawing of the superconducting cavity with filter and couplers

Parameter		URMEL-T 7,000	URMEL 25,000	Measured*
Basic Mode Frequency	f_0	2,790.8 MHz	2,792.9 MHz	2,829 ± 1 MHz
Total Geometry Factor	G	150.1 Ω	141.7 Ω	140 ± 10 Ω
Localisation max. E-Field		Border Cathode	Iris	
Gauge Factor max. E-Field	E_p^2/W	5,780 $(MV/m)^2/J$	7,857 $(MV/m)^2/J$	
Gauge Factor max. H-Field	H_p^2/W	19,298 $(kA/m)^2/J$	20,227 $(kA/m)^2/J$	
Cathode Geometry Factor	G_C	7.91 MΩ	8.48 MΩ	
Guage Factor E Cathode	E_C^2/W	5,780 $(MV/m)^2/J$	5,387 $(MV/m)^2/J$	

* at room temperature

Table 6 Geometrical RF Parameters of the Half-Cell Cavity according to Calculations with URMEL (Resolution 25,000 Meshpoints) and URMEL-T (7,000 Points)

The photocathode is located on the cavity axis (beam axis), plane with the end plate. However, not the cavity surface serves as substrate, but the top face of a stem with 6 mm diameter. This stem can be transferred under vacuum between cavity and preparation chamber while the cavity remains cold. There is no direct electrical contact between cathode stem and cavity wall, but they are separated by a 0.5 mm gap. Due to the isolating layer of niobium oxide on niobium, a direct touch would inevitably lead to point contacts, which can cause enhanced RF losses. The stem is beared directly behind the top in a ring of single crystal Al_2O_3 to enhance its thermal contact to the helium bath. The Al_2O_3 ring does not load the cav-

ity quality due to its excellent dielectric properties ($\varepsilon_r \approx 10$; $\tan(\delta) < 10^{-5}$). Further back the stem must have an electrical contact to the cavity, but shielded from the RF field. There it is beared in a fine thread at the same time enabling an exact longitudinal positioning.

4.2.2. The Bandpass Filter

The stem together with the surrounding vacuum tube forms a coaxial line which is coupled to the cavity by the gap and acts as a drain of RF power. The external quality induced by this system is about 5×10^4 according to measurements at a model cavity. A rough analytical estimation gave the same order of magnitude. The external quality is inversely proportional to the gap width, but the width cannot be reduced below about 0.5 mm due to mechanical reasons. Thus a bandpass filter (choke) has been inserted behind the Al_2O_3 ring, which reflects the extracted charge back into the cavity, if accurately tuned. The bandpass filter has been designed coaxially, its exact shape has been optimized by numerical calculations (code URMEL) as well as by measurements on a model cavity with variable filter geometry [7].

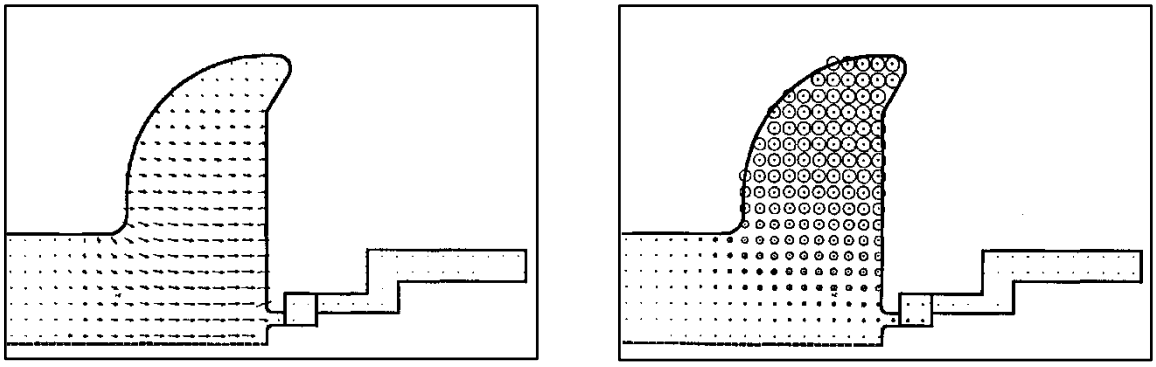

Figure 15 Cavity with bandpass filter: Electrical (left) and magnetical (right) field distribution of the π-Mode at 2.8 GHz

The effect of the bandpass filter can be understood if one considers cavity and filter as two coupled resonators with similar basic frequency, but different impedance: One gets a passband with two resonances. In the 0-mode both resonators oscillate parallel (the magnetic field has the same circulation direction in both parts), but the field is nearly exclusively concentrated in the filter. This 0-mode has a frequency of about 2 GHz; it is strongly coupled to the further coaxial line and has no meaning for the experiment. In the π-mode the field is mainly located inside the cavity (see Figure 15). Both systems oscillate antiparallel, and the knot of the oscillation (the zero area of the magnetic field) is located exactly where the coaxial line is connected (resp. where losses can occur). The knot is shifted if the resonance frequency of the filter is changed: as lower the filter frequency, as nearer the knot to the cavity. The filter is exactly tuned if the knot is located exactly at the critical point (electrical contact or antenna connection). The magnetic field is zero there, and the losses are minimized.

The model of two coupled resonators correctly describes the field distribution, however, it cannot completely explain the shape of the spectral response (Figure 17). The best-suited model for this purpose is a substitute circuit diagram: The cavity is a weakly coupled oscillator and the filter a closed side line at a 50 Ω line (Figure 16), which has a length of λ/4 at correct tuning.

In the π-mode, the field strenght in the filter is much lower than in the cavity, but not negligible (see Table 7). Filter and stem thus were also manufactured from niobium and are superconducting during operation, because normalconducting components at the filter would cause significant power dissipation. In fact, cavity and filter are welded together, which simplifies the construction of flanges at the cavity. The field relations between filter and cavity as

well as the geometry factors in the filter are difficult to determine with codes like URMEL-T, because the mesh cannot sufficiently resolve the small gap between cavity and filter. Calculations for various gap widths (Table 7 top) show that the results behave reasonably only within their order of magnitude. However, at a fixed gap width the relations of the results to each other (Table 7 bottom) seem to be reliable.

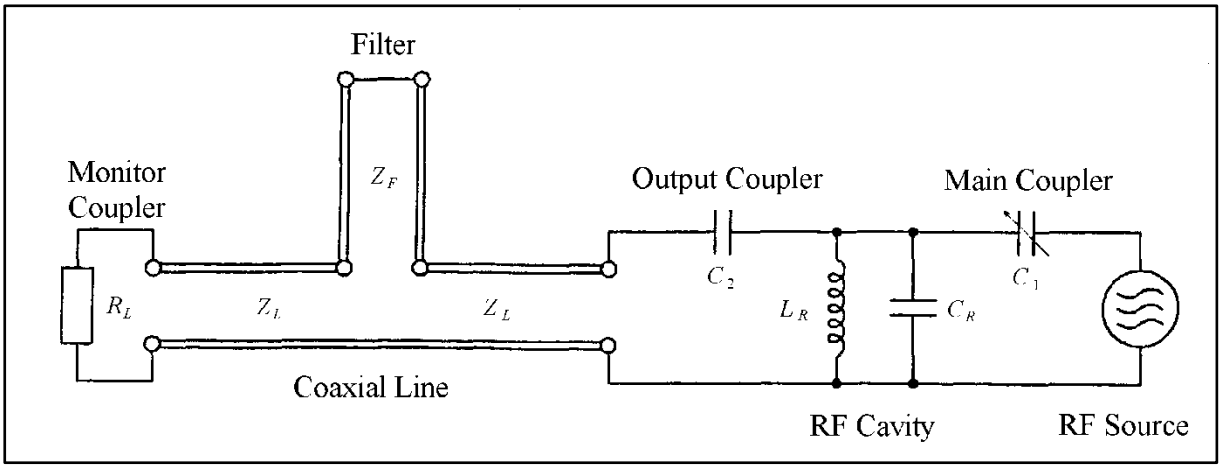

Figure 16 Substitute circuit diagram for cavity and filter

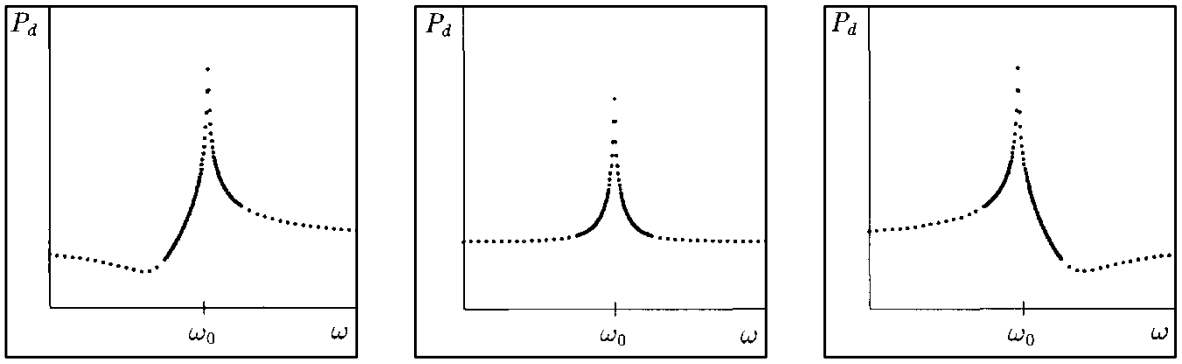

Figure 17 Transmission curve for cavity with bandpass filter for too low (left), correct (center), and too high (right) filter frequency

The superconducting design of the filter theoretically enables to achieve very high quality factors up to 10^{10} as long as no photocathode is evaporated yet. A normalconducting copper layer already reduces the quality below 5×10^8; a completely normalconducting filter made from copper would reduce the quality down to about 3×10^7. The unloaded quality of the cavity can also be determined without cathode stem, when the complete filter area is not excited. However, field distortions especially occur near the hole for the cathode in this situation; the cavity frequency increases by about 1.2 MHz.

The remaining signal on the coaxial line behind the filter is collected with an antenna (see Figure 14). This signal is used for fine tuning of the filter and as monitor signal (transmitted signal P_d) from the cavity: It is proportional to the field strength in the cavity and gives a phase reference for the frequency control circuit. When the cathode stem is drawn back from the cavity, the coupling strength of the monitor is decreasing (Figure 18); without cathode stem it disappears completely. In this state, the cavity can be measured without being loaded by stem and filter. However, the monitor signal must then be yielded from the reflected signal of the main coupler. Due to the superposition with the input signal, which has at least the same size, the errors are unavoidably bigger than with an independent monitor signal. The

main coupling strength must then be chosen critical ($Q_1 \approx Q_0$) to obtain a sufficiently large phase signal for the frequency control.

Gap Width	H_F^{max}/H_p	G_F
0,5 mm	0.023	360 kΩ
1,0 mm	0.009	2,351 kΩ
1,5 mm	0.015	846 kΩ
2,0 mm	0.039	125 kΩ

Geometry Factors at 0,5 mm Gap Width		
Complete Filter Area		360 kΩ
Outer Surface Coax Line	A	938 kΩ
Inner Surface Coax Line	B	868 kΩ
Surface in λ/4-Filter	C	1,786 Ω
Energy Portion of Al_2O_3 Ring		2.48×10^{-5}

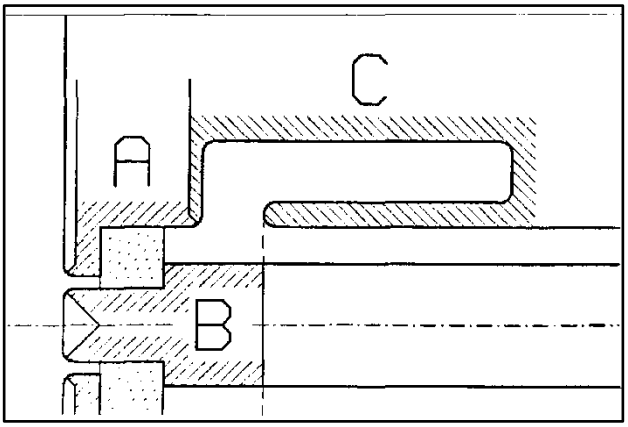

Table 7 Field strengths and geometry factors of the ir-Mode in the filter area, according to calculations with the code URMEL-T (resolution 7,000 mesh points)

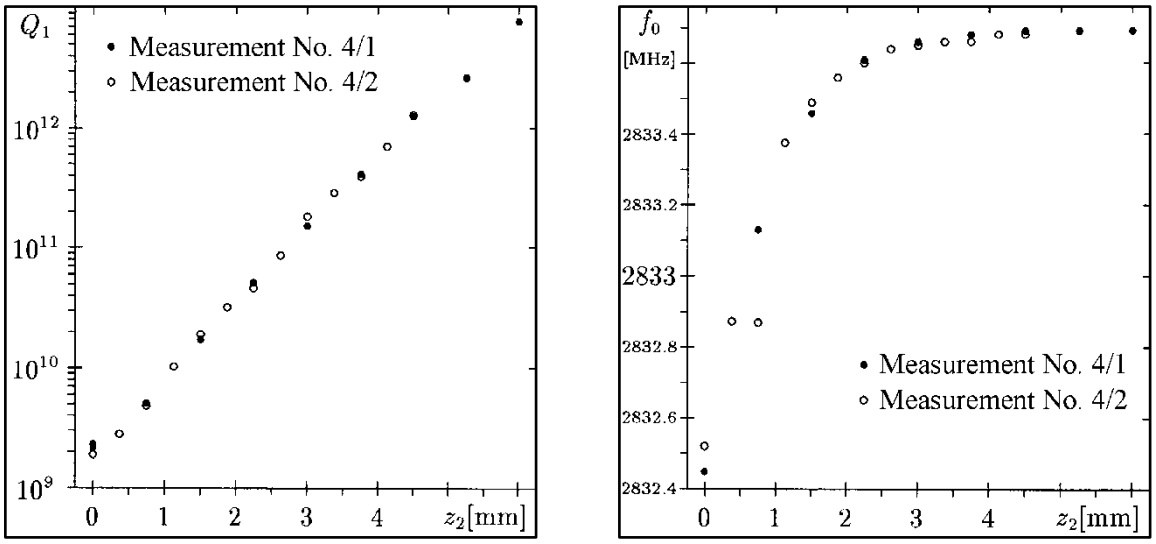

Figure 18 Variation of external quality Q_2 and resonance frequency f_0 during drawback of the cathode stem

The cavity is not tuned during operation, but its frequency is running free. The RF generator is locked to the cavity frequency by a phase-coupled control circuit; reference is the phase of the monitor signal. Variations in the resonance frequency are mainly caused by pressure fluctuations in the helium tank of the cryostat. The reaction of the cavity on pressure variations is much stronger than the reaction of the filter due to its lower mechanical stability. Thus besides the frequency variations also the tuning between cavity and filter is changed. By this effect oscillations in the helium tank lead to a statistical failure of the frequency control, when the cavity frequency crosses the exact rejection frequency of the filter. This effect can be seen as seam of narrow peaks on the reflected and transmitted signal. During the cooldown from room temperature to liquid helium temperature the resonance frequency is increased by

6 MHz due to thermal contraction (about 0.22% for niobium). Because cavity and filter are contracted equally, a tuning done at room temperature remains valid.

4.2.3. The Beam Tube

The beam tube itself is a vacuum tube with 35 mm inner diameter guiding out of the cryostat. Inside there is another coaxial tube of 15 mm outer and 13 mm inner diameter. This tube ends about 50 mm away from the cavity carrying on its top a niobium tip with 25 mm outer diameter (see Figure 14 right). This tip is movably beared in an isolating Al_2O_3 ring about 100 mm away from the cavity. The other bearing of the inner tube is a vacuum feedthrough outside the cryostat. With a membrane bellows the whole inner tube can be moved longitudinally. The distance z_1 between the top of the stem and the cavity end plate can be varied between 58 and 88 mm. Beam tube and inner tube are made from stainless steel to keep the heat transfer from outside to the helium bath low.

The electrons emitted from the cathode are accelerated towards the beam tube by the RF field. There they enter the inner tube and are collected at its walls. Due to its length of about 1.5 m the inner tube is a nearly ideal faraday cup: The probability that electrons leave it again on the other side is quite low and can be further suppressed by a magnetic field. The collected current can be measured, because the inner tube is isolated. According to our measurements and to corresponding simulation results from L. Serafini (see Table 8 at page 55), this extraction mechanism is already efficient at E_C = 0.5 MV/m. The extraction is efficient even at E_C = 0.1 MV/m with additional bias voltage of +150 V at the tube. The bias voltage of +150 V considerably improves the extraction efficiency (see Figure 19) although it causes only a very small additional electric field at the cathode (<< 100 V/rn). We don't yet understand completely the reason for this effect; probably the low-energy electrons entering the beam tube are bent to the inner tube increasing the effective collection area from 491 mm^2 to 962 mm^2. It is not possible to extract the electrons only with the DC bias voltage, because the gradient produced at the cathode is too low. However, we intend to increase the shift range of the inner tube to 100 mm by using a longer bellows. Then its top will penetrate into the cavity enabling a direct measurement of quantum efficiency there without RF field.

The coaxial tube system also serves as RF power coupler for the cavity. Its coupling strength can be varied by shifting the inner conductor. The variation range of the external coupling quality Q_1 extends from 10^7 for z_1 = 58 mm to 10^{10} for z_1 = 88 mm (Figure 20). The impedance along the 100 mm long tip of 25 mm diameter is 20 Ω, along the tubes themselves the impedance is 50 Ω. The length of this coaxial line is about 1,500 mm, thus coincidences between the resonance frequencies on this line with the cavity resonance frequency (coupling resonances) are quite inevitable (see Figure 20). As a matter of fact, the line resonance No. 31 coincides with the cavity frequency at z_1 = *77* mm. However, this coupling resonance is narrow and affects the coupling only for 75 mm < z_1 < 79 mum; any desired external quality can be realized with a z_1 outside this range. Except for the coupling resonance, the course of the external quality can be explained by exponential damping of the TM-01 mode (cutoff frequency 6.56 GHz); it is definitely not in agreement with exponential damping of the TE-11 mode (cutoff frequency 5.02 GHz). The RF absorption of the line between feedthrough and cavity away from the coupling resonance is about 2.25 dB at 3 GHz. If required it could be reduced by a factor three by covering the tubes with a thin copper or silver layer. The incoming power is limited to about 500 W by the vacuum feedthrough (outside the cryostat). However, the coupler itself could even transfer a much higher power if the feedthrough would be replaced.

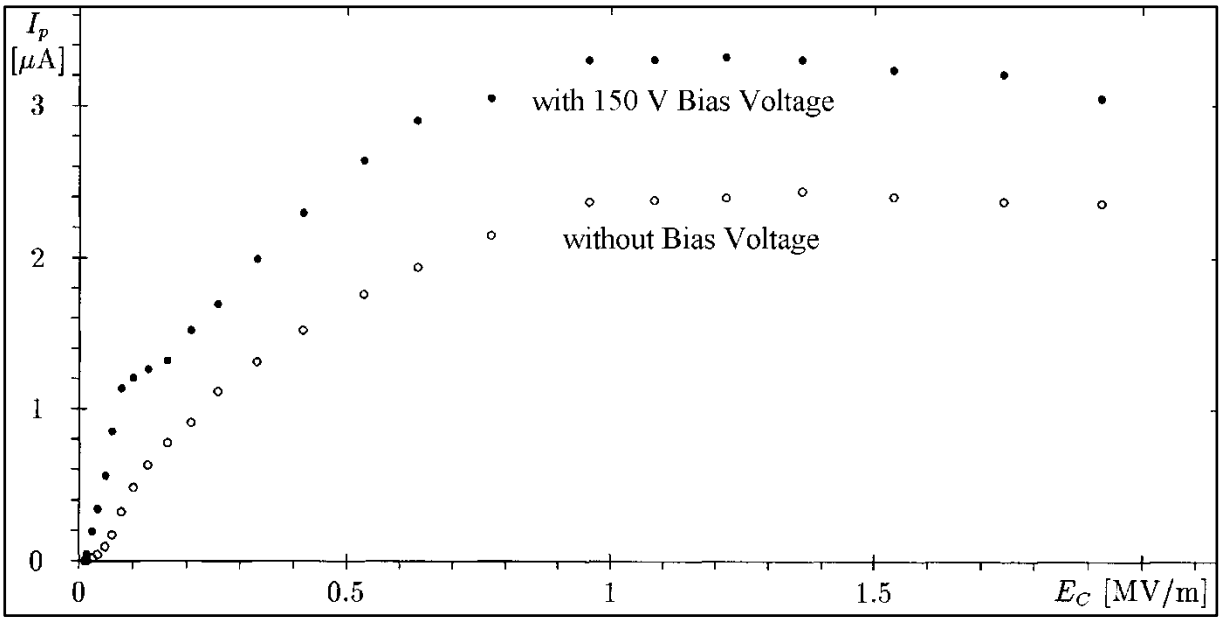

Figure 19 Dependence of the extracted electron current on the RF field strength with and without 150 V bias voltage; measurement *I(E)* No. 5/6

The beam tube is also used to evacuate the cavity: Outside the cryostat it is connected to a roughing port with all-metal valve, to a 30 l/s ion getter pump, and to an ionization vacuum gauge. However, the effective pumping speed at the cavity is only 0.2 l/s because pumping is done through the narrow inner tube (the channel between inner and outer tube is closed by the Al_2O_3 bearing). Thus the pressure in the cavity can be two orders of magnitude higher than near the ion pump, where the vacuum gauge is located, if most of the gas is coming from the cavity walls. This problem is aggravated by the fact that the environment of the cavity cannot be baked out, because the indium seals between niobium and stainless steel components would melt. A sealing material with the same performance as indium, but resistivity against higher temperatures, was not yet available. In addition, this part is located inside the cryostat, and the access for heating is difficult. Due to this disadvantageous situation the lowest pressure which we achieved near the pump was 10^{-8} mbar; inside the cavity the pressure could even be as high as 10^{-6} mbar. The filter area, where the access through the beam tube is difficult due to the small opening to the cavity, is pumped from the preparation chamber with an effective pumping speed of about 0.6 l/s. These data are valid only when the cavity is at room temperature. When the cavity is cooled to liquid helium temperature the relations are reversed: The pressure at the outer ends of the pumping lines change ony slightly (typically less than one order of magnitude), but in the cavity area all gases except helium and hydrogen are completely frozen at the walls.

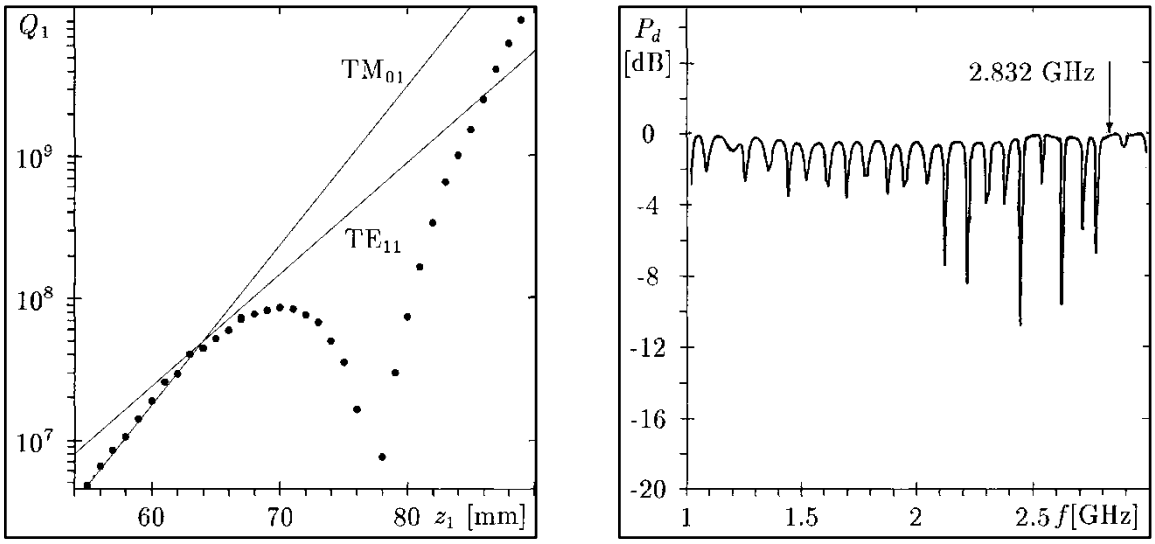

Figure 20 Main power coupler: Variation of the external quality Q_1 with the position z_1 of the inner tube (left) and resonances visible on the reflected signal (right)

4.2.4. The Cryostat

The whole cavity is mounted inside a horizontal helium bath cryostat. In contrary to a vertical cryostat, this one enables external access from both sides. The inner tank has a length of 1 m and a diameter of 220 mm (inner dimensions) and can be filled with about 30 l liquid helium. Pump down of the filled tank from 4.2 K to 1.9 K already consumes about 30% of the total helium amount, because the components of the helium tank (especially the heavy flanges) have a large heat capacity. The static heat load of the cryostat is about 3 W, thus the remaining helium is sufficient for about 8 hours operation, if the additional RF power dissipation is negligible. The existing pumping system can achieve a minimum pressure of 25 mbar with that heat load, resulting in a minimum temperature of 1.9 K. The main portion of the heat load comes from the lateral flanges, which have no superisolation, in contrary to the other walls. A guided improvement of the flange isolations should help to increase the operation time significantly as well as to reduce the operation temperature.

The cryostat consists of an outer and an inner tank both made from stainless steel. Between those a radiation baffle is located, made from aluminium and cooled with liquid nitrogen. Both inner tank and radiation shield are isolated on their outer jacket with about 30 layers of superisolation (alternating layers of aluminium foil and glass fiber). The whole volume between outer and inner tank is evacuated for isolation: It is actively pumped with an oil diffusion pump, its pressure is between 10^{-5} mbar at room temperature and 10^{-6} mbar with cryogenic cooling. The flanges of the inner tank, which are sealed with indium, are especially sensitive against leaks. A magnetic shielding made from Kryoperm foil [210] is mounted inside the inner tank; the residual static magnetic field near the cavity is below 2 µT.

The cavity is mounted horizontally in a support inside the cryostat. The axis of cavity and beam tube lies 30 mm below the cryostat axis for better use of the helium amount. A platinum resistor for temperature control is mounted besides the cavity as well as a helium levelmeter. A rotating temperature and gamma-ray mapping system, as used in testing single and multicell accelerator cavities [139][153], is not installed in this experiment. However, they can be added if required, because cavity and filter are rotationally symmetric.

4.2.5. Laser and Optical System

The inner tube inside the beam tube is open at both ends, and the beam tube itself is closed with a viewport. Therefore the illumination of the photocathode can be done directly along the beam axis. The illumination reaches the cathode even in the preparation chamber along the same axis, when the cathode stem is retracted. Thus the photocathode efficiency measurements in preparation chamber and cavity are directly comparable. The illumination system is actually the same as for the independent preparation chamber (see section 3.2.3): The light source is a continuous helium-neon laser with about 0.5 mW power at 543 nm (green light). The laser beam is reflected onto the beam axis by a small prism; the cathode surface can be scanned with the beam by tilting this prism. Broadening or focussing of the laser beam is enabled by a simple two-lens optics. With careful alignment the beam can pass the narrow inner tube (13 mm diameter and 1,500 mm length) without power loss.

A Galilei telescope with about ten times magnification has been mounted at the same optical axis, where the cathode can be observed from outside the cryostat. This telescope is indispensable for focusing and alignment of the laser beam as well as controlling the cathode transfer. In addition we found that several optical effects occur around the cathode during high-field operation (see section 4.4.3 at page 64). Due to the bad geometrical conditions, however, optical quality and brightness of the telescope picture are rather low.

The laser described above is not well suited for illuminating the photocathode inside the cavity, because it is emitting continuously, and its intensity is rather low. The continuous emission causes a high portion of backaccelerated electrons hitting the cathode again which are known to alter the cathode performance; the low power makes studies on cathode lifetime during operation difficult. The perfect laser would have a pulse width below 50 ps (about 60° RF phase) synchronized with the RF phase and with an average power of about 1 W. However, lasers with these properties are quite expensive, and at the moment we have to restrict ourselves to the system described above. Nevertheless, the more sophisticated system will be indispensable in a future stage of our project.

4.2.6. The Photocathode Preparation Chamber

All processes connected to the preparation of photocathodes should be done in a special chamber outside the cryostat: Generation of a complete layer by successively evaporating layers of antimony and alkali metals, refreshment with low amounts of cesium vapour, activation by tiny amounts of oxygen, and cleaning of the stem by annealing up to 600°C. The cathode stem is transferred from the cavity to the preparation chamber, prepared there, and afterwards transferred back into the cavity. Actually, only one cathode stem can be handled inside the vacuum system at the same time; a preparation for storage is not yet possible.

This preparation chamber connected to the cryostat resembles the independent preparation chamber (see section 3) in a lot of details, however, considerably less effort has been done here to achieve a good vacuum. It consists of a stainless steel recipient with large ion getter pump (pumping speed 300 l/s) and a series of metal-sealed flanges for its various components (Figure 21). Also this system is baked to condition the vacuum, but only up to about 250°C, because the transfer system would be damaged at higher temperature (bearings made from PTFE, fluoro-elastomer sealings at the shutter valve). An externally connected turbomolecular pump is used during the evacuation process and during bakeout; the bakeout process is identical with that of the other chamber. Recipient and ion pump once have been part of a vacuum furnance for Nb_3Sn preparation. Due to the long-time previous operation, they inavoidably contain adsorbates, which slowly desorb again. Due to these fair conditions the achieved basic pressure is typically 2×10^{-9} mbar – two orders of magnitude more than in the other chamber.

The composition of the residual gas is quite similar: Besides hydrogen the gas contains about 10^{-10} mbar CO and methane in the 10^{-11} mbar range; the pressure of active gases like oxygen or water is however also in the 10^{-11} mbar range (see Table 9). Also here the instruments for vacuum control are an ionization gauge and – temporarily connected – a quadrupol mass spectrometer.

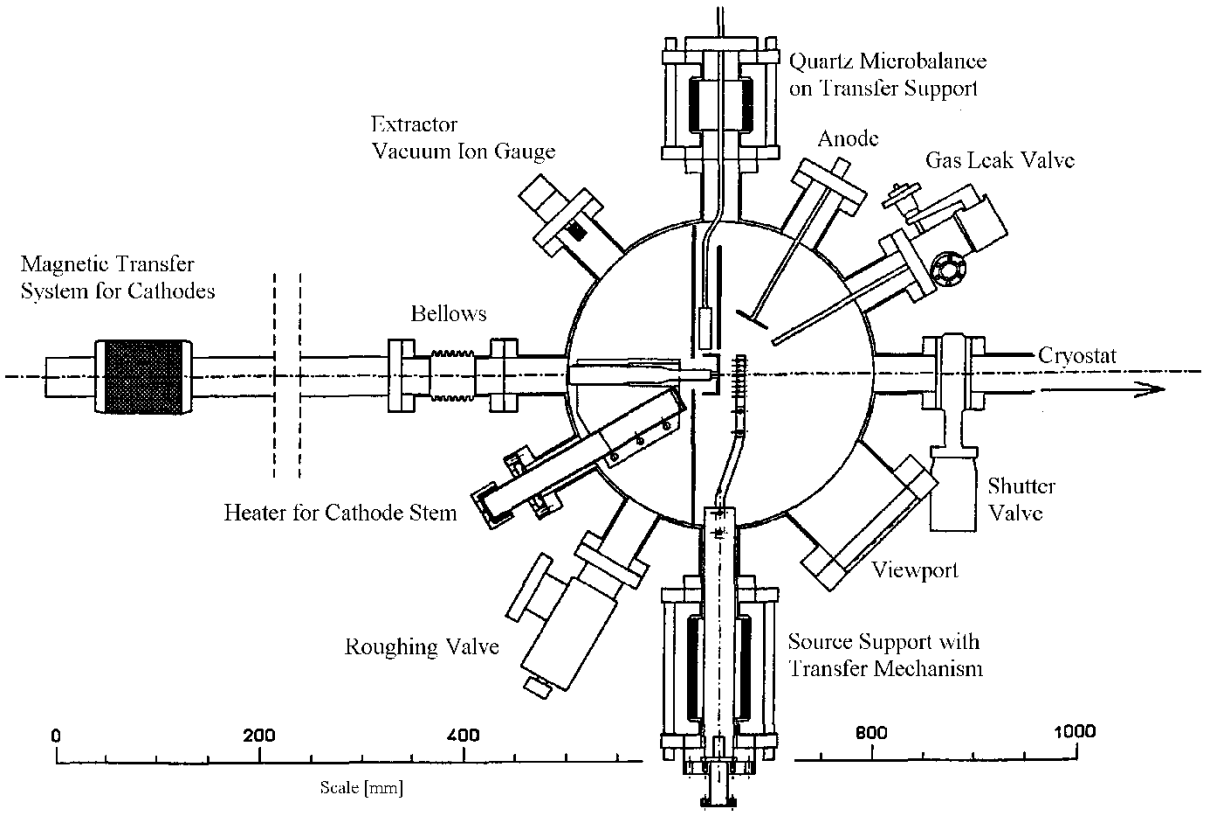

Figure 21 Overview sketch of the preparation chamber connected to the cryostat

After its transfer to the preparation chamber, the cathode stem is screwed into a copper log, which serves as heater and support. This system was built for heating the cathode substrate up to 600°C, but showed to be unsuited for this purpose, because the stem is pinned in the copper thread and because the heat transfer is much lower than expected. Actually, the maximum temperature achievable at the top of the stem is about 150°C. In contrary to the other preparation chamber, the evaporation of alkali metals is done from dispenser sources here. At a temperature between 550°C ands 850°C alkali metal is generated by a redox reaction of alkali chromate with a zirconium-aluminium alloy [215][219]. The outstanding advantages of these sources are their small dimensions (typically $2 \times 2 \times 25$ mm^3) and the simple control of their emission by the heating current. Their main disadvantages are their low alkali metal contents (typically a few milligrams per source) and the variation of their emission characteristics even during their short lifetime. The low alkali metal contents can be compensated partially by mounting several sources at the same time. After carefully degassing, the gas rates desorbed during operation are not higher than with other alkali sources (see Table 9) [209][213][216].

Antimony is evaporated directly as pure metal, too, in this chamber. However, this is done in tubes of the same shape as the alkali metal sources, specially provided by the SAES Getters SpA. company. Two sources for antimony and four sources for alkali metals are mounted in parallel on a support. They are placed directly in front of the cathode during preparation, the distance between cathode and source being only about 20 mm. This arrangement however

prevents the control of quantum efficiency during preparation, because the sources shield the laser and the anode field from the cathode. The calibration of the evaporation rates is again done by a quartz microbalance, which can be moved to the exact location of the cathode. A gas leak valve with a capillary tube directed to the cathode is already installed, but not yet the corresponding gas supply system.

The lower and the back part of the chamber are shielded with copper sheets against metal vapours. But also the other surfaces of the cathode stem behind the cathode and especially its Al_2O_3 bearing must be protected against vapour condensations, otherwise they would produce additional RF losses and field emission in the high RF field of the cavity. For this purpose a titanium foil with a hole exactly as big as the cathode surface is moved in front of the stem during preparation. The control of quantum yield is quite similar to the procedure in the other chamber: The anode is a simple stainless steel disc near the cathode, being isolated against the rest of the chamber. The illumination with the laser is done either along the beam axis through the cavity or through the laterally mounted viewport.

The photocathode stem is transferred between cavity and preparation chamber with a magnetically coupled linear and rotational feedthrough with 1 m translation distance. The cathode stem is plugged onto the top of the feedthrough rod. Its translation can be controlled optically through the chamber wiewport and with the telescope on the beam axis. In the preparation chamber as well as in the cavity the stem is beared in a fine thread enabling adjustment of the cathode and a fixed bearing when the translator rod is withdrawn. The stem can be separated from the translator, which is important to reduce the heat transfer to the cavity. Nevertheless not more than one stem can be handled in the vacuum system, because there is no storage facility yet. The transfer vacuum tube to the bandpass filter is pumped by the preparation chamber ion pump. This vacuum section is closed with a shutter valve during the preparation procedure to protect it against metal vapours. This shutter valve between preparation chamber and cryostat also enables opening of one component while the other remains under vacuum.

4.3. Simulation Calculations of Electron Dynamics

4.3.1. Two-Dimensional Calculations, Program ITACA

The dynamics of emitted electrons have been investigated by simulation with computer codes. Knowledge of the beam dynamics is important also for this experiment to estimate the intensity of cathode bombardment by electrons and to calculate the quantum efficiency from the extracted current.

Within our collaboration with INFN Milano, L. Serafini has made calculations for our cavity using his code ITACA. He considered especially that we are often forced to operate our cavity at very low field levels (below 1 MV/m). The space-charge effects can be neglected due to the low charge density obtainable with our laser. The most important result of these two-dimensional simulations (consideration of axial and radial components) is that the emitted electrons remain radially correlated down to field strengths of E = 0.5 MV/m: They are either backaccelerated to the cathode or leave the cavity through the beam tube (and are collected at the inner tube), but only a very low amount hits other regions of the cavity (see Table 8). The electrons hitting the cathode have a time of flight of less than one RF period, their radial expansion is negligible. The other electrons are focused by the RF field. Even at 0.5 MV/m, where the electrons need about 35° RF periods to cross the cavity, only about 4% of them don't reach the collector, but hit the cavity wall somewhere. Only at yet lower gradients the beam diverges already inside the cavity, and the portion of dissipated charge increases. As a matter of fact, however, in this region the bias voltage at the inner tube (which

has not been considered in the simulations) is noticeable already inside the cavity and supports the extraction. According to our data, with bias voltage the electrons are extracted efficiently already at about 0.1 MV/m (see Figure 19).

Gradient at the Cathode	[MV/m]	0.1	0.25	0.5	1.0	5.0	10	20
Critical Emission Phase	φ_C					91.5°	93.5°	99°
Dissioated Charge Portion		33%	22%	2%	2%			
Charge Portion Cathode								
Average* Kinetic Energy	[eV]			43.5	170	4.17 k	15.8 k	54.3 k
Maximum Kinetic Energy	[eV]			104	418	10.3 k	39.3 k	141 k
Charge Portion Beam Tube								
Beam Divergence**	[mrad]	314	212	166	130	88		52
Minimum Kinetic Energy	[eV]			31	118	2.9 k	10.8 k	22 k
Average* Kinetic Energy	[eV]			71.4	280	6.68 k	23.5 k	130 k
Maximum Kinetic Energy	[eV]			108	405	9.9 k	39.6 k	238 k

* Averaging over all incoming electrons at continuous emission

****** Start conditions R_0 = 1.5 mm, $E_k^{(0)}$ = 0.2 eV, without space charge effects

Table 8 Electron beam dynamics calculations with the code ITACA: Overview of the most important results

4.3.2. One-Dimensional Calculations, Program TRACKING

Knowing the low divergence of the beam, we can completely neglect radial effects and continue with one-dimensional calculations. This gives us a possibility to make detailed investigations using a lot of calculation points with moderate numerical effort. For this purpose we have written a simple computer code called TRACKING which can be used with personal computers. Based on the acceleration field of our cavity, phase y and energy E_k of the electrons leaving the cavity resp. hitting the cathode are calculated depending on the emission phase φ_0. The resulting data correspond quite well with the results of the ITACA simulations (Table 8).

For every gradient E there exists a critical emission phase φ_c, where for an emission phase $0° < \varphi_0 < \varphi_c$ the electrons are extracted, and for $\varphi_c < \varphi_0 < 180°$ the electrons are backaccelerated to the cathode (Figure 22 left). At small gradients $E_C \ll mc^2/(eL)$ the electrons need several RF phases to cross the cavity. L is the acceleration distance of the cavity; for our cavity L = 25 mm, and $mc^2/(eL)$ = 20 MV/m. There they periodically gain and loose energy, and their final energy, when they leave the cavity, is the same order of magnitude as the energy gained within a single RF phase. The critical emission phase is only very slightly above 90° for these gradients. With continuous emission resp. illumination the extracted current is about one quarter of the current extractable with a DC field. The time of flight for the electrons hitting back the cathode is always smaller than one RF period. At low gradients their final energy does not differ significantly from the final energy of extracted electrons. The kinetic energies of both components increase about quadratically with the gradient, as expected according to the non-relativistic approximation (Figure 22 right).

Starting at about $E_C \approx mc^2/(eL)$, the electrons can cross the cavity within one RF period, and the critical emission phase φ_c increases significantly. The increase of the kinetic energy with the gradient is only linear, because the energy gain is limited by the acceleration distance. The time necessary for crossing the cavity approaches the limit L/c, because the electrons cannot be faster than the velocity of light. The energy of the electrons hitting the cathode increases linearly with the gradient, too, and is significantly smaller than the energy of extracted electrons.

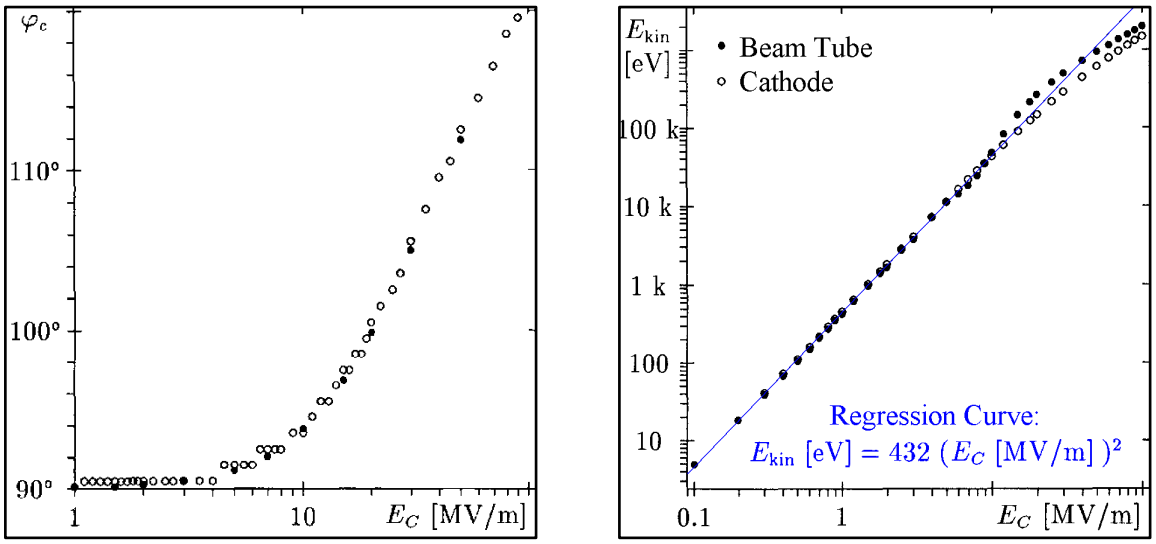

Figure 22 Critical emission phase φ_c and maximum kinetic energy E_{kin} dependent on the gradient E_c at the cathode for the 3 GHz cavity

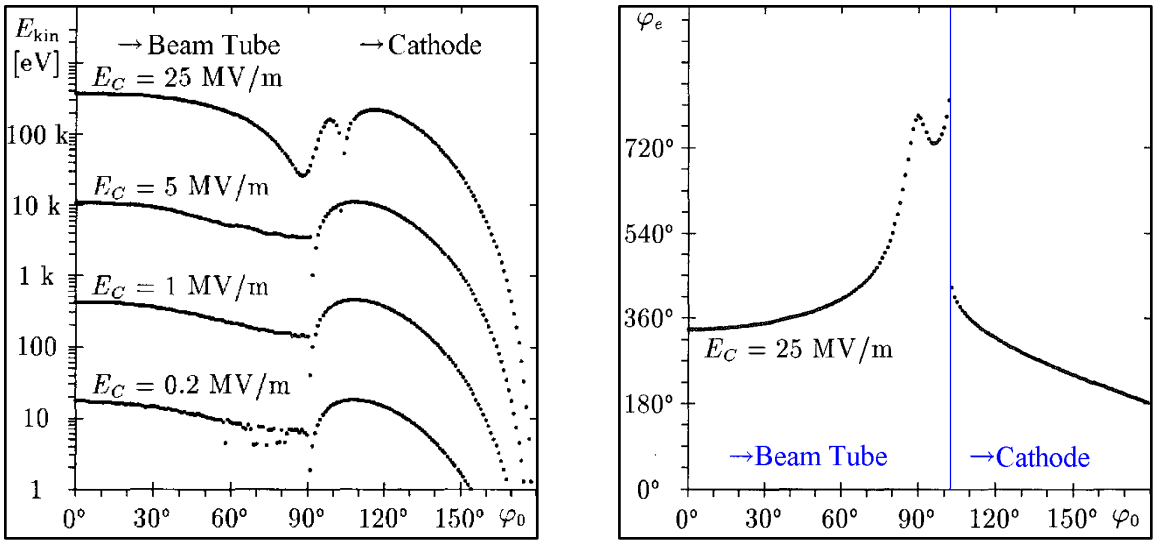

Figure 23 Kinetic energies and phases of the electrons leaving the cavity resp. hitting the cathode dependent on the emission phase φ_0

4.3.3. Consideration of Secondary Electron Emission at the Photocathode

Electrons emitted at a phase $\varphi_0 > \varphi_c$ hit the cathode again at a RF phase between 180° and 450°. They dissipate their kinetic energy in the cathode, which leads to an alteration of its photoelectric properties [83][84] and possibly to sputtering of cathode material besides the heat load. In addition, they can also generate secondary electron emission between 360° and 450° RF phase. The only difference between secondary emission and photoemission is that the emitted electrons are not excited by impinging photons, but by impinging electrons [123]. Consequently, Cs_3Sb has a high yield also for secondary emission: The secondary emission coefficient δ has its maximum $\delta_{max} \approx 6$ for electrons impinging with an energy of 750 eV [110][86].

The secondary emission has been included into the one-dimensional simulations in order to investigate its contribution to the extracted current. For this purpose the secondary emission curve $\delta(E_{kin})$ had to be parametrized. However, the shape of the normalized curve δ/δ_{max} (E_{kin}/E_{kin}^{peak}) is about the same for all materials; only the maximum coefficient δ_{max} and the corresponding kinetic energy are material dependent [120]. Thus the curve has been parametrized according to the simple equation

$$\delta(E_{kin}) = \frac{3\delta_{max}}{\sqrt[3]{4}} \cdot \frac{X}{1+\sqrt{X}^3} \text{ mit } X = \sqrt[3]{4}\,\frac{E_{kin}}{E_{kin}^{peak}} \tag{16}$$

As visible in Figure 24, this parametrization is in excellent harmony with the available measurement data. However, one should consider that at gradients above E = 3 MV/m electrons with energies above 4.5 keV will occur. Their secondary emission coefficient is no longer covered by the measurements, but assumed by extrapolation only.

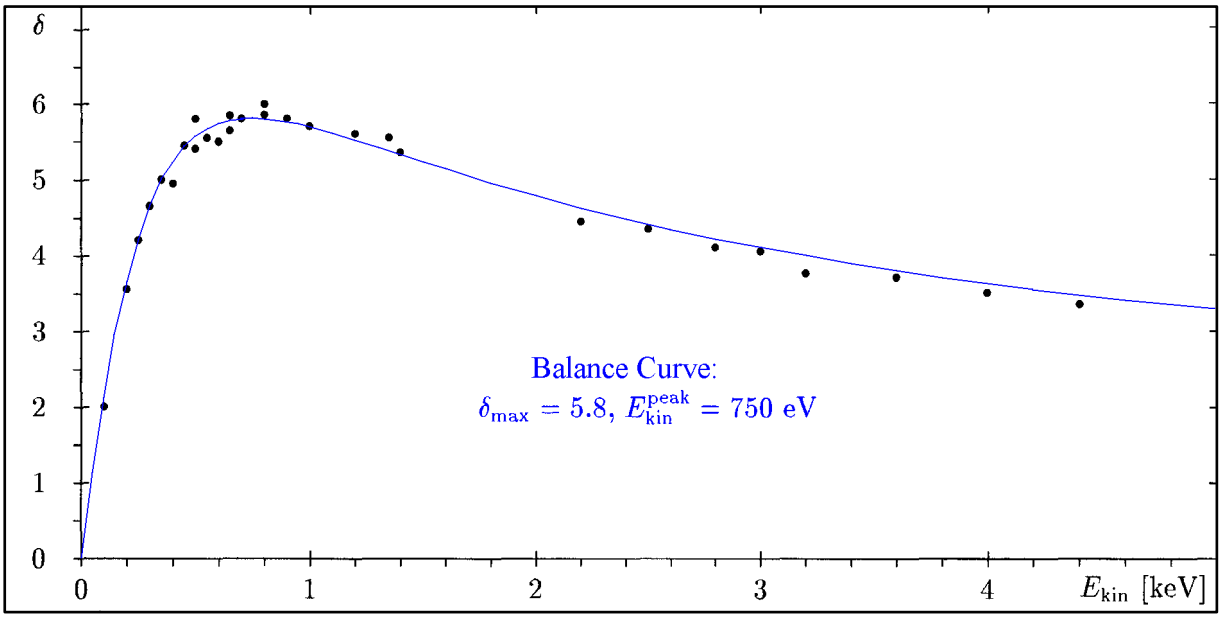

Figure 24 Shape of the secondary emission coefficient for Cs_3Sb, according to measurements [110], and parametrized according to equation (16)

The secondary emission leads to a significant increase of the extracted current up to a factor two for gradients between 1 and 2 MV/m. The contribution of secondary emission decreases again at higher gradients, and the effect of the increasing critical phase starts to dominate. Primary and secondary current can be distinguished using the simulation results: From the measurement of the extracted current in relation to the gradient one can determine the quantum efficiency of photoemission as well as the two parameters of secondary emission

(Figure 25). This enables a complete photocathode characterization with only three parameters. Although the exact analytical correlations are very complex, the three parameters can be determined with surprising accuracy from the I_p (E_C) measurement data $I_p^{(0)}$, $I_p^{\max}$, and E_C^{peak} (see Figure 29) using the equations

(17) $$\eta_Q = 4\frac{hc}{e\lambda}\cdot\frac{I_p^{(0)}}{P_{\text{Laser}}}$$

(18) $$\delta_{\max} = 8\left(\frac{I_p^{\max}}{I_p^{(0)}} - 1\right) \text{ and } E_{\text{kin}}^{\text{peak}} = \left(E_C^{\text{peak}}\right)^2 \cdot 240\left[\frac{\text{eV}}{(\text{MV/m})^2}\right]$$

The errors of this approximaton are completely dominated by the measurement errors on I_p and E_C.

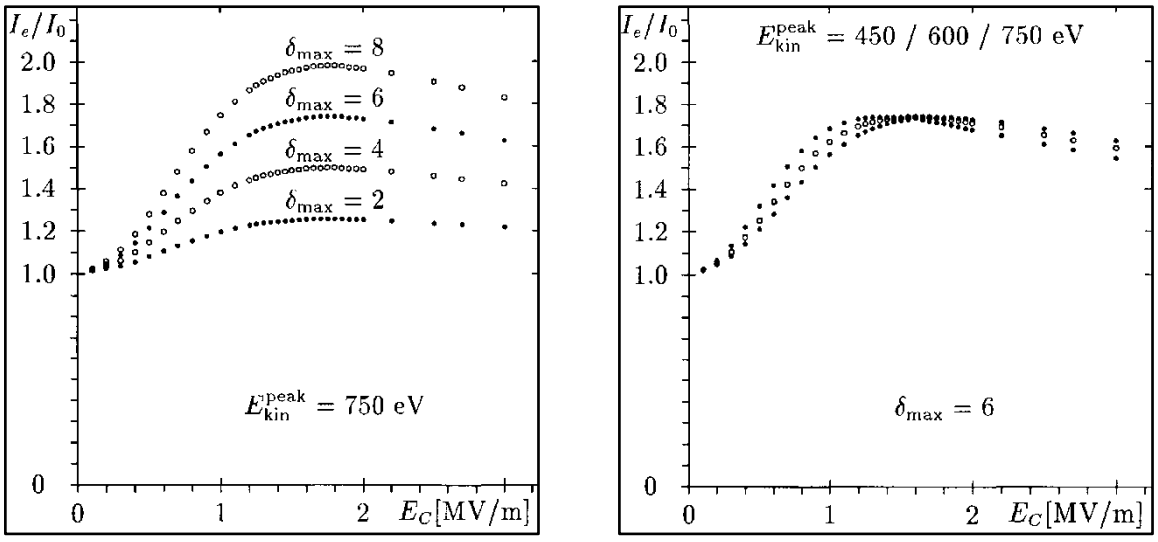

Figure 25 Extracted current dependent on the gradient for various shapes of the secondary emission coefficient $\delta(E_{\text{kin}})$

The secondary emission is continuously decreasing from 0° to 90° RF phase, thus the secondary electrons are mainly concentrated in the upper range of the energy spectrum (Figure 26). Above 90° RF phase no more secondary electrons are emitted at all, therefore no resonant secondary emission can occur, at least under these simplified conditions. In the center of the photocathode this statement will be valid also under real conditions. Concerning the border of the cathode, however, where the fields are strongly distorted and the one-dimensional approximation is certainly not valid, no corresponding statement can be made. Resonant secondary emission (multipacting) would require that a location exists, where an emitted electron hits again after exactly one RF period and causes secondary emission with a coefficient $\delta > 1$. The corresponding current increases exponentially and limits the gradient in the cavity by its power dissipaton. The high secondary emission coefficient of the photocathode promotes this effect, because the condition $\delta > 1$ is easier to fulfil.

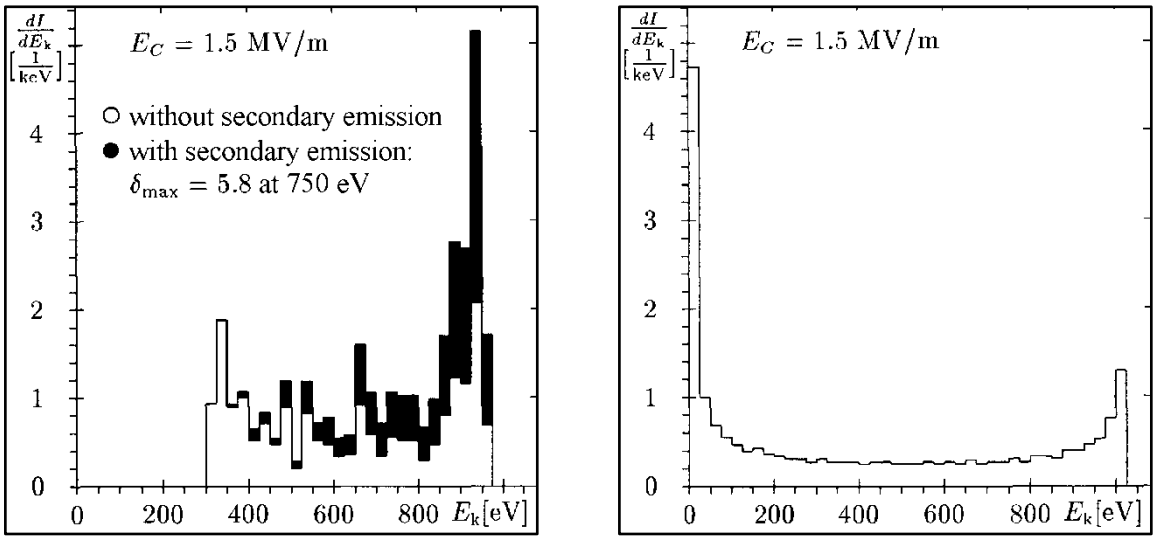

Figure 26 Energy spectra of extracted electrons with and without secondary emission (left) and of electrons hitting the cathode (right) at E_C = 1.5 MV/m

4.4. Putting Into Operation

4.4.1. Preparation Chamber and Corresponding Components

The preparation chamber has been put into operation in October 1991 as first component of the whole setup. The first aim was to condition the vacuum system and to find a suitable photocathode preparation process. In the first test of the whole system useful photocathodes should already be available. Both procedures are time-consuming and therefore were started two months in advance of the first complete system test.

The inner walls of the chamber as well as all mounted components were carefully cleaned and chemically etched if possible. Already after a few bakeout cycles (at 300°C, some components only at 250°C) a basic pressure of 2.5×10^{9} mbar could be achieved reproducibly. Also here the residual gas was composed mainly of hydrogen with about 10% carbon monoxide and 2.5% methane. But in contrary to the other chamber (section 3), also active gases could be detected here, namely water (3x $l0^{-11}$ mbar) and carbon dioxide (10^{-11} mbar). Noble gases are nearly undetectably low, the most frequent compound was argon at about 2×10^{-12} mbar. The total pressure is two orders of magnitude higher than in the other chamber, which is probably caused by the history of this device, especially of the ion pump: In contrary to the components of the other system, these components were not new, but already used for other purposes during a long time. Considerable amounts of gas are alredy gettered inside the ion pump, a small part of which is desorbed again during the further operation. Thus the equilibrium pressure of the pump is considerably increased.

In this preparation chamber we used for the first time the alkali metal dispenser sources of the company SAES Getters SpA., where the reducing alloy (84% Zr, 16% Al) at the same time serves as getter material for generated gases [213][219]. All the time several Cs sources have been mounted in parallel; we didn't use other alkali metals yet. After the standard bakeout cycle these sources showed an acceptably low gas generation during operation, in agreement with corresponding publications [209]. It is difficult to calibrate the evaporation rates of these sources, because they vary continuously during the short lifetime of the sources. In addition, the data of a single calibration show a certain spread (see Figure 27 right). The reason for that spread is not yet clear; possibly the used quartz microbalance is not well suited for cesium. As a rule, the evaporation process of cesium was guided by the measured pho-

toemission, which required no calibration of the source. The employed antimony sources had the same technical setup, but were filled with pure antimony only. Their calibration curves were much more stable (see Figure 27 left), but varied also between several sources and even for one source during its lifetime. It seems to be important whether the antimony inside the source has already been molten once and wetted the surface. The gas generation of the antimony sources was quite low, too (Table 9). The gas leak valve for controlled gas exposition of the cathode has been neither calibrated nor used yet.

Operating Situation	Partial pressure [mbar] of components					
	H_2	CH_4	H_2O	N_2+CO	Ar	CO_2
Basic pressure of the chamber	3×10^{-9}	8×10^{-11}	3×10^{-11}	3×10^{-10}	2×10^{-12}	10^{-11}
Operation oft he cathode heater; cathode temperature 59°C	$1.5\ 10^{-8}$	3×10^{-10}	2×10^{-10}	2×10^{-9}	10^{-11}	10^{-10}
Operation of an Sb source; heater current 4.7A	6×10^{-8}	10^{-9}	2×10^{-10}	10^{-8}		10^{-9}
Operation of an Cs source; heater current 6.5A	2×10^{-8}	6×10^{-10}	2×10^{-10}	4×10^{-9}		10^{-10}

Table 9 Residual gas composition of the preparation chamber at various operation conditions

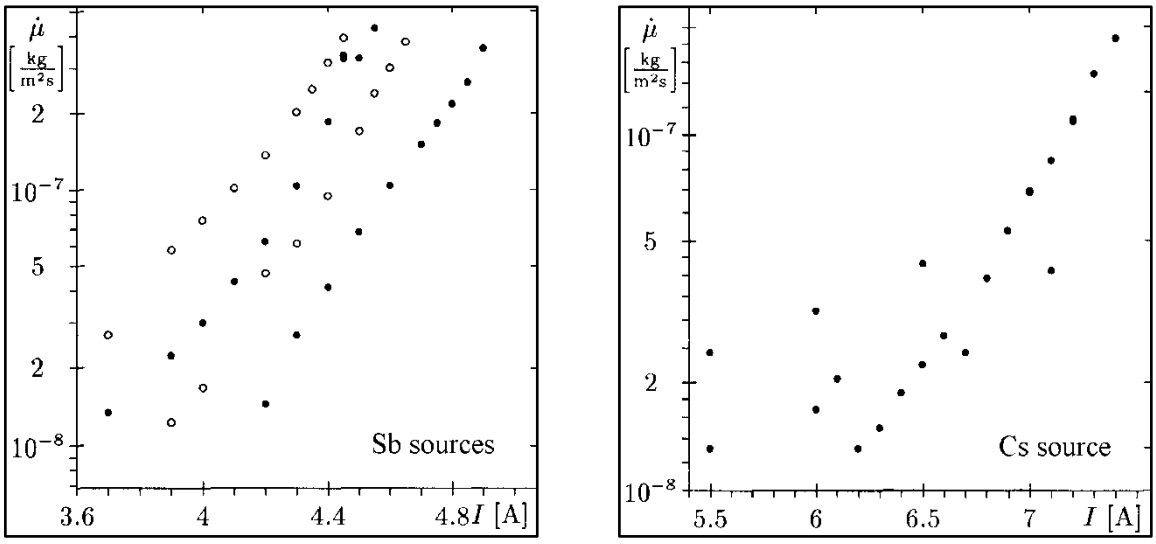

Figure 27 Characteristic evaporation rates of the antimony (left) and cesium sources (right), according to measurements with the quartz microbalance

The heater for the cathode stem showed to be only partially suited for the intended purpose: The bad thermal transfer between cathode stem and heater causes a strong temperature gradient, and the cathode itself can be heated only to about 150°C instead of the desired 600°C. Thus a cleaning of the cathode stem (by annealing) is actually not possible in situ. The stem must be taken out of the chamber for cleaning, if required. However, the temperature range necessary for photocathode preparation is fully available and can be controlled with a thermocouple pressed onto the cathode surface.

When the chamber was open, we could measure with the photoradiometer that only about 50% of the laser power reach the cathode inside the chamber. A considerable amount of light is lost at the vacuum viewport (of the beam tube), which is made from Al_2O_3 to allow also

measurements with ultraviolet light. The anode shows the typical current-voltage characteristics (Figure 28). From the lower voltage region a perveance of about $10^{-8}\ \mathrm{A/V^{3/2}}$ can be determined. Although at 150 V bias the current is not yet completely saturated, this value has been used for all further measurements without correction. The corresponding field strength at the cathode is about 3 kV/m. However, the sources are in front of the cathode during evaporation and shield it from the electric field of the anode, and they hamper the illumination of the cathode with the laser. Additionally, they emit a non-negligible thermionic current during operation. Therefore the photoemission current practically cannot be controlled during cesium evaporation with the actual setup. Thus the cesium evaporation is done in short stages (between three and ten minutes) with intermediate control of the quantum efficiency. A continuous control would be possible, if the photoemission current could be measured via the cathode instead of the anode. With a negative bias voltage of the cathode also the thermionic emission of the sources would no longer disturb.

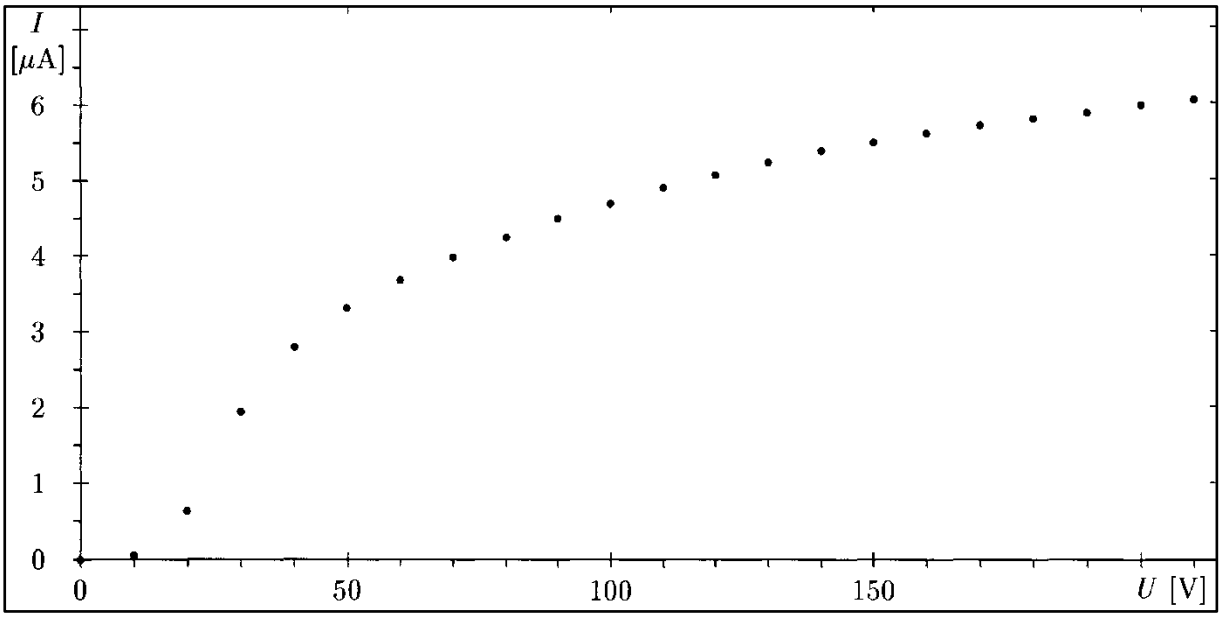

Figure 28 Current-voltage characteristic of the anode-cathode setup; the regularly applied bias voltage is +150 V at the anode

4.4.2. Preparation of Photocathodes

The standard procedure for the preparation of Cs_3Sb photocathodes [97], which also has been successful in the independent preparation chamber, could not be adapted here without modifications. The layers prepared according to this procedure showed no or only very low quantum efficiency (below 3×10^{-4}). Only after one month of laborious experiments photocathodes with 1-2% quantum efficiency could be prepared for the first time. Another month of work was necessary to clear the influences of the various parameters, until these preparations could be done with acceptable reproducibility.

The most important modification concerned the temperature of the cathode during cesium evaporation. Usually the preparation is done at substrate temperatures between 120°C and 150°C. The experiments in the independent chamber showed in addition that a preparation at lower temperature is also possible, only the diffusion of cesium into the antimony layer and the formation of the correct stoichiometry took a longer time. However, successful preparations could only be done between 50°C and 65°C in this chamber. The reason will probably not be found in different preparation conditions, but in incorrect temperature determination: The temperature of the cathode is measured with a small thermocouple pressed onto the ca-

thode surface with a titanium spring. A direct contact to the cathode (for example by point welding) is not possible, because the cathode stem must remain movable for transfer. Thus a considerable thermal gradient can be formed between cathode and thermocouple, which is quite difficult to estimate. In addition, the cesium source with an operation temperature between 550°C and 850°C during evaporation is only 20 mm away from the cathode [213]. If the cathode layer has a bad thermal conductivity, the crucial uppermost layer could be considerably superheated by heat radiation without considerable effect on substrate and thermocouple. As a matter of fact, a temperature increase between 5-10°C is observed at the thermocouple during operation of the sources. Both effects shift the true cathode temperature in the correct direction, however it could not yet be determined whether they can completely explain the discrepancy between expected and measured value.

The most important result is, nevertheless, that successful preparations can reliably be done when the temperature is correctly chosen, and that the results are comparable with other experiments. Quantum efficiencies between 1% and 3% could be achieved in a lot of preparations on the niobium stem; successful preparations are listed in Table 10. However, the procedure was not yet reliable in the sense that every preparation directly produced a good photocathode. In a lot of trials, the antimony layer could not or only weakly be activated by cesium. The preparations showed yet more peculiarities: The lifetime of the layers was only about 12 hours, which cannot be explained exclusively with the fair vacuum conditions. The cesium consumption was much higher than expected, and varied strongly between the individual preparations; the same is valid for antimony: Until now, photocathodes based on extremely thin antimony layers, as done in the other chamber (3-7 $\mu g/cm^2$ Sb), could not be successfully prepared here. Above all, the extremely high quantum efficiencies of 5-10%, as realized in the other chamber, could not be achieved here.

During these preparations we noticed that much better photocathodes were generated on the shield directly besides the cathode than on the cathode stem itself, although the preparation conditions were quite the same. The only remaining difference was the material of the substrate, namely copper and titanium instead of niobium. Consequently, in February 1992 we covered the top of the niobium stem with copper and tried to prepare photocathodes onto this copper layer. We instantaneously got very good results, and most of the problems described above disappeared. Therefore all further preparations until now were done onto an intermediate copper layer.

The simplest and best procedure to cover the niobium stem with a copper layer is evaporation in high vacuum; galvanic procedures yielded no useful copper layers. Until now, the thickness of the copper layers was not controlled, by estimation it is in the order of 100 nm to 1 μm. The covering with copper has been performed externally hitherto, however, a copper evaporation source could be included in the preparation chamber, too. Then the layer thickness could be measured with the quartz microbalance. The preparation process onto the intermediate copper layer is the same as onto the bare niobium stem. The same low substrate temperature is used, however, the cesium consumption to achieve maximum quantum efficiency is considerably lower. At the same time the achievable quantum efficiencies are increased by a factor two, they now are between 3% and 5% (see Table 10). The preparations are now more reliabe than without copper layer. Also the lifetime of the cathodes is increased, it now amounts several days and can be explained with the vacuum conditions in the chamber. However, we were not yet successful to prepare useful photocathodes with extremely thin antimony layers on the copper substrate, too.

Sb layer [μg/cm²]	Temperature of cathode	Quantum eff. at 543 nm
33	60°C	0.93%
Reactivated	60°C→50°C	2.1%
+40	55°C	1.8%
20	54°C→45°C	1.2%
+13	52°C	1.7%
+27	50°C	0.32%*
27	62°C	1.7%
+13	59°C	1.8%
+37	58°C	2.7%
+20	58°C	1.2%
+13	58°C	1.35%
+13	62°C	1.85%
Reactivated	25°C	1.8%
+13	60°C	1.6%

* Inside the cavity in Test No.1

Sb layer [μg/cm²]	Temperature of cathode	Quantum eff. at 543 nm
33	62°C	2.85%
+13	60°C	5.0%
80	56°C→48°C	1.35%*
+13	56°C	0.65%*
33	55°C	4.65%
+13	54°C	5.1%
33	55°C	2.95%**
+13	56°C	4.05%**
+33	56°C	4.75%**

* Inside the cavity in Test No.4

** Inside the cavity in Test No.5

Table 10 Successful preparations of Cs_3Sb on niobium stems without (left) and with copper layer (right)

The fact that Cs_3Sb photocathodes can be prepared easier and better on copper than on niobium is astonishing, especially because we were able to produce excellent photocathodes on niobium in the other chamber. In fact, they were yet superior to the ones prepared on copper here. An important difference between that chamber and this one is the possibility to anneal the niobium substrate at 600°C in situ. Niobium exposed to the normal atmosphere is covered with a thin but firm Nb_2O_5 layer, which is dissolved at temperatures above 600°C (the oxygen diffuses into the bulk niobium). Possibly the niobium pentoxide prevents the formation of Cs_3Sb, while copper and pure niobium promote it. First results from successive Auger spectroscopy at Cs_3Sb layers (performed by our collaboration partners at INFN Milano together with the University of Modena) show a sharp boundary between (oxide-covered) niobium and Cs_3Sb, while copper and Cs_3Sb diffuse into each other. We couldn't yet investigate whether this effect also occurs with oxide-free niobium. In order to clear this question we would like to anneal the niobium stem at 600°C also in this chamber.

As a conclusion we can say that we can reliably produce photocathodes using the modified preparation process, if we employ an intermediate copper layer. These photocathodes have a high quantum efficiency and are suitable to be operated inside the superconducting cavity. The achieved lifetimes make it possible to produce the photocathodes without deadline pressure and to store the layers for some hours before transfer, if required. Yet desired improvements are good photocathodes on bare niobium as well as the preparation of extremely thin Cs_3Sb layers in order to reduce their RF losses inside the cavity.

4.4.3. Superconducting RF Cavity

The half-cell of the cavity was deep-drawn from niobium sheet and has been provided by the TH Darmstadt. End plate and filter were turned from niobium logs; the filter groove was spark-cutted. All these components were produced from niobium of high thermal conductivity (RRR 250). Beam tube and cathode stem were produced from niobium tube resp. rod of lower quality. We have then etched the semi-finished components (about 50 μm removal), plugged them together, and measured their RF properties. Next, the filter was tuned to the cavity under careful consideration of the future weld shrink. Then the components were electron-beam welded at our collaboration partner CEBAF. After careful inspection of the weld joints the filter was again tuned to the cavity, and finally the complete system etched with about 20 μm removal.

Before the first test the cavity was annealed in an UHV furnance at 1350°C with titaniun envelope. All impurities on the cavity surface vaporize or diffuse into the bulk niobium under these conditions, and the cavity theroretically has a defect-free surface after annealing [145]. Titanium also vaporizes perceptably at this temperature; a portion of the evaporated titanium is condensed again at the outer surface of the cavity. The established titanium layer getters interstitial impurities from the bulk niobium (hydrogen, oxygen, nitrogen), which are movable at this temperature. The bulk niobium is purified and achieves a higher thermal conductivity, potential defects in the superconducting surface are better cooled and stabilized. The openings of the cavity were covered with niobium caps to protect the inner surfaces against titanium vapour. However, these caps were not allowed to seal the cavity completely, because the internal volume yet had to be pumped efficiently. An excellent vacuum is necessary, otherwise the residual gases would diffuse into the bulk niobium and generate new interstitial impurities there. No chemical etching has been performed between the annealing with titanium envelope and the first test for two reasons: On one hand, the defect-free surface generated by the annealing should be preserved. On the other hand, we feared that an additional surface removal would deteriorate the tuning of the filter again; the material removal by etching has a much stronger frequency effect on the filter than on the cavity. The cavity is mounted to the cryostat system under dust-free conditions as far as possible. However, a completely dust-free mounting is not possible with this system, because the vacuum volume of the cavity cannot be locked with a valve, and is inevitably open during the transport to the cryostat.

The first test of the whole system (including operation with liquid helium) has been performed in December 1991. The quality factor of the superconducting cavity was disappointingly low: At 4.2 K the unloaded quality was 1.5×10^7; cooldown to 1.9 K produced only an improvement to about 2.5×10^7. We had expected an unloaded quality of about 5×10^7 at 4.2 K with an improvement of up to two orders of magnitude at 1.9 K. Also the power coupling did not work as expected, and due to the low quality we could achieve only about 1.5 MV/m gradient at the cathode with the available RF power (Table 11). At these gradients no electron loading could be detected in the cavity (without Cs_3Sb photocathode). However, the unloaded quality showed significant jumps during operation at the highest achievable gradients.

Initially, we assumed that the low quality of the cavity was caused by impurities at the cavity surface, especially because we had some problems during installation, which could have produced this contamination. Before the next test, the cavity was cleaned with concentrated nitric acid, but not etched in order not to disturb the filter tuning, and finally annealed at 850°C in the UHV furnance. In the following test (No. 3; test No. 2 had to be abandoned due to problems with the main coupler), however, the quality was exactly as bad as before. The values of the two tests were so exactly the same that we had to assume a common reason,

namely that some titanium vapour penetrated to the inner surface during the first annealing. It is well known that low amounts of titanium diffused into niobium surfaces strongly increase the residual surface resistance, and can only be removed by a complete surface removal of about 50 μm.

Consequently, the cavity was chemically etched and about 40 μm of its surface removed before the next test. A strongly buffered acid mixture has been used (BCP 1:1:4) to prevent a superheating in the filter area. Then the cavity was rinsed with ultrapure water and dust-free mounted as far as possible, but not annealed again. In fact, in the next test the quality was between 3.6×10^7 and 4.3×10^7 at 4.2 K, close to the expected value. During cooldown to 1.9 K the quality increased to about 7.5×10^8. However, this vaue could not be reproduced after the second helium filling: The quality reached only 4×10^8at 1.9 K, before any photocathode had been transferred to the cavity. For the first time, higher gradients could be achieved in the cavity under these conditions. At about 1 MV/m gradient (reference value is always the gradient at the location of the cathode), the cathode stem (not yet covered with a photocathode) became normalconducting and limited the cavity quality to about 2×10^7. This jump was shifted up to about 3.5 MV/in gradient in pulsed operation. A more accurate investigation showed that the thermal coupling of the cathode to the helium bath is much too weak. However, a solution of this problem requires extensive construction modifications at cathode stem and cavity. Thus, the maximum gradient was power-limited to about 9 MV/m (at $Q_0 = 2\times10^7$) with cathode stem. Without cathode stem, electron loading of the cavity occured at about 10 MV/m, finally limiting the gradient to 14 MV/m.

We suspected that the quality was yet limited by titanium contaminations of the niobium surface, and again chemically removed about 20 μm. Thereafter a renewed tuning of the filter was necessary. Finally, the cavity was again chemically etched for a very short time, rinsed with ultrapure water, and mounted under dust-reduced conditions. However, in the following test No. 5 only qualities of 3×10^7 at 4.2 K and 10^8 to 1.7×10^8 at 1.9 K could be achieved. Titanium can no longer be the reason for the low quality. Actually, we assume that adsorbed gases at the cavity surface limit the quality. This hypothesis is supported by the fact that the vacuum in the beam tube was normally quite fair during cooldown: At the ion pump we typically measured about 10^{-7} mbar, which enables up to 10^{-5} mbar inside the cavity. For the present this effect can only be avoided by a long pumping period, because a bakeout of the cavity vacuum is not possible without modifications. Nevertheless, also in this test gradients up to 12 MV/m could be achieved, where again strong electron emission occured.

The field strength in the cavity was limited by technical problems during the first three tests; the very low values of $E_C^{\max}$ are therefore without interest. In the tests No. 4 and No. 5 dark electron emission occured already below E_C = 10 MV/m, finally limiting the maximum field strength. The dark currents could be seen as drop of the quality curve (electron loading) and at the same time were extracted to the inner tube. With the installed telescope we could see two or three tiny but bright spots at the border of the cathode bore shining simultaneously with the dark current. A diffuse reflexion was an indication for further spots, probably located at the iris. The size of the shining spots could not be resolved with the telescope, they must have been smaller than about 0.1 mm. As far as observable, the spectrum of their light was continuous and indicated thermal, not plasma radiation. The bright spots could not definitely be identified as the dark current sources, but they exclusively occured at locations of high electric field, and their brightness was strongly correlated to the intensity of the dark currents. These spots must at least have caused thermionic emission; according to their colour their temperature must have been far above 1000°C. With higher gradients, a diffuse violet glowing could be observed at the same time in an annular area around the cathode, which however

had no sharp boundary. This glow coud not be located along the beam axis; it could have been generated near the cathode as well as near the viewport.

Test No.	Preparation procedure	Q_0 (4,2 K)	Q_0 (1,9 K)	E_C^{Onset} [MV/m]	E_C^{max} [MV/m]	I_e^{max} [nA]
1	After welding: Filter tuning; chemical etching 20 μm, UVH annealing at 1350°C with titanium envelope	1.5×10^7	2.5×10^7	-	1.5	-
2	Cleaning with HNO_3, UHV annealing at 850°C	Problem at the RF coupler; test abandoned				
3	No new preparation; cavity remained mounted	1.5×10^7	2.5×10^7	-	4.2	-
4	Chemical etching (BCP 1:1:4) 40 μm, water rinsing	4.2×10^7	7.5×10^8	10	14	2300
5	Chemical etching 20 μm, filter tuning, chemical etching 5 μm, water rinsing	3.3×10^7	1.7×10^8	8	12	96

Table 11 Preparations and initial measurement values of the cavity at various tests

Actually, we discuss two possible models to explain the bright spots: The first model assumes that they are locations of defects, which initially produce RF field emission due to geometrical field superelevation [138][124]. Those badly cooled defects are heated resistively by the field emission current, until an equilibrium with the radiation cooling is installed. The resulting current is caused by a combined thermionic and RF field emission; it is finally limited by the formed space-charge. This model favours very small defects, because field superelevation and resistivity increase with decreasing dimensions of the defect. The other model also starts with badly cooled, but dielectric defects, which are heated by the high electric RF field. Thermionic emission occurs at a sufficiently high temperature, and the emitted current is extracted. This effect however favours bigger defects, because the relative efficiency of radiation cooling is decreasing with increasing radius. Until now, we have no satisfying explanation for the diffuse violet glowing. Possibly it is emitted by a plasma generated from the electrons hitting the wall of the inner tube.

4.5. Test Results

Since starting of the system in December 1991 until now, six photocathode layers could be transferred into the cavity and measured there. As a rule, these measurements were done according to the following scheme: Initially, the cavity was measured without photocathode (the cathode stem either bare or withdrawn). Then a Cs_3Sb layer was prepared onto the cathode stem and characterized yet inside the preparation chamber. Subsequently, the photocathode was transferred to the cavity as soon as possible. There it was measured under various operation conditions (see below). Finally, the photocathode was transferred back to the preparation chamber and characterized there again. In parallel, also the empty cavity was measured again to control eventual contaminations from the photocathode. A series of interesting results could already be achieved using this scheme, although the test system yet has several shortcomings. In particular, the operation of photocathodes in the cavity was always combined with electron bombardment of the cathode, because only the continuously emitting laser was available.

Already in test No. 1, for the first time a Cs_3Sb photocathode layer could be operated inside the cavity. However, due to the low cavity quality and due to probems with the coupler, it

could be operated with gradients up to 0.3 MV/m only (finally up to 0.5 MV/m). In addition, this layer had a quite low quantum efficiency of about 0.5% and was very instable already during the measurements. Thus the results gained in that test are only of minor interest. In the tests No. 4 and No 5, in contrary, two resp. three good photocathodes could be transferred to and operated inside the cavity. All those measurements have been performed with a bias voltage of +150 V at the inner tube serving as anode. The extracted current was considerably lower without bias, although this DC voltage causes only very small gradients inside the cavity. Probably the bias voltage focuses the electrons which enter the beam tube to the inner tube and prevents them from being blown to the outer tube by their own space charge. One must consider that at 0.6 MV/in gradient the extracted electrons have an energy of 150 eV.

4.5.1. Behaviour of the Photocathodes Inside the Superconducting Cavity

The photoelectric characterization of a cathode inside the cavity was normally done by measuring a complete I_p (E_C) curve: The current I_p, extracted with illumination was measured from very low gradients $E_C < 0{,}1$ MV/m up to the onset of dark currents (or in the reverse direction). Due to the large contribution of secondary emission to the extracted current single measurements at a fixed gradient are not sufficient to completely characterize the layer. The obtained curve shapes were always consistent with the predictions of the simulation calculations (including secondary emission). Besides the quantum efficiency η_Q^{HF} also the maximum secondary emission coefficient δ_{max} and the corresponding kinetic energy E_{kin}^{peak} could be obtained from the curves. A typical example of such a curve, its correspondence with the simulation results, and its parametrization is shown in Figure 29. The sharp decrease of the extracted current below 0.1 MV/m is caused by the decreasing extraction efficiency at low gradients.

The complete investigation of a Cs_3Sb layer inside the cavity normally consists of a characterization at the beginning and after various operation stages (see Table 12). It can be observed how the parameters of the photocathode are varied by the different operation conditions. In fact, the parameters of photo- and secondary emission showed strong variations during operation. The reasons of these changes can be divided into two groups: On one hand the pure operation of the photocathodes inside the cavity with corresponding photo- and field emission, on the other hand the transfer of the layers between cavity and preparation chamber and the helium refill into the cryostat.

Quantum efficiencies between 0.5% and 13.5% at a wavelength of 543 nm have been measured with this method at photocathodes inside the cavity. The statistical error of these measurements amounts between 10% and 20%, depending on the quality of the curve. The main error source is the extrapolation $I_p^{(0)}$ of the curve towards zero gradients. We don't yet know why the quantuni efficiencies η_Q^{HF} initially and finally measured in the cavity do not correspond with the values η_Q^{DC} measured before resp. afterwards in the preparation chamber: They differ by up to a factor two. It is noticeable that the quotient η_Q^{HF}/η_Q^{DC} is about the same for there and back transfer for a single layer, but varies from layer to layer within a single test (compare Table 12). This systematics cannot be explained with variations of the layer during transfer; it indicates either a strong systematic error in our measurements or a temperature dependence of the quantum efficiency. However, we expect only a slight change of the yield with the temperature, because we operate the layers considerably above the threshold energy [67]. A direct DC measurement of the quantum efficiency inside the cavity would help a lot to understand this effect. For this purpose, the inner tube must project into the cavity, which will soon be possible thanks to a longer shift distance.

Activities / parameters of continuous operation					Parameters of the photocathode			
Operation mode*	E_C [MV/m]	I_e [μA]	T [s]	W_C [J]	$I_p(E_C)$ No.	η_Q^{HF} (543 nm)	δ_{max}	E_k^{peak} [eV]
Layer No. 1-1 prepared: η_Q^{DC} = 0.32%; Transfer					1/1b	0.72%	n.d.	n.d.
Layer No. 4-1 prepared: η_Q^{DC} = 1.35%; Transfer					4/1a	2.6%	7.5	400
PE	2.0	2	300	1.2				
Measurement of field emission up to 4.6 MV/m								
Operation with cathode withdrawn								
Helium refill					4/1b	2.0%	6.5	≅ 600
PE	1.9	0.97	600	1.0				
FE	5.0	40	1200	600				
Backtransfer: η_Q^{DC} = 0,9%								
Layer No. 4-2 prepared: η_Q^{DC} = 0.65%; Transfer					4/2a	1.1%	(≅ 2)	≅ 400
Measurement of field emission up to 5.5 MV/m					4/2b**	1.4%	≅ 8	n.d.
Helium refill					4/3a**	0.85%	≅ 9	≅ 550
PE	2.6	0.47→0.555	600	1.0				
FE	6.7→4.3	40→0.8	300	10				
PE	3.0→2.6	0.48→0.6	600	1.3	4/3b**	1.2%	7.5	≅ 550
Operation with cathode withdrawn								
Backtransfer: η_Q^{DC} = 0.36%								
Layer No. 5-1 prepared: η_Q^{DC} = 2.7%; Transfer					5/1	1.3%		n.d.
PE	2.7→2.5	0.425→0.93	1800	5	5/2	2.0%	≅ 11	n.d.
Heliurn refill					5/3	2.2%	7	600
PE	5.0→3.8	0.69→0.81	600	5	5/4	1.3%	12.5	800
FE	5.6	1.2→0.03	300	1				
PE	6.0→4.7	0.36→0.27	600	3	5/5	0.65%	12	750
Backtransfer: η_Q^{DC} = 2.3%								
Layer No. 5-2 prepared: η_Q^{DC} = 3.9%; Transfer					5/6a	4.4%	(14)	(360)
Rückwärts-Messung					5/6b	5.8%	8.5	n.d.
PE	1.25	3.5→2.5	1200	3	5/7	4.4%	9	≅ 400
Measurement of field emission up to 5.3 MV/m					5/8	4.4%	8	400
PE	2.5	2.2	600	4.1	5/9	4%	9	450
Helium refill					5/10	1.75%	(11)	n.d.
PE	3.0	1.2→1.67	900	6	5/11	3.5%	7.5	500
FE	6.7→5.9	160	600	2000	5/12	0.55%	6	350
PE	2.25	0.3	300	0.2	5/13	0.65%	6.2	400
Backtransfer: η_Q^{DC} = 0.4%								
Layer No. 5-3 prepared: η_Q^{DC} = 4.65%; Transfer					5/14	9%	(15)	n.d.
Wiederholung der Messung					5/15	13.5%	5.8	700
PE	0.7→0.5	4→3	300	0.25	5/16	9.1%	≅ 8	n.d.
Backtransfer: η_Q^{DC} = 4.8%								

* FE: Operation with field emission; PE: Operation with photoemission

****** Curve shows an enhancement with peak at 1.0 MV/m; see text on page 70

Table 12 Parameters of photo- and secondary emission dependent on operation conditions for the Cs_3Sb layers investigated inside the cavity

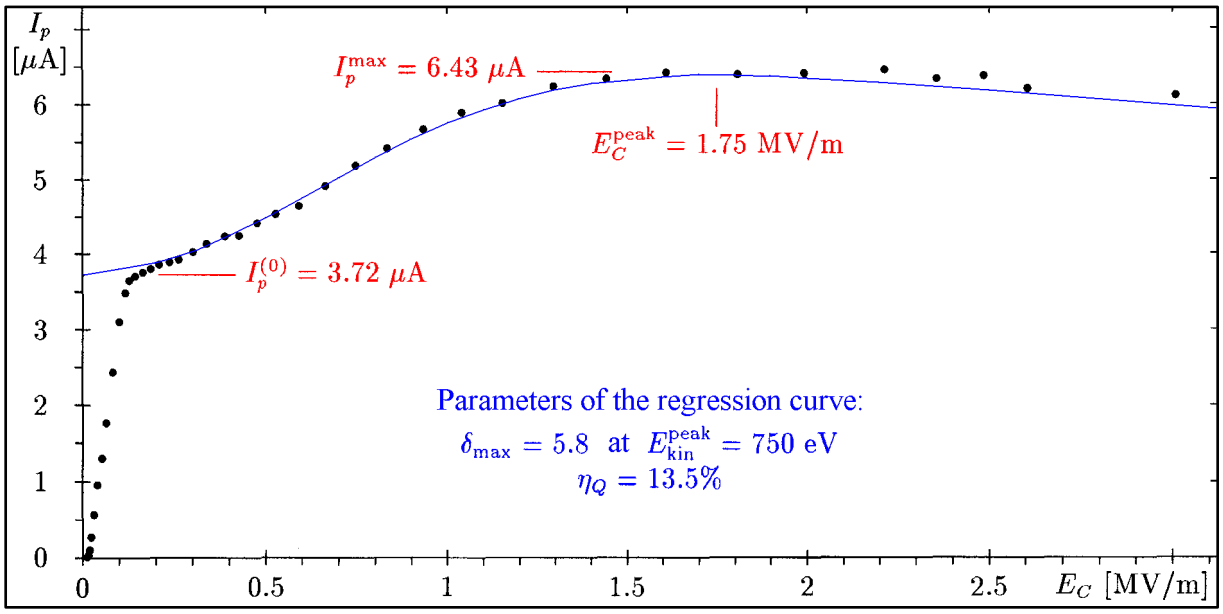

Figure 29 I_p *(Ec)* Curve of a Cs_3Sb layer: Measured points, simulation result, and pararnetrization, according to measurement No. 5/15

The secondary emission coefficients δ_{max} measured in the RF field are between 6 and 12, up to a factor two higher than quoted in literature. Surprisingly, their variations show no correlation with the simultaneously measured quantum efficiencies. However, a systematic error is quite unlikely here, because the result is the quotient of two data and thus bases only on relative measurements. The relative error of these values is also between 10% and 20%; it is mainly caused by the extrapolation of $I_p^{(0)}$ from the curve, too, because the peak value can be determined quite accurately. The kinetic energy E_{kin}^{peak} corresponding to the maximum of the coefficient gave results between 400 eV and 800 eV from our measurements. However, they are rather inaccurate due to the flat shape of the curve near the peak. The relative error amouts to values between 25% and 50%; in several cases no reliable value for E_{kin}^{peak} could be determined at all.

Changes of the quantum efficiency and also of the secondary emission coefficient in both directions have been observed during operation of the Cs_3Sb photocathodes. Obviously, the changes depended on the emitted current and on the accelerating gradient besides the actual status of the photocathode. Probably, this is not an effect of the emission itself (which would depend on the current, but not on the gradient), but an effect of the bombardment with back-accelerated electrons. Such effects have already been reported earlier from Cs_3Sb photocathodes [83] and were expected here. However, an additional effect caused by the emission itself cannot be excluded; a corresponding investigation would require a synchronized-pulsed light source. These measurements have been performed with pulsed operation as far as possible in order to suppress changes of the photocathode already during measurement of the I_p (E_C) curve; the laser has been opened only for a short time at each data point. Nevertheless, this effect sometimes occured, especially with new Cs_3Sb layers, which above all led to wrong values of δ_{max}; in Table 12 these values are put in brackets.

The parameters of continuous operation, as listed in Table 12, are the field strength E_C, the emission current I_e, the operation period t, and the energy W_C deposited at the cathode by backaccelerated electrons. The existing measurements indicate that newly prepared cathodes can be modified easily and with low energy by electron bombardment. They gradually stabilize and require more and more energy for further changes. We could not yet decide whether

only the power density or also the energy spectrum of the backaccelerated electrons determines their effectiveness. Changes of quantum yield during operation occured in both directions; we could observe an increase by a factor two as well as a decrease by a factor ten. We couldn't yet find systematics for this effect, too. Further measurements are necessary to improve the statistics of the data base. Sometimes even both effects occured during a single operation, as shown in Figure 30. However, photo- and secondary emission are not separated in this measurement. Possibly, the increase is caused by the secondary emission and the decrease by the photoeinission resp. vice versa. As a rule the secondary emission is more stable and changes much slower than the photoemission, but changes in both directions have already been observed for this parameter, too.

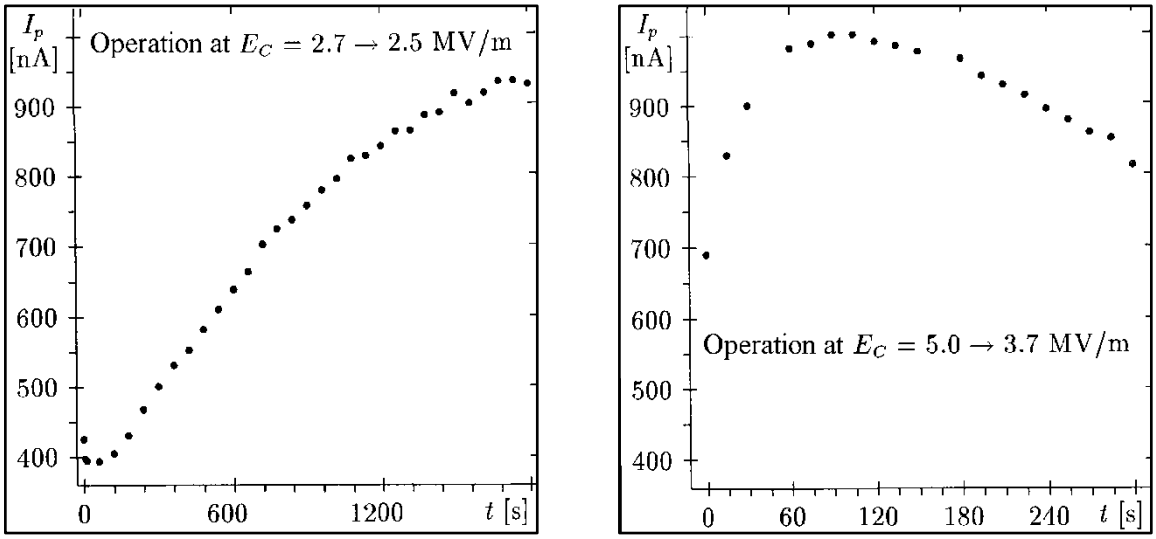

Figure 30 Variation of the extraction current during operation, according to continuous I_p (E_C) measurements No. 5/1 and No. 5/2

The changes which the parameters of photo- and secondary emission showed after transfer or helium refill were surely caused by reaction with residual gases. The vacuum tube used for the transfer partially remains at room temperature, but cannot be baked out. Thus it provides much worse vacuum conditions than the preparation chamber or the cold cavity, which affects the cathode during the transfer. During the refill of liquid helium, initially a small amount of warm helium gas floats into the croystat. It heats the cavity which is no longer covered with liquid helium and causes the partial desorption of gases frozen at the inner walls of the cavity. As a rule, this mechanism leads to a significant decrease of quantum efficiency and secondary emission coefficient. However, in one case also a slight increase of quantum yield could be observed after helium refill. It must be noted that Cs_3Sb layers affected by residual gases are again more sensitive to electron bombardment.

Deviating from all other layers, the layer No. 4-2 shows a peak in its I_p (E_C) curve superimposing the usual shape at about 1.0 MV/m. The I_p (E_C) curve of the fresh layer initially showed the usual shape just after transfer. The peak occured for the first time after an operation at high gradients with field emission. It consists of an increase of the extracted current respective to the normal behaviour between 0.5 and 1.5 MV/ni; at the maximum near 1.0 MV/m the curve is at least four times superelevated. After a subsequent helium refill the peak is only visible between 0.8 and 1.2 MV/m yet. The superelevation in the maximum is only about 20%, but the maximum is still located at the same gradient. After another continuous operation with photo- and field emission the peak has become higher again, but not broader: The maximum is still located at 1.0 MV/m and shows a superelevation of at least a factor two (Figure 31). This strange shape cannot be explained with our simple one-

dimensional calculations. We assume that it is caused by resonant secondary emission at the border of the cathode, which especially would explain the fixed gradient of 1.0 MV/m given by the geometric resonance condition. The varying height of the peak would then indicate varying secondary emission coefficients at the location of this effect.

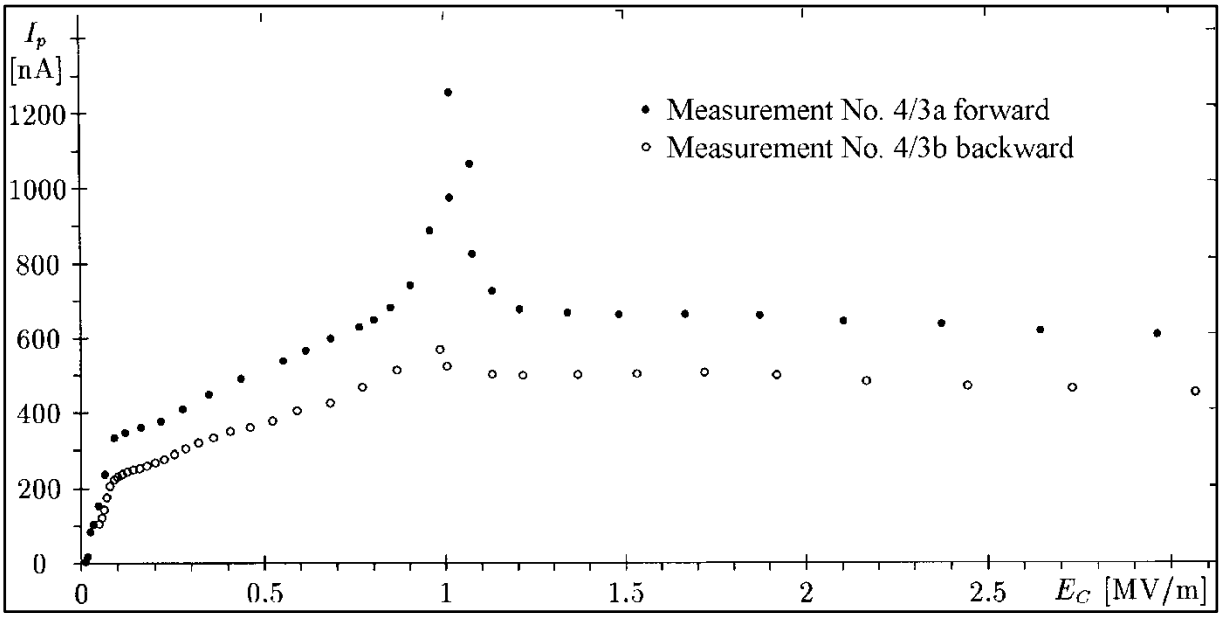

Figure 31 Shape of the I_p (E_C) curve of layer No. 4-2 with the peak at 1.0 MV/m, according to measurement No. 4/3

4.5.2. RF Properties of the Photocathode Layers

All Cs_3Sb layers transferred into the cavity have loaded the cavity quality significanty, although their surface contribution was quite low. The cathode quality factor Q_C given in Table 13 is the quality of the cavity with photocathode, inversely reduced by the quality of the bare cavity. The resulting strong RF losses cannot be explained with a purely magnetic loss mechanism (surface currents to shield the RF magnetic field), particularly since the magnetic field is quite low at the location of the cathode. If one nevertheless converts the quality factors with a geometry factor G_C = 8 MΩ, the resulting surface resistances amount around 1 Ω for all photocathode layers. This requires a field penetration depth of about 100 µm, while the Cs_3Sb layers are only about 500 nm thick: The RF field thus penetrates the layers completely and is shielded only by the substrate below. The power dissipation is of dielectric nature and is caused by the currents $j = \sigma E_C$ induced by the normal electric field E_C in the volume of the Cs_3Sb layer. Assuming that the shielding of the nornial electric field by charges on the Cs_3Sb surface is negligible (u <<*WE)*, the conductivity of the layer can be calculated from the equation

$$\sigma = 2\omega\left(\frac{E_C^2}{W}\cdot A_C d_C \cdot Q_C\right)^{-1} \tag{19}$$

In fact, all Cs_3Sb layers with a quantum efficiency above 2% lead to the same conductivity σ = 0.045 A/Vm with surprising accuracy. Only the layers No. 1-1 and No. 4-2, which also showed a lower quantum efficiency, deviated from this value. The low absolute value of the conductivity can be understood, if one considers that the photocathode is a semiconductor at very low temperature. A conductivity of about 6 A/Vm has been reported for Cs_3Sb at room temperature [93].

Layer No.	Substrate	Sb amount [μg/cm^2]	Cs_3Sb thickn. d_C [nm]	Quality Q_C [10^6]	Resistance* R_S [Ω]	Conductivity σ [mA/Vm]
1-1	Niobium	60 ± 6	540 ± 54	5.8 ± 0.9	1.38 ± 0.22	70 ± 14
4-1	Cu (thin)	80 ± 8	720 ± 72	7.1 ± 1.0	1.13 ± 0.16	42 ± 6
4-2		93 ± 9	840 ± 84	13.8 ± 2.4	0.58 ± 0.10	18± 4
5-1	Copper	33 ± 3	300 ± 30	14.3 ± 2.6	0.56 ± 0.10	51 ± 10
5-2		47 ± 5	420 ± 42	12.5 ± 1.8	0.64 ± 0.09	42 ± 7
5-3		80±8	720± 72	6.8±0.2	1.18±0.04	45±5

* virtual surface resistance, calculated with the magnetic geometry factor G_C

Table 13 Thicknesses and RF losses of the Cs_3Sb photocathodes transferred into the cavity

The strong RF losses at the cathode are undesired in a regular electron source operation, because they require a powerful cooling of the cathode. A reduction of the RF losses at the photocathode would be desirable. The possibilities to influence the conductivity of this material seem to be quite limited, because its optimization with respect to the quantum efficiency is already difficult enough. In addition, the measured data give no indication that the conductivity of Cs_3Sb is varied under certain preparation conditions. A yet lower conductivity would also lead to additional problems for the extraction of high currents, because the voltage drop over the layer thickness would be considerable. The simplest way to reduce the RF power dissipation seems to be the reduction of the layer thickness. The generation of high quantum efficiency Cs_3Sb photocathodes, which thickness is a factor ten to twenty lower, should be possible with an improved preparation process, as already demonstrated in the other chamber. The reduction of thickness would linearly result in a reduction of power dissipation. A layer directly evaporated on niobium, which thickness is smaller than the correlation length in niobium (35 nm), could even become superconducting by proximity effect. The RF field would already be shielded in the photocathode layer, and the RF losses were further reduced.

The Cs_3Sb layers inside the cavity produced dark currents already at relatively low gradients between 2 and 5 MV/m. Obvious reason is the low work function of the photocathodes; their tendency towards field emission is well known [66][31]. In contrary to the effects at bare niobium described in section 4.4.3, this effect is apparently pure field emission. In most cases no bright spots could be seen inside the cavity even at large extracted currents (up to 200 μA). The behaviour of this emission, however, is quite the same as the known behaviour of emitters in niobium cavities [149]: The extracted current I_f is very instable during the first increase of gradient. Its curve normally shows sections of approximate Fowler-Nordheim behaviour, separated by wide jumps of the current (Figure 32). Obviousy emitters are changed by the emission current and disappear completely at a certain gradient (processing). Once the maximum gradient is achieved, a completely regular Fowler-Nordheim curve is seen during the backwards measurement as a rule. The yet active emitters are stable at the present gradient. This curve can be reproduced by increasing the gradient again, and even continuous operation at the maximum field strength does hardly change the emitters. In single cases processing of the emitters also led to an increased emission current.

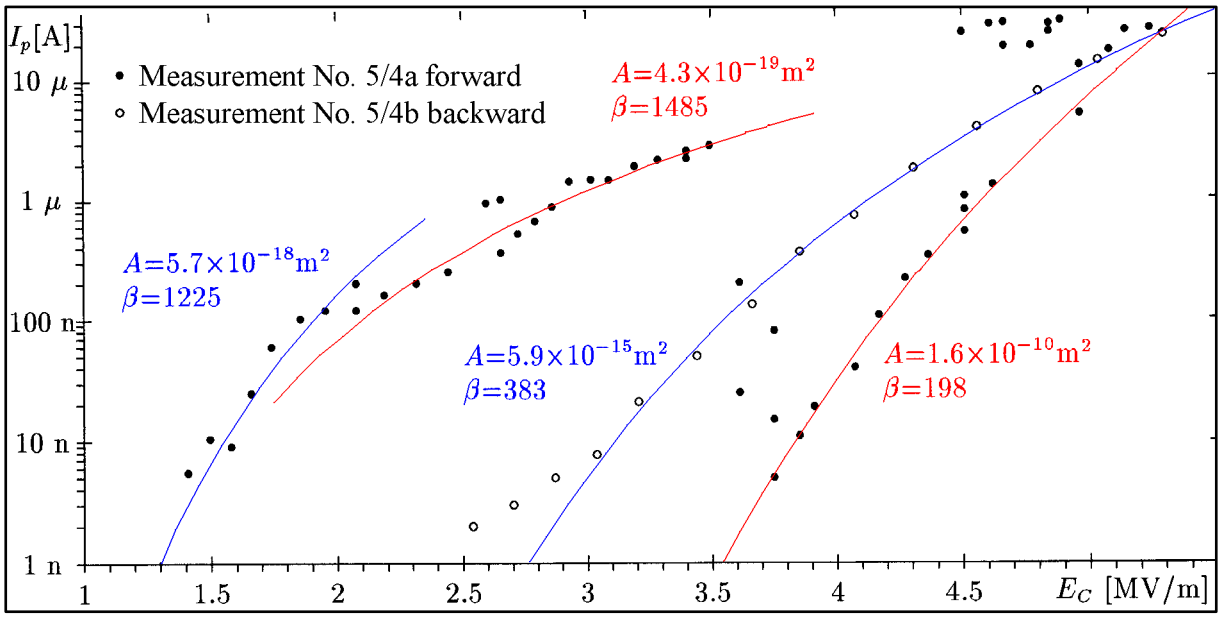

Figure 32 Field emission curve before and after achieving the maximum gradient, and approximations by Fowler-Nordheim curves; $I_f(E_C)$ measurement No. 5/4

By linear regression, a curve of the shape

$$I_f[A] = 28.32\frac{A_{FE}[m^2](\beta E_C[V/m])^{3/2}}{(\Phi[eV])^{8/3}}\cdot\exp\left(-6.833\cdot10^9\frac{(\Phi[eV])^{3/2}}{\beta E_C[V/m]}\right) \tag{20}$$

which approximately describes the theoretical behaviour according to Fowler and Nordheim, could be fitted to the data points [121]. In most cases this curve harmonized excellently with the measured data. The parameters yielded by the fitting are the field enhancement factor β at the location of the emitter and the apparent emission area A_{FE}. In Table 14 the field strength E_C, where the extracted emission current amounted to 1 nA, is listed additionally. The value 1 nA has been chosen, because this is our detection limit for the field emission current. We assumed a work function of 2.05 eV in the calculations of β and A_{FE}. With values between 150 and over 1000 the resulting β values are higher than the values normally observed at niobium surfaces. The table shows that operation at high gradients normally leads to a reduction of the enhancement factor and to an increase of the onset gradient E_C (1 nA). The operation at lower gradients as well as the reaction with residual gases, which both had a strong influence on the photoelectric properties, did not change the field emission properties of the photocathodes. Either the processes changing the quantum efficiency don't alter the work function of Cs_3Sb, or the material of the field emitters is not Cs_3Sb at all. From the regression curves only the parameters $\beta/\Phi^{3/2}$ and $A_{FE}/\Phi^{8/3}$ can be determined, but not the work function Φ itself.

The field emission at the cathode is also undesirable for a regular electron source operation. It causes uncontrolled currents which are emitted at the wrong phase and with uncontrollable intensity; finally it takes energy from the RF field. In our experiments it always limited the gradients in the cavity to values between 5 and 7 MV/m. In addition, a part of the emitted current is backaccelerated and contributes to cathode destruction. The same problem was also present in normalconducting RF guns with alkali antimonide cathodes [31]. There it could be suppressed by polishing the substrate: K_2CsSb layers prepared on a substrate with only 2 nm surface roughness showed no more appreciable field emission up to 30 MV/m gradient. We'll

investigate in our next tests whether this trick can also be applied to photocathodes prepared on niobium substrates.

Remarks Measurement direction	Measurem. $I_f(E_C)$	E_C (1 nA) [MV/m]	β (2,05 eV)	A_{FE} [nm^2]	E_C^{max} [MV/m]	I_f^{max} [μA]
Layer No. 4-2						
forward	4/2a	1.86	(566)*	(6800)*	5.19	80
backward	4/2b	2.43	547	91	5.44	17
Operation at gradients up to 3 MV/m; Helium refill						
forward	4/3a	2.46	540	87	6.83	35
FE operation for 300 s at 6.7 → 4.3 MV/m: FE current 40 → 0.8 μA						
backward	4/3b	2.82	418	740	6.38	32
Layer No. 5-2						
forward	5/4a	1.30	(1.225)*	(5,7)*	4.89	29
backward	5/4b	2.76	383	5.900	5.29	22
Operation at gradients up to 3 MV/m; Helium refill						
forward	5/5	2.89	368	5.100	6.79	150
FE operation for 600 s at 6.7 → 5.9 MV/m: FE current stable at 160 μA; optical effects						
backward	5/6	2.32	515	590	6.39	199

* values at low gradients; at higher gradients the emitters are processed

Table 14 Parameters of field emission in the RF field from photocathodes No. 4-2 and No. 5-2

4.5.3. Contamination of the Cavity Caused by the Photocathode

Besides the RF losses and the field emission at the cathode itself, it is also important whether material is transported from the photocathode to the cavity surface. It can cause again field emission there, or RF losses, eventually coupled with a superconductivity breakdown (quench). In this case, not only a periodical preparation of the photocathode would be necessary, but also the cavity would have to be cleaned periodically. A material transfer from cathode to cavity could be caused by thermal desorption, which however should be negligible at 4.2 K, or by laser or ion ablation. Also the electrons being backaccelerated to the cathode could cause desorption of cathode material; this effect should be the dominant one in our hitherto experiments. The size of this effect can be investigated by measuring the Q_0 (E_C) curves of the bare cavity and its field emission behaviour before and after the operation of a photocathode.

All measurements of the empty cavity (without photocathode stem) have been necessarily made with a singly coupled RF system until now, because the second coupler works via the cathode stem. The results have rather big errors for the quality as well as for the acceleration gradient, because the singly coupled frequency control system is quite instable. A compilation of these results is given in Table 15. The quality factor $Q_0^{res} = (Q_0^{-1}\,(\text{after}) - Q_0^{-1}\,(\text{before}))^{-1}$ is a measure for the additional RF losses in the cavity. Oniy in one case the quality of the cavity

decreased provably. However, in this case the cavity was not measured again until six days after removal of the cathode, and in the meantime the cavity was warmed up to 125 K. In two cases, the qualities of the cavity before and after testing the photocathode are identical within the error limits, and in one case the quality was even improved a bit (see Figure 33). Variations of the quality in this order of magnitude are also observed in accelerator cavities, thus they cannot provably be traced back to the presence of the photocathode.

Cavity before cathode operation		Layer No.	Cavity after cathode operation		Effects
Q_0 [10^8]	E_C [MV/m]		Q_0 [10^8]	E_C [MV/m]	Q_0^{res} [10^8]
0.2 ± 0.05	1.6 (Coupler)	1-1	No measurement		n.d.
5.5 ± 1.5	14 (FE)	4-1	2 ± 0.4	21.5 (FE)	3 ± 1*
2 ± 0.4	21.5 (FE)	4-2	3.2 ± 0.5	18 (Controls)	-5 ± 3
		600 J	sporad. FE at 7.8 MV/m; unstable		
1.3 ± 0.4	12 (FE)	5-1	1.5	19 (FE)	> 12
1.5	19 (FE)	5-2	1.6 ± 0.3	14 (FE)	> 10
E_C(1 nA) = 10.35 MV/m; β = 343		2 kJ	E_C(1 nA) = 7.07 MV/m; β = 546		
1.6 ± 0.3	14 (FE)	5-3	No measurement		n.d.

* Measured not until 6 days after cathode removal; intermediate warm-up to 125 K

Table 15 Properties of the bare cavity before and after operation of photocathodes inside it

The situation concerning the field emission is quite similar. Only in one case the field emission was significantly increased after the operation of a photocathode in the cavity (the onset gradient was reduced from 10.35 to 7.05 MV/m; see Figure 34). In two cases, however, the field emission was even significantly reduced afterwards. In another case, sporadic field emission occured already at a gradient of 7.8 MV/m after removal of the photocathode, but could immediately be processed. Finally, the cavity was free of dark currents up to the maximum gradient of 18 MV/m. Also here the measurements don't prove a significant correlation between the operation of a photocathode and the subsequent field emission in the cavity. However, it must be noticed that the increased field emission occured after the one test, where the photocathode received by far the strongest bombardment of electrons with an energy deposition of 2 kJ. The test which contained the second strong electron bombardment (600 J energy deposition) caused the sporadic field emission afterwards. This could be an indication that we are just at the limit of detectable contamination, and that yet stronger bombardment could cause significant effects.

The present measurements do not prove any permanent affection of the cavity by the operation of Cs_3Sb photocathodes within their accuracy limits. However, the accuracy of the measurements is yet quite low, and also the power of the processes, which possibly cause a contamination, is yet much lower than in a prototype electron source.

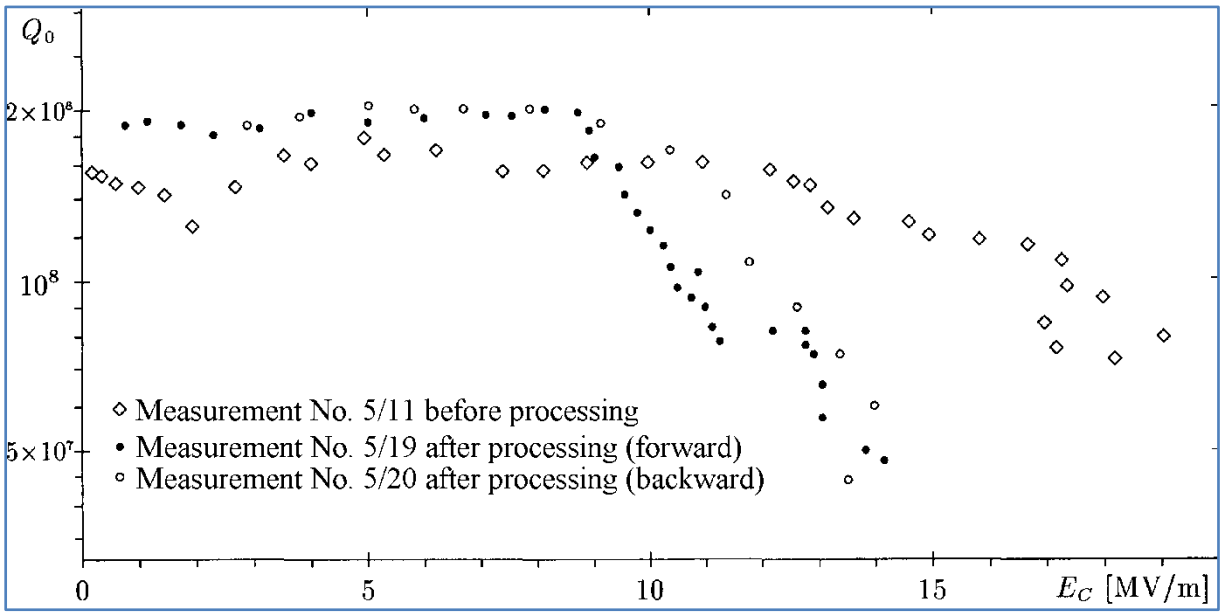

Figure 33 Dependence of the quality on the gradient before and after operation of photocathode No. 5-2 inside the cavity

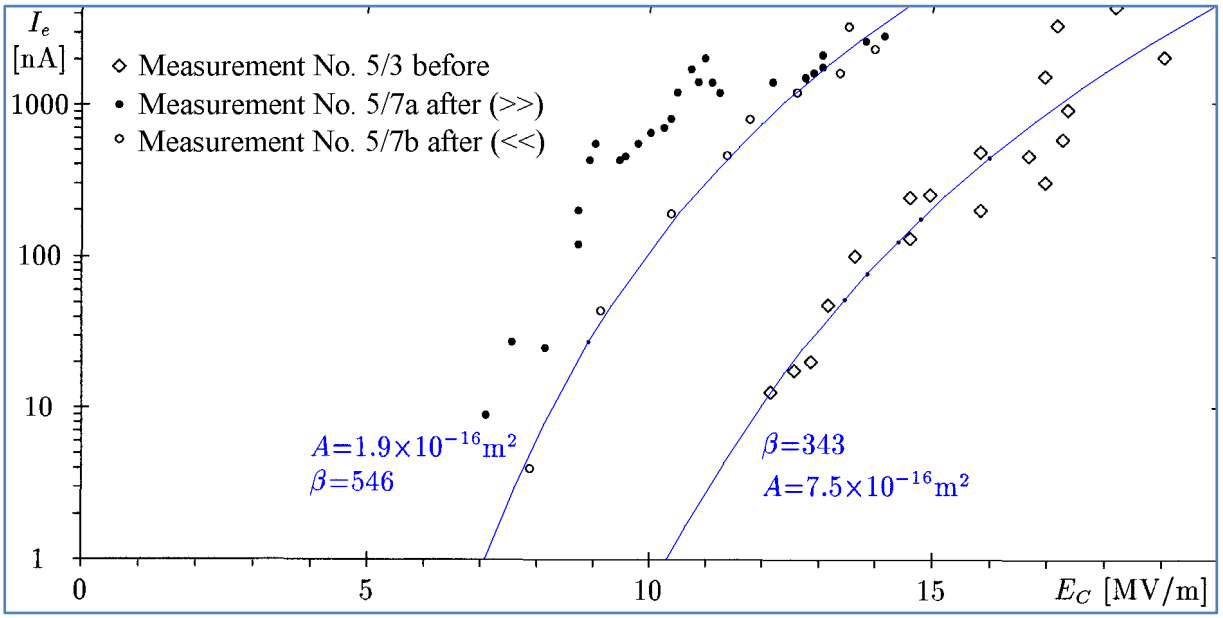

Figure 34 Dependence of the dark current on the gradient before and after operation of photo- cathode No. 5-2 inside the cavity

4.5.4. Summary of the Measurement Results

For the first time we could transfer and operate a high-quantum efficiency Cs_3Sb photocathode inside a superconducting cavity. In summary, we have operated six Cs_3Sb layers inside the superconducting cavity until now; the most important results being collected in Table 16.

Layer No.	d_C (Cs_3Sb) [nm]	η_Q^{DC} (543 nm)	η_Q^{HF} (543 nm)	E_C (1 nA) [MV/m]	Q_C [10^6]	Q_0^{res} [10^8]
1-1	540	0.32%	0.72%	> 1.1	5.8 ± 0.9	n.d.
4-1	720	1.35%	2.6% 2.0%	1.75 ± 0.15 2.15 ± 0.25	7.1 ± 1.0	3 ± 1
4-2	840	0.65%	1.4% 1.2%	2.43 > 2.96	13.8 ± 2.4	-5 ± 3*
5-1	300	2.7%	2.2% 1.3%	4.6 ± 0.15 4.84	14.3 ± 2.6	> 12
5-2	420	3.9%	5.8% 3.5%	1.45 ± 0.07 2.89	12.5 ± 1.8	> 10
5-3	720	4.8%	13.5%	> 3.3	6.8 ± 0.2	n.d.

* Increase of cavity quality observed after operation of the photocathode

Table 16 Summary of the most important parameters of the Cs_3Sb photocathode layers tested inside the cavity

The Cs_3Sb layers showed no unexpected behaviour inside the superconducting cavity. The dependence of the extracted current I_p on the RF field strength E_C can be explained as superposition of photo- and secondary electron emission. The values for quantum efficiency and secondary emission coefficient measured with the RF field show slight deviations from the values measured outside the cavity. The emission properties of the photocathodes vary strongly during operation, which can be dominantly explained by the electron bombardment of the cathode. The true lifetime of photocathodes inside the superconducting cavity could not yet be determined, because this electron bombardment cannot yet be avoided.

By their presence inside the cavity the Cs_3Sb layers cause strong RF power dissipation, which is of dielectric origin. They also show strong field emission already at very low RF field strengths. Both effects severely affect the application of this type of photocathodes in a prototype electron gun. However, in both cases there is hope to suppress the effects by at least one order of magnitude using munch thinner photocathode layers resp. polishing the substrate before preparation.

A permanent contamination of the cavity also after removal of the Cs_3Sb photocathodes could not yet be detected. However, the investigated range of parameters for the processes which could remove material from the cathode is yet far below the operation conditions of a prototype source.

4.6. Intended Improvements of the Setup and Expansions of the Test Program

The actually intended improvements and expansions of the experiment described above can be divided into three groups, according to the technical and financial effort required, and thus according to their chance of realization. The first group contains only expansions of the test program, which can be realized without modification of the actual setup. In particular,

these are the more accurate determination of quality and field emission of the bare cavity before and after operation of a photocathode, a more reproducible adjustment of the laser for measurements of the quantum efficiency and scanning of the whole cathode surface for homogeneity, the operation of photocathodes inside the cavity during a longer period (at least several hours), and an improved preparation, mounting, and evacuation of the cavity before cooldown in order to obtain better qualities at 1.9 K. An investigation of K_2CsSb photocathodes in comparison with Cs_3Sb layers, together with corresponding measurements in the other preparation chamber, also belongs here.

The second group comprises several improvements of the experimental setup, which require a considerable constructional, but (except for the cavity) only a moderate financial effort. As described above, the experiment is designed as a dynamic system which shall be optimized during operation. A series of minor improvements has already been done during and between the first tests. However, several more extensive modifications now have to be done, which efficiently should be done all at the same time. The guiding modification is the usage of a much shorter cathode stem (only about 35 mm long instead of 145 mm now) to improve its thermal coupling to the helium bath. This requires subsequent modifications at the cavity as well as in the preparation chamber: A new cavity with modified filter geometry is necessary to bear the shorter cathode stem. This cavity shall be equipped with an additional beam tube side coupler, replacing the monitor coupler behind the filter. In spite of the possible direct coupling between the two adjacent antennas, this concept promises a more stable frequency control (especially when the cathode stem is withdrawn) and thus more accurate measurements. Another modification is scheduled for the main coupler in the beam tube: Its shift distance shall be increased from actually 30 mm to 100 mm. Then its top can project into the cavity itself, enabling direct measurement of the quantum efficiency with a DC voltage. Inside the preparation chamber, the heater for the cathode stem must be modified; the new one shall be designed for a real cathode temperature up to 600°C. Actually, we think about an inductive heater element. In this case the cathode stem is heated directly, and no heat transition losses can occur. A minor modification of the sources support and the metal vapour shields will also be necessary. A cathode stem exchange magazine for at least six stems shall be installed in the preparation chamber at the same time. Then several photocathodes can be produced on storage, and also a bare stem will be available at any time.

The third group comprises supplements of the experiment, which have a high scientific interest, but require considerable amounts of money and thus actually have comparably low chances of realization. This primarily concerns a more powerful, pulsed laser, which pulses are synchronized to the RF signal. Its necessary properties are an average power up to 1 W in the green spectral range and a pulse length of 45 to 60 ps, corresponding with 45° to 60° RF phase. The standard solution would be a mode-locked, frequency-doubled Nd:YAG laser; a possible alternative would be an Ar^+ ion laser at 514 nrn. A monochromatic light source (of low power) with tunable wavelength is another desirable device. With that source one could characterize the photocathodes not only at one wavelength (actually 543 nm), but over the whole visible spectrum to achieve a better understanding of their properties.

Finally, I would like to mention that additional possible applications exist for the described experimental setup beyond our project of a Superconducting Photoemission Source. This setup provides the possibility to insert arbitrary material probes into the high electric RF field of the superconducting cavity and to test their RF properties under visual control. The only additional component which one needs for such experiments is a vacuum sluice for the cathode stem carrying the probes. For example, the RF field emission of specially prepared niobium surfaces could be tested in parallel to the DC investigations at the field emission microscope also performed in Wuppertal [125].

Conclusions

General Part

Photoemission RF sources actually have a leading role in the development of high-brightness electron sources due to their technical advantages. Several of these sources have already been built, which proved their performances concerning the beam brightness. However, in order to operate their normalconducting cavities with the required high RF field, these sources must be pulsed with typical duty cycles of 10^{-4}. They are not suitable for applications with superconducting accelerators, because those are just distinguished by their continuous operation (resp. operation with long macropulses).

The natural solution of this problem seems to be a photoemission RF gun with superconducting cavity. This device could supply the superconducting accelerators with the required high-brightness electron beam in continuous operation. However, it cannot simply be the reproduction of a normalconducting RF gun. The superconducting cavity puts completely different demands on its environment, including the photocathode, than a normalconducting cavity, and also provides a completely different environment.

Within our project to develop a superconducting photoemission source we initially studied the requirements on the various components in detail. Special attention has been naturally directed to the superconducting cavity and to the photocathode, but also to the laser for cathode illumination. Based on the properties already known from other applications, we have developed possible technical solutions for these components. It occured that especially for the photocathode no ideal solution exists, but a tradeoff must be done between robustness and high yield, which result varies according to the application.

Applications with high average current seem to favour alkali antimonide photocathodes. Their high quantum efficiency provides the best physical conditions, although their high sensitivity requires a considerable effort in vacuum technology. Based on this special application, we developed a complete design for a prototype source and estimated its presumable beam qualities with simulation calculations. Parallel with our experimental activities we have subsequently updated this design regularly. In particular, we have included a second, strongly improved cavity shape based on proposals from our collaboration partners at INFN Milano.

Experimental Part

However, some questions of fundamental importance for the selection of the components can only be decided experimentally, because corresponding measurement data are not yet available. In particular, this concerns the mutual affection of high-quantum efficiency photocathodes and the superconducting cavity in common operation. Thus we have set up two experiments and performed corresponding measurements on Cs_3Sb photocathodes.

Our first experiment is an UHV chamber to prepare and characterize alkali antimnonide photocathodes. Initially, it had a more technical than scientific meaning. It helped us to learn the handling of Cs_3Sb layers and to define a preparation process reliably leading to photocathodes with high quantum efficiency. Finally, we regularly achieved quantum efficiencies η_Q (543 nm) of 5%; with a somewhat more sophisticated preparation layers of even 10% efficiency could be produced. We also investigated the lifetime of these layers and their reaction with some residual gases. As a rule, the photocathodes showed no significant change of their quantum efficiency after two to four weeks storage in the chamber. The photocathode with 10% quantum efficiency was even stored for six months without losing its quality. Pure nitrogen at partial pressures of 5×10^{-5} mbar for 30 minutes does not affect the photocathodes. The

dependence of the quantum efficiency from the layer thickness on a niobium substrate was investigated. A decrease of quantum yield starts only at thicknesses below 30 nm.

In our second experiment, Cs_3Sb photocathodes are transferred into a superconducting cavity and operated in its high RF field. However, for reasons of simplicity a beam with defined properties is not produced in this setup. This restriction allows a very simple and flexible system with respect to a prototype source: The cavity has a simple geometry and is operated at 3 GHz, thus being small and handy. Beam-optical devices are not necessary, and the requirements on the laser for cathode illumination concerning power and pulse structure are quite low. Nevertheless all mutual influences between Cs_3Sb photocathode and superconducting Nb cavity can be studied in detail under various operation conditions.

We constructed and built up this experiment during two years; it has been put into operation in December 1991. The cavity has been carefully prepared and could (without photocathode) achieve gradients up to 20 MV/in at the location of the photocathode. The quality Q_0 (1.9 K) of the system however was yet limited to about 5×10^8; further improvements on the cavity preparation are necessary. The preparation process for Cs_3Sb photocathodes defined in the independent preparation chamber could not simply be adapted. However, we found a modified process which led to photocathodes with quantum efficiencies between 1.5% and 2% on a niobium substrate. After covering the niobium stem with a copper layer we could even produce photocathodes up to 5% quantum efficiency there. The lifetime of these photocathodes in the preparation chamber amounted to several days, because the vacuum conditions were much worse with respect to the first setup. Actually, this experiment is only equipped with a continuously emitting helium-neon laser of low power. Consequently, an electron bombardment of the photocathode during RF operation cannot be avoided.

Until now six Cs_3Sb photocathodes have been transferred to the superconducting cavity and operated there. The behaviour of the layers inside the cavity was as expected. However, due to the electron bombardment of the cathode a considerable amount of secondary electron emission could be observed. Comparing the measured curves with simulation results, the quantum efficiencies of the photocathodes could be determined as well as their secondary emission parameters. For a yet unknown reason the quantum efficiencies determined from the RF measurements deviate up to a factor two from the values measured with a DC field at room temperature; however they are consistent among themselves. The measured secondary emission coefficients are also bigger than expected up to a factor two.

Quantum efficiency and secondary emission show variations during the operation of the photocathodes, which can be traced back to mainly two reasons: Bombardment by backaccelerated electrons and reaction with residual gases. The electron bombardment may alter the quantum efficiency of the photocathodes in both directions; an increase by a factor two as well as a decrease by a factor ten have been observed already. The systematics behind this behaviour could not yet be found; obviously it depends on the actual state of the photocathode as well as on the energy spectrum and the current density of the impinging electrons. As a rule the sensitivity of the photocathode against the bombardment is gradually reduced during operation. The reaction with residual gases generally leads to a reduction of the quantum efficiency. It is suppressed inside the cold cavity, but occurs during helium refill and cathode transfer. However, the photocathodes become sensitive again for electron bombardment, and in two cases the initial quantum yield could nearly be restored by subsequent electron bombardment. The lifetime of a Cs_3Sb layer inside the cavity, which is relevant for a prototype source, can only be determined when a pulsed laser enables operation without electron bombardment.

The results concerning the RF properties of the Cs_3Sb layers most severely affect the realization of a prototype electron source. The specific conductivity of the semiconducting Cs_3Sb has been determined as 45 mA/Vm at 4.2 K. The conductivity is so low that the photocathode layers don't shield the RF field but cause dielectric losses. The energy dissipation is large, because the photocathodes shall just be operated in the region of maximum electric field. In addition, the Cs_3Sb layers show field emission starting already at very low field levels between 2 and 3 MV/m. Its currents limited the achievable gradient at the cathode to 5 – 7 MV/in until now. Field emission is undesired in an electron source, because it leads to a phase-shifted background current and to an electron bombardment of the cathode. The same problem also occured in normalconducting RF sources; there it could be suppressed by polishing the photocathode substrate. We yet have to test whether this solution can also be applied in a superconducting photoemission source.

We also tested whether the Cs_3Sb photocathodes caused a permanent contamination of the superconducting cavity. Within the limits of our accuracy, such a contamination could not be detected. Furter investigations are however necessary, because our operation conditions concerning laser power and current density are yet far below the range of a real electron source.

Conclusively, we can say that we have performed studies for the design of a superconducting photoemission source. For the first time we have operated alkali antimonide photocathodes inside a superconducting cavity and experimentally investigated the mutual interferences of these two components. No fundamental restrictions for the realization of a superconducting photoemission source have been found. However, the most severe problems seem to be given in the RF properties of the alkali antimonide photocathodes.

References

Articles Concerning the Proper Project

[1] H. Chaloupka, H Heinrichs, M. Jeck, A. Michalke, H. Piel, C. K. Sinclair, F. Ebeling, T. Weiland, U. Klein and H. P. Vogel. A proposed superconducting photoemission source of high brightness. In Kojima [195], page 583-589.

[2] H. Chaloupka, H. Heinrichs, A. Michalke, H. Piel, C. K. Sinclair, T. Weiland, F. Ebeling and U. Klein. A proposed superconducting photoemission source of high brightness. In Gover and Granatstem [192], page 327-332.

[3] H. Chaloupka, H. Heinrichs, H. Piel, C. K. Sinclair, F. Ebeling, T. Weiland, U. Klein and H. P. Vogel. A proposed superconducting photoemission source of high brightness. In Tazzari [207], page 1312-1314.

[4] A. Michalke, H. Piel, C. K. Sinclair and P. Michelato. First operation of a high-quantum efficiency photocathode inside a superconducting RF cavity. In Homeyer [194], page 1014-1016.

[5] A. Michalke, H. Piel, C. K. Sinclair, P. Michelato, C. Pagani, L. Serafini and M. Peiniger. A proposed superconducting photoemission source of high brightness. In Proch [205], page 1-6.

[6] C. Pagani et al. Proposal of a superconducting photoemission RF gun for TESLA, March 1992.

[7] Peter vom Stein. Aufbau eines Systems zur Untersuchung photoemissiver Schichten innerhalb eines supraleitenden Resonators. Externer Bericht, Bergische Universität-Gesamthochschule Wuppertal, 1992. WU D 9248.

Articles Concerning RF Photoemission Guns

[8] K. Batchelor et al. Performance of the Brookhaven photocathode RF gun. In Goldstem and Newnam [191], page 372-376.

[9] K. Batchelor, H. Kirk, J. Sheehan, M. Woodle and K. McDonald. Development of a high-brightness electron gun for the accelerator test facility at Brookhaven National Laboratory. In Tazzari [207], page 954-957.

[10] R. Bossart, J. C. Codot, H. Kugler, J. H. B. Madsen, A. Riche and J. Ströde. RF-Gun construction, tuning and high power tests. In Homeyer [194], page 1026-1028. Also published as CERN report CERN PS 92-19 (LP).

[11] B. E. Carlsten. New photoelectric injector design for the Los Alamos National Laboratory XUV FEL accelerator. In Gover and Granatstem [192], page 313-319.

[12] R. Chaput. Electron gun for the FEL CLIO. In Mann and Mandrillon [200], page 544-546.

[13] M. Curtin, G. Bennett, R. Burke, S. Benson and J. M. J. Madey. First demonstration of a free-electron laser driven by electrons from a laser irradiated photocathode, 1988.

[14] J.-M. Dolique and J.-C. Coacolo. Self-field-driven rms emittances of a field-photoemitted intense short relativistic electron beam. In Homeyer [194], page 732-734.

[15] William Donaldson. Superconducting RF gun. In Nation [203].

[16] J. W. Early et al. The Los Alamos FEL photoinjector drive laser. In Goldstem and Newnam [191], page 381-388.

[17] J. C. Gallardo and R. B. Palmer. Emittance correction of photocathode gun. In Buzzi and Ortega [190], page 345-347.

[18] J. Gao. Theoretical investigation of optimizing the microwave electron gun. In Buzzi and Ortega [190], page 348-352.

[19] J. Gao et al. Candela photoinjector status report. In Homeyer [194], page 1020-1022.

[20] Luca Giannessi. Synchrotron radiation triggered RF gun. In Nation [203].

[21] Louls N. Hand. Superconducting RF laser-driven electron gun. Project Proposal, Cornell University / Rochester University Collaboration, 1991.

[22] Y. Kawamura, K. Toyoda and M. Kawai. Generation of relativistic photoelectrons induced by excimer laser irradiation. *Applied Physics Letters,* 45(4):307-309, August 1984.

[23] K. J. Kirn and Y. J. Clien. RF and space-charge induced emittances in laser-driven RF guns. In *Proc. of the 1988 Linear Accelerator Conf.*, Williamsburg VA, October 1988. Also published as Lawrence Berkeley Laboratory Report LBL-26050.

[24] Kwang-Je Kirn. RF and space-charge effects in laser-driven RF electron guns. *Nuclear Instruments and Methods in Physics Research,* A275:201-218, 1989.

[25] D. A. Kirkpatrick et al. High-brightness electron beam sources for FEL applications. In Goldstem and Newnam [191], page 349-352.

[26] C. Lee, P. E. Oettinger, A. Sliski and M. Fishbein. Practical laser-activated photoemissive electron source. *Review of Scientific Instruments,* 56(4):560-562, April 1984.

[27] Chungshin Lee. High current density photoemissive electron source. *Applied Physics Letters,* 44(5):565-566, March 1983.

[28] I. S. Lehrman et al. Design of a high-brightness, high-duty factor photocathode electron gun. In Goldstem and Newnam [191], page 270-274.

[29] C. L. Lin, S. C. Chen, J. S. Wurtele, R. Tempkin and B. Danly. Design and modeling of a 17 GHz photocathode RF gun. In Lizama and Chew [199], page 2026-2028.

[30] A. H. Lumpkin et al. Initial observations of high-charge, low-emittance electron beams at HIBAF. In Buzzi and Ortega [190], page 379-385.

[31] Alex H. Lumpkin. Observations on field-emission electrons from the Los Alamos FEL photoinjector. In Lizama and Chew [199], page 1967-1969.

[32] K. T. McDonald. Beam dynamics of the RF electron gun of the BNL accelerator test facility.

[33] P. E. Oettinger. A selection of high brightness, laser-driven cathodes for electron accelerator applications. In J. Murphy and C. Pellegrini, editors, *Proc. of the ICFA Workshop on Low Emittance e^+e^--Beams,* Brookhaven, March 1987. BNL.

[34] P. E. Oettinger, I. Bursuc, R. E. Shefer and E. Pugh. Brightness of an intense electron beam generated by a pulse-laser irradiated photocathode. *Applied Physics Letters,* 50:1867-1870, 1987.

[35] P. E. Oettinger, R. E. Shefer, D. L. Birx and M. C. Green. Photoelectron sources: Selection and analysis. *Nuclear Instruments and Methods,* A272:264-267, 1988.

[36] P. G. O'Shea et al. Performance of the photoinjector accelerator for the Los Alamos free-electron laser. In Lizama and Chew [199], page 2754-2756.

[37] Patrick O'Shea. APEX 40 MeV photoinjector linac. In Nation [203].

[38] Zohreh Parsa. Beam emittance and the effects of the RF, space charge and wake fields – Application to the ATF photoelectron beam. In Lizama and Chew [199], page 511-513.

[39] W. Peter, R. J. Faehl and M. E. Jones. Analysis of a microwave electron gun for accelerator applications. *Particle Accelerators*, 21:59-67, 1987.

[40] J. B. Rosenzweig. Flat-beam rf photocathode sources for linear collider applications, In Lizama and Chew [199], page 1987-1989.

[41] L. Serafini, M. Ferrario, C. Pagani and R. Rivolta. TOPGUN: A new way to increase the beam brightness of rf guns. Technical report, INFN Milano, San Francisco, May 1991.

[42] L. Serafini, R. Rivolta, L. Terzioli and C. Pagani. RF gun emittance correction using unsymmetrical rf cavities. *Nuclear Instruments and Methods in Physics Research*, 1992.

[43] C. K. Sinclair. A 500 kV photoemission electron gun for the CEBAF FEL. In Goldstem and Newnam [191], page 410-414.

[44] Charles K. Sinclair and Roger H. Miller. A high current, short pulse, RF synchronized electron gun for the Stanford Linear Accelerator. *lEBE Transactions on Nuclear Science*, NS-28(3), June 1981.

[45] M. Takabe et al. 0.9-MeV microwave electron gun system for an FEL. In Goldstem and Newnam [191], page 367-371.

[46] Christian Travier. Rf guns: A review. In LeDuff [197], page 105-141. Also published as LAL/RT 90-13.

[47] Christian Travier. Rf guns: Bright injectors für FEL. In Buzzi and Ortega [190]. Also published as LAL/SERA/90-248 RFG.

[48] Christian Travier. Review of microwave guns. Technical Report LAL/SERA/91-286, Laboratoire de l'Accelerateur Lineaire, Université Paris-Sud, Centre d 'Orsay, F-9 1405 Orsay Cedex, July 1991. Submitted to Particle Accelerators.

Articles Concerning Other Electron Guns

[49] Michael Bieler. *Untersuchungen zur Emissionsdauer-Verlängerung einer Laser- getriebenen Hohlstrahlkanone.* Dissertation, Universität Hamburg, Fachbereich Physik, November 1990. DESY M-90-12.

[50] J. E. Ciendenin et al. Polarized electron sources für linear colliders. In HEACC-92 [193].

[51] G. D'Auria, J. Gonichon and T. Manfroi. Preliminary design for a thermionic R.F.-gun. In Lizama and Chew [199], page 1978-1980.

[52] K. R. Eppley et al. SLC polarized beam source electron optics design. In Lizama and Chew [199], page 1964-1966.

[53] H. Gundel, H. Heydari, D. Suchland, K. Schmidt and H. Henke. Profile measurements on a pulsed ferroelectric electron beam. In Homeyer [194], page 1023-1025.

[54] W. Hartmann et al. Source of polarized electrons. In Tazzari [207], page 1335-1336.

[55] T.-Y. Hsu, G. Kirkman-Amemiya and M. A. Gundersen. Electron beam generation from a superemissive cathode. In Lizama and Chew [199], page 1990-1992.

[56] Y. Huang and J. Xie. Measure to alleviate the back bombardment effect of thermionic rf electron gun. In Lizama and Chew [199], page 2017-2019.

[57] K. K. Jain, B. N. Ding and M. J. Rhee. Scaling study of pseudospark produced electron beam. In Lizama and Chew [199], page 1972-1974.

[58] A. Kadish, W. Peter and M. E. Jones. Current-voltage relation in a time-dependent diode. *Applied Physics Letters,* 47(2):115-117, July 1985.

[59] C. B. McKee and J. M. J. Madey. Optimization of a thermionic microwave electron gun. In Buzzi and Ortega [190], page 386-391.

[60] C. B. McKee and John M. J. Madey. Computer simulation of cathode heating by back-bombardment in the microwave electron gun. page 716-719, Naples FL, October 1989. Duke University, Durham NC, Nuclear Instruments and Methods in Physics Research, Vol. A296.

[61] T. Nakanishi et al. Development of polarized electron sources using AlGaAs-GaAs superlattice and using strained GaAs. In Lizama and Chew [199], page 2032-2034.

[62] G. A. Westenskow and J. M. J. Madey. Microwave electron gun. *Laser and Particle Beams,* 2(2):223-225, 1984.

[63] J. Xie, J. Gao, Y. Huang, R. Zhang, H. Liu and Y. Wang. Development of thermionic-cathode RF electron gun at IHEP, In Lizama and Chew [199], page 2020-2022.

Articles Concerning Photoemission and Photocathodes

[64] D. J. Bamford, M. H. Bakshi and D. A. G. Deacon. The search for rugged, efficient photocathode materials. In Goldstem and Newnam [191], page 377-380.

[65] R. L. Bell. *Negative Electron Affinity Devices.* Clarendon Press, Oxford, 1973.

[66] J. A. Cochrane and R. F. Thumwood. The effects of high electric fields on photocathodes. In Morgan et al. [202], page 441-448.

[67] R. H. Fowler. The analysis of photoelectric sensitivity curves for clean metals at various temperatures. *Physical Review,* 38:45-56, July 1931.

[68] J. S. Fraser, R. L. Sheffield, E. R. Gray, P. M. Giles, R. W. Springer and V. A. Loebs. Photocathodes in accelerator applications. In *Proc. of the 1987 IEEE Particle Aceelerator Conf.*, number 17, page 1705-1709, Piscataway, NJ, 1987. IEEE.

[69] H. R. C. Garfield. Multialkali photocathodes. In McGee et al. [201], page 339-355.

[70] J. P. Girardeau-Montaut and Y. Chaouki. Experimental behaviour of cesium-antimony photocathodes under laser irradiation. In Mann and Mandrillon [200], page 694-696.

[71] J.P. Girardeau-Montaut, C. Girardeau-Montaut and R. Dei-Cas. Production of very high electron density assisted by lasers. In *Proc. of the 15th Int. Symp. ori Discharges and Electrical Isolation in Vacuum,* page 519-521, Paris, 1988.

[72] P. Görlich. Über zusammengesetzte, durchsichtige Photokathoden. *Zeitschrift für Physik,* 101:335-342, 1936.

[73] W. Greschat, H. Heinrich and P. Römer. Quantum yield of Cs_3Sb photocathodes as function of thickness and angle of incidence. In Morgan et al. [202], page 397-408.

[74] Minoru Hagino and Tadashi Takahashi. Thickness of Cs-Sb films relative to the original Sb films. *Journal of Applied Physics,* 37(10):3741-3743, September 1966.

[75] P. J. Hockley and H. Thomas. Electron emission from GaAsP NEA cathodes. In Turner [208], page 69-72.

[76] K. H. Jack and M. M. Wachtel. The characterization and crystal structure of caesium antimonide, a photo-electric surface material. *Proc. of the Royal Society (London),* A239:46-60, 1957.

[77] E. Kansky. Some physico-chemical aspects of the synthesis of antimonide photocathodes. In McGee et al. [201], page 357-368.

[78] Claus Kunze. Untersuchungen an Cs-Sb-Schichten. *Annalen der Physik,* 7(6):89-106, 1960.

[79] Chungshin Lee. Photoelectron energy distribution of Cs_3Sb. *Journal of Applied Physics,* 54(8):4578-4580, August 1983.

[80] T. Maruyama, E. L. Garwin, R. Prepost, G. H. Zapalac, J. S. Smith and J. D. Walker. Strain enhanced electron spin polarization observed in photoemission from InGaAs. In Lizama and Chew [199], page 2029-2031.

[81] T. Maruyama, E.L. Garwin, R. Prepost and G.H. Zapalac. Electron spin polarization in photoemission from strained GaAs grown on GaAsP. Technical Report SLAC-PUB-5731, WISC-EX-92-322, SLAC / Univ. of Wisconsin, February 1992. Bei Physical Review Letters eingereicht.

[82] D. McMullan and J. R. Powell. Residual gases and the stability of photocathodes. In Morgan et al. [202], page 427-439.

[83] Kiyoshi Miyake. Effect of electron bombardment on secondary and photo-electron emission of cesium-antimonide. *Journal of the Physical Society of Japan,* 10:164-165, 1955.

[84] Kiyoshi Miyake. Effect of electron bombardment on secondary and photoelectric emission of cesium-antimonide. *Journal of the Physical Society of Japan,* 10:912-913, 1955.

[85] Kiyoshi Miyake. Fatigue of photoelectric emission of cesium-antimonide. *Journal of the Physical Society of Japan,* 10:913-915, 1955.

[86] N. D. Morgulis and B. I. Djatlowizkaja. Emissionje swoistwa surmjano-zesiewich katodow. *Jurnal Technitschjeskoi Fisiki,* X(8):657-670, 1940.

[87] A. L. Musatov, S. L. Filippov and V. L. Korotkikh. Photoemission from back-biased schottky diodes p-InP-Ag. In Turner [208], page 53-56.

[88] C. Piaget, R. Polaert and J. C. Richard. Gallium indium arsenide photocathodes. In Morgan et al. [202], page 377-385.

[89] D. C. Rodway and D. J. Bradley. Mean transverse emission energy and surface topography on GaAs(Cs,O) photocathodes. *Journal of Physics D: Applied Physies,* 17:L137-L141, 1984.

[90] C. J. Scott, X. Tang and M. G. Spencer. Enhanced photoemission from a bi-metallic LaB_6/Au photocathode. *Applied Physies Letters,* 58(16):1795 f., April 1991.

[91] A. Septier, F. Sabary, J. C. Dudek, H. Bergeret and B. Leblond. A binary Al/Li alloy a new material for the realization of high-intensity pulsed photocathodes. In Buzzi and Ortega [190], page 392-395.

[92] Richard L. Sheffield. Photocathodes. In Nation [203].

[93] A. H. Sommer. Photo-electric alloys of alkali metals. *Nature,* 148:468, October 1941.

[94] A. H. Sommer. Spectrally selective (solar blind) uv photomultipliers with fluoride windows. *Review of Scientific Instruments,* 32:356, 1962.

[95] A. H. Sommer. A new alkali antimonicle photoemitter with high sensitivity to visible light. *Applied Physics Letters,* 3(4):62-63, August 1963.

[96] A. H. Sommer. Photoelectric emission. In S. Larach, editor, *Photoelectronic Materials and Devices,* chapter 4, page 175-221. Van Nostrand Reinhold Co., New York, 1965.

[97] A. H. Sommer. *Photoemissive Materials.* Elsevier Science Publisher, Princeton, 1968.

[98] W. E. Spicer. Photoemissive, photoconductive, and optical absorption studies of alkali-antimony compounds. *Physical Review,* 112(1):114 122, October 1958.

[99] W. E. Spicer. Photoemission and related properties of the alkali-antimonides. *Journal of Applied Physics,* 31(12) :2077-2084, December 1960.

[100] W. E. Spicer. Photoemission and band structure of the semiconducting compound CsAu. *Physical Review,* 125(4):1297-1299, February 1962.

[101] R. W. Springer and B. J. Cameron. Photocathode transfer and storage techniques using alkali vapor feedback control. In Goldstem and Newnam [191], page 396-400.

[102] T. Srinivasan-Rao. Photoemission studies using femtosecond pulses for high brightness electron beams. In LeDuff [197], page 267-284.

[103] G. Suberlucq. Photocathodes en iodure de césium utilisées à fort courant. Technical Report CERN PS 92-29 (LP), CLIC Note 162, CERN PS Division, May 1992.

[104] E. Taft and L. Apker. Photoemission from cesium and rubidium tellurides. *Journal of the Optical Society of America,* 43(2):81-83, February 1953.

[105] R. L. Ternes, S. Z. Bethel and D. O. Janky. A statistically-designed experiment for assessing cesium-potassium-animonide photocathode fabrication parameters. In Goldstem and Newnam [191], page 401-409.

[106] P. W. Timofejew and Ju. I. Luikowa. Surmjano-zesiewie emitteri. *Jurnal Technitschjeskoi Fisiki,* X(1):20-23, 1940.

[107] Cs. Toth, Gy. Farkas, D. Charalambidis, E. Hontzopoulos and C. Fotakis. High brightness electron beam production by laser induced various order multiphoton photoeffects of gold. In LeDuff [197], page 285-303.

[108] T. Tsang, T. Srinivasan-Rao and J. Fischer. Photoemissiori using femtosecond lasers. In Goldstem and Newnam [191], page 270-274.

[109] A. T. Young et al. Quantum yield measurements of photocathodes illuminated by pulsed ultraviolet laser radiation. In Lizama and Chew [199], page 1993-1995.

Articles Concerning Other Emission Mechanisms

[110] G. Appelt and O. Hachenberg. Sekundärelektronenemission von Antimon-Caesium und Wismut-Caesium Schichten verschiedener Zusammensetzung. *Annalen der Physik,* 7(6):67-81, 1960.

[111] D. Boimond et al. High-current electron and ion sources based on ferroelectrics switching. In HEACC-92 [193].

[112] M. Boussoukaya. Laser triggered field emission. In LeDuff [197], page 91-104. Invited Paper.

[113] M. Boussoukaya, H. Bergeret, R. Chehab and B. Leblond. Pulsed photofield emission in ps regime obtained from new type of microemitters. In *Proc, of the l3th Int. Symp. on Discharges and Electrical Isolation in Vacuum,* page 522-524, Paris, 1988.

[114] H. E. Elsayed-Ali et al. Time-resolved observation ofelectron-phonon relaxation in copper. *Physical Review Letters,* 58(12):1212-1215, March 1987.

[115] Louis R. Falce. Thermionic cathodes: A review. In LeDuff [197], page 1-48. Invited Paper.

[116] R. H. Fowler and L. Nordheim. Electron emission in intense electric fields. *Proc. of the Royal Society (London),* A119:173-181, 1928.

[117] J. G. Fujimoto et al. Femtosecond laser interaction with metallic tungsten and non-equilibritim electron and lattice temperatures. *Physical Review Letters,* 53(19): 1837-1840, November 1984.

[118] O. Gärtner, P. Janiel, J. E. Crombeen and J. Hasker. Top layer scandate cathodes by plasma-activated CVD. In Turner [208], page 25-28.

[119] K. Geissler et al. Enhancement of laser-induced electron emission from ferroelectrics by surface charge refreshment. *Physics Letters,* 1992.

[120] O. Hachenberg and W. Brauer. Secondary electron emission from solids. In L. Marton, editor, *Advances in Electronics and Electron Physics,* number 11, page 413-500, 1959.

[121] H. Hübner. *Untersuchung der Feldemission bei Frequenzen zwischen 12 und 18 GHz.* Dissertation, Universität Karlsruhe, Institut für Kernphysik, October 1982. KfK 3398.

[122] J. H. Ivers, R. Advani, J. A. Nation and L. Schachter. Electron emission from ferroelectric ceramics. In Lizama and Chew [199], page 2104-2106.

[123] Robert G. Lye and A. J. Dekker. Theory of secondary emission. *Physical Review,* 107(4):977-981, August 1957.

[124] E. Mahner et al. Field emission measurements on niobium cathodes of high purity. In Proch [205], page 694-699.

[125] E. Mahner et al. Enhanced field emission of niobium single crystals. In Homeyer [194], page 1653-1655.

[126] Ph. Niedermann et al. Investigation of field emitting microstructures by scanning electron and scanning tunneling microscopy. In Turner [208].

[127] L. W. Nordheim. The effect of the image force on the emission and reflexion of electrons by metals. *Proc. of the Royal Society (London),* A121:626-639, 1928.

[128] H. Riege. Features and applications of the new methods of ferroelectric emission, photoemission from perovskite ceramics, and plasma-assisted particle emission. Tech-

nical Report CERN PS Note 89-15 (AR), CERN, CERN, CH-1211 Geneva 23, Switzerland, December 1989.

[129] H. Riege. The diffuse vacuum discharge as an intense particle beam source. In LeDuff [197], page 323-344.

[130] R. W. Schoenlein et al. Femtosecond studies of nonequilibrium electronic processes in metals. *Physical Review Letters,* 58(16):1680 1683, April 1987.

[131] W. Schottky. *Zeitschrift für Physik*, 14:80 ff, 1923.

[132] C. M. Tang, A. C. Ting and T. Swyden. Field emission arrays - a potentially bright source. In Goldstem and Newnam [191], page 353-357.

[133] Cha-Mei Tang. Field emission arrays. In Nation [203].

Articles Concerning Superconducting Cavities

[134] C. Benvenuti et al. Superconducting cavities produced by magnetron sputtering of niobium on copper. In Shepard [206], page 445-468.

[135] D. Bloess. Preparation and handling of surfaces for superconducting radio frequency cavities. In Shepard [206], page 359-366.

[136] G. Cavallari et al. Status report on superconducting RF cavities at CERN. In Proch [205], page 23-36.

[137] Chen Chia-Erh et al. The status of RF superconducting activities at Peking University. In Homeyer [194], page 1257-1259.

[138] C. Chianelli et al. Microscopic analysis of niobium field electron emitters. In Proch [205], page 700-705.

[139] M. Fouaidy et al. Surface temperature measuremerits on superconducting cavities in superfluid helium. In Proch [205], page 547-576.

[140] J. Graber et al. High peak power RF processing studies of 3 GHz niobium cavities. In Proch [205], page 758-765.

[141] J. Halbritter. Theoretical aspects in RF-superconductivity. In Kuntze [196], page 190-214.

[142] J. Halbritter. On RF residual losses in superconducting cavities. In Lengeler [198], page 42 7-445.

[143] Udo Klein. *Untersuchungen zu Feldbegrenzungsphänornenen und Oberflächenwiderständen von supraleitenden Resonatoren.* Dissertation, Bergische Universität-Gesamthochschule Wuppertal, 1981. WUB-DI 81-2.

[144] H. Lengeler. Design of superconducting accelerator cavities. In Kuntze [196], page 219-236.

[145] G. Müller and H. Padamsee. High-temperature annealing of superconducting cavities from high-purity niobium. In *Proc. of the 1987 Partiele Accelerator Conf.,* Washington, DC, March 1987.

[146] Günter Müller. Superconducting niobium in high RF magnetic fields. In Shepard [206], page 331-358.

[147] H. Padamsee. Recent status of superconducting accelerator cavities. In *Proc. of the IGFA Workshop on AG Superconductivity*, KEK, Tsukuba, Japan, June 1992.

[148] H. Padamsee. Review of the superconducting approach to linear colliders. In Homeyer [194], page 378 384.

[149] H. Padamsee et al. RF field emission in superconducting cavities. In Lengeler [198], page 251-272.

[150] M. Peiniger et al. Work on Nb_3Sn cavities at Wuppertal. In Shepard [206], page 503-532.

[151] M. Pham Tu, K. Mbaye and L. Wartski. Niobium nitride coated superconducting cavities. In Shepard [206], page 673-680.

[152] H. Piel. Fundamental features of superconducting cavities for high energy accelerators. Technical Report WUB 86-14, Univ. Wuppertal, Wuppertal, Germany, September 1985. Talk at CERN Accelerator School, Oxford.

[153] D. Reschke et al. High gradients in 3 GHz nine-cell cavities for superconducting linear colliders. In Proch [205], page 743-750.

[154] R. W. Röth et al. Results of postpurified 3 GHz accelerator structures. In Kojirna [195], page 437-444.

[155] R. W. Röth et al. Thermal stability of superconducting Nb cavities at 3 GHz. In Homeyer [194], page 1325-1327.

[156] Ralf W. Röth. *Anomale Verlustmechanismen in supraleitenden Resonatoren aus hochreinem Niob*. Dissertation, Bergische Universität-Gesamthochschule Wuppertal, 1992. WUBDIS 92-12.

[157] Suehiro Takeuchi. Superconducting RF activities at JAERI. In Proch [205], page 76-83.

[158] B. H. Wiik et al. A proposal to construct and test prototype superconducting R.F. structures for linear colliders. Technical report, DESY Hamburg and partners, Notkestr. 85, Hamburg, Germany, April 1992.

Articles Concerning Linear Colliders and Free-Electron-Lasers

[159] J. Auerhammer et al. Project review of the near infrared free electron laser at the **S-DALINAC.** In Goldstem and Newnam [191], page 184-188.

[160] P. Balleyguier et al. Production of high-brightness electron beams für the ELSA-FEL. In Buzzi and Ortega [190], page 308-310.

[161] K. Batchelor et al. Status of the visible free-electron laser at the Brookhaven Accelerator Test Facility. In Goldstem and Newnam [191], page 159-164.

[162] I. Ben-Zvi et al. Proposed UV-FEL user facility at BNL. In Goldstem and Newnam [191], page 201-207.

[163] Charles A. Brau. *Free-Electron Lasers*, Band Suppl. 22 von *Advances in Electronics and Electron Physics.* Academic Press, Boston, MA, 1990.

[164] M. Castellano et al. Progress report of the machine construction and FEL program on LISA at LNF. In Goldstem and Newnam [191], page 168-172.

[165] K. C. D. Chan et al. Los Alamos advanced free-electron laser. In Goldstem and Newnam [191], page 148-152.

[166] M. E. Couprie et al. Measurements performed on the Super-ACO free-electron laser with a dissector. In Goldstem and Newnam [191], page 59-64.

[167] R. Dei-Cas et al. Photoemission studies and commissioning the ELSA-FEL experiment. In Goldstem and Newnam [191], page 121-126.

[168] G. J. Ernst et al. Status of the TEU-FEL project. In Goldstem and Newnam [191], page 173-177.

[169] D. W. Feldman et al. Performance of the Los Alamnos HIBAF accelerator at 17 MeV. In Buzzi and Ortega [190], page 133-139.

[170] K. L. Meier. Engineering considerations of the advanced free-electron laser facility. In Goldstem and Newnam [191], page 153 158.

[171] G. R. Neil et al. FEL design using the CEBAF linac. In Goldstem and Newnam [191], page 212-215.

[172] B. E. Newnam et al. The Los Alamos POP project: FEL oscillator experiments in the ultraviolet and beyond. In Goldstem and Newnam [191], page 197-200.

[173] C. Pellegrini. The free electron laser and its possible developments. *IEEE Transactions on Nuclear Science,* NS-26(3):3791 3797, June 1979.

[174] A. Renieri. Free electron lasers. In Tazzari [207], page 144-147.

[175] M. Sawamura et al. Status of the JAERI FEL - beam test for injection system. In Goldstem and Newnam [191], page 153-158.

[176] Richard L. Sheffield. Short wavelength FELs. In Lizama and Chew [199], page 1110-1114.

[177] Todd I. Smith. Intense low emittance linac beams for free electron lasers. In *Proc. of the 1986 Linear Accelerator Conf.,* Stanford Linear Accelerator Center, 1986. Invited paper, also published as HEPL-PUB 976.

[178] S. Takeda. Review of linear colliders (KEK, SLAC, CERN, DESY, **...).** In Homeyer [194], page 372-377.

[179] K. Yamada et al. Visible oscillation of storage-ring free electron laser on TERAS. In Goldstem and Newnam [191], page 33-37.

Articles Concerning Accelerators in General

[180] V. Aab et al. The superconducing 130 MeV electron accelerator at Darmstadt. In Shepard [206], page 127-140.

[181] R. Bailey et al. Three years operational experience with LEP. In Homeyer [194], page 63-65.

[182] Ilan Ben-Zvi. The BNL accelerator test facility and experimental program. In Lizama and Chew [199], page 550-554.

[183] R. Boni et al. Status of the ARES R&D program. In Lizama and Chew [199], page 2973-2975.

[184] D. Degle. The EP collider HERA. In Homeyer [194], page 3-8.

[185] S. Hartman et al. Photocathode driven linac at UCLA for FEL arid plasma wakefield acceleration experiments. In Lizamna and Chew [199], page 2967-2969.

[186] E. Keil. Review of high energy ee colliders. In Homeyer [194], page 22-26.

[187] J. D. Lawson. Brightness, emittance, and temperature. Number 178 in NATO ASI Series B: Physics, page 5-20, Pitlochry, Scotland, July 1986. Plenum Press, New York.

[188] G. H. Rees. Review of high energy pp colliders. In Homeyer [194], page 17-21.

[189] M. Reiser. Physics of high brightness sources. American Institute of Physics, 1989.

Proceedings and Collections of Articles

[190] J. M. Buzzi and J. M. Ortega, editors. *Proc. of the l2th Int. Free Electron Laser Conf.,* Paris, September 1990. Nuclear Instruments and Methods in Physics Research, Vol. A304.

[191] J. C. Goldstem and B. E. Newnam, editors. *Proc. of the l3th Int. Free Electron Laser Cortf.,* Santa Fe, NM, August 1991. Nuclear Instruments and Methods in Physics Research, Vol. A318.

[192] A. Gover and V. Granatstem, editors. *Proc. of the 10th Int. Free Electron Laser Conf.,* Jerusalem, Israel, August 1988. Nuclear Instruments and Methods in Physics Research, Vol. A285, Nos. 1,2.

[193] *Proc. of the 15th Int. Conf. ort High Energy Accelerators,* Hamburg, July 1992.

[194] H. Horneyer, editor. *Proc. of the 3rd European Particle Accelerator Conf.,* Berlin, March 1992. Editions Frontieres, Gif-sur-Yvette.

[195] Y. Kojima, editor. *Proc. of the 4th Workshop ort RF Superconductivity,* KEK, Tsukuba, Japan, Januar 1989. KEK Report 89-21.

[196] M. Kuntze, editor. *Proc. of the Workshop on RF Superconductivity,* KfK Karlsruhe, July 1980. KfK Report 3019.

[197] Joel LeDuff, editor. *Proc. ofthe Workshop on Short Pnlse High Current Cathodes,* Bendor, France, June 1990. Editions Frontières, Gif-sur-Yvette.

[198] H. Lengeler, editor. *Proc. of the 2nd Workshop on RF Superconductivity,* CERN, Geneva, July 1984.

[199] Loretta Lizama and Joe Chew, editors. *1991 IEEB Particle Accelerator Conf. Record,* San Francisco, May 1991. IEEE.

[200] P. Mann and P. Mandrillon, editors. *Proc. of the 2nd European Particle Accelerator Conf.,* Nice, France, June 1990. Editions Frontières.

[201] J. D. McGee, D. McMullan and E. Kahan, editors. *Proc. of the 5th Syrnp. on Photo-Electronic Image Devices,* Imperial College, London, September 1971. Published in: Advances in Electronics and Electron Physics, Vol. 33A+B, ed. L. Marton, Academic Press, 1972.

[202] B. L. Morgan, R. W. Airey and D. McMullan, editors. *Proc. of the 6th Symp. on Photo-Electronic Image Devices,* Imperial College, London, September 1974. Published in: Advances in Electronics and Electron Physics, Vol. 40A+B, ed. L. Marton, Academic Press, 1976.

[203] John Nation, editor. *Proc. of the 3rd Int. Workshop on Advartced Accelerator Concepts,* Port Jefferson, NY, June 1992. Massachusetts Institute of Technology.

[204] Hasan Padamsee, editor. *Proc. of the 1st TESLA Workshop,* Cornell University, Ithaca NY, July 1990. CLNS-90-1029.

[205] D. Proch, editor. *Proc. of the 5th Workshop ort RF Superconductivity,* Hamburg, August 1991.

[206] K. W. Shepard, editor. *Proc. of the 3rd Workshop On RF Superconductivity,* Argonne,IL, September 1987.

[207] S. Tazzari, editor. *Proc. of the European Particle Accelerator Conf.,* Rome, June 1988. World Scientific, Singapore.

[208] R. E. Turner, editor. *Proc. of the 2nd Int. Conf. on Vacuum Microelectronics,* number 99 in Institute of Physics Conf. Series. Institute of Physics, July 1989.

Various Publications

[209] P. Balzarotti and A. Renzo. Gas emission from Cs dispensers under heating. Technical Report 118/1990, SAES Getters SpA., RD Central Labs, 20151 Milano/Italy, November 1990.

[210] R. Boll and L. Borek. Elektromagnetische Schirmung. *NTG-Fachberichte,* 76, 1980.

[211] F. Ebeling, P. Schütt and T. Weiland. Selfconsistent simulation of high power tubes with TBCI-SF. In Tazzari [207], page 678-682.

[212] *Gmelins Handbuch der Anorganischen Chemie.* Verlag Chemie, Weinheim / Gmelin-Verlag, Clausthal.

[213] S. J. Heuer. Measurement of gaseous impurities in alkali metal vapor generated by a dispenser. Technical report, SAES Getters SpA., 20151 Milano, Italy.

[214] B. A. Lengyel. *Lasers.* Wiley Series in Pure and Applied Optics. Wiley-Interscience, New York, 1971.

[215] P. Della Porta, C. Emil and S. J. Hellier. Alkali metal generation and gas evolution from alkali metal dispensers. Technical Report TR 18, SAES Getters SpA., 20151 Milano, Italy.

[216] A. Renzo. Prove di outgassing durante l'attivazione dei dispenser di Cs. Technical Report 65/1991, SAES Getters SpA., R&D Central Labs., 20151 Milano/Italy, June 1991.

[217] L. Serafini and C. Pagani. ITACA: A new computer code for the integration of transient particle and field equations in axi-symmetrical cavities. In Tazzari [207], page 866 ff.

[218] C. V. Shank. *Generation of Ultrashort Optical Pulses,* Band 60 von *Topics in Applied Physics,* Kapitel 2, page 5 34. Springer-Verlag, 1988.

[219] M. Succi, R. Canino and B. Ferrario. Atomic absorption evaporation flow rate measurements of alkali metal dispensers. *Vacuum,* 35(12):579 582, July 1985.

[220] T. Weiland. On the computation of resonant modes in cylindrically symmetric cavities. *Nuclear Instruments and Methods in Physics Research,* 216:329-348, 1983.

List of Figures

List of Tables